The Development and Application of the AstroFit Program for Complementary Dark Matter Studies

Dissertation
zur Erlangung des Doktorgrades
des Fachbereichs Physik
der Universität Hamburg

vorgelegt von

Ngoc-Lan Nelly Nguyen

Hamburg 2012

Gutachter der Dissertation:	Prof. Dr. Dieter Horns
	Prof. Dr. Peter Schleper
Gutachter der Disputation:	Prof. Dr. Günter Sigl
	Prof. Dr. Georg Weiglein
Dekan der MIN Fakultät:	Prof. Dr. Heinrich Graener

Abstract

This doctoral thesis describes the development and application of the AstroFit program. Many studies have shown the existence of dark matter (DM), a mass component that constitutes over eighty percent of the entire matter in the Universe. From historical astrophysical evidence to latest reconstructions with sophisticated methods, the gravitational effect of DM can be shown, but its nature remains unknown. Many theoretical explanations aim at describing DM, for example as weakly interacting massive particles (WIMPs), within particular frameworks. The majority of these frameworks extend the existing standard model of particle physics (SM), so that new particles are added to the known set of elementary particles. One of these frameworks is the constrained supersymmetric standard model (CMSSM) that naturally introduces a DM candidate in form of the lightest supersymmetric particle (LSP).

Searches for DM particles are undertaken in three different ways. First, directly with fixed-target experiments that measure WIMPs coming towards the Earth with nuclei of the target material. Second, indirectly by reconstructing DM signatures in particle spectra of known particles observed with ground-based telescopes, space-borne satellites or balloon-borne experiments. And third, indirectly via direct production of DM at particle colliders such as the Large Hadron Collider (LHC) and energy reconstructions where missing transverse energy is presumably carried away by the DM particles. Global fit programs used in particle physics, such as Fittino, are designed to fit parameters of theories beyond the SM simultaneously that are in accordance with the experimental and observed data in order to probe models and constrain the parameter space. To explore complementarity in DM research, the AstroFit interface program has been developed to combine all available information from direct and indirect searches for DM as well as collider searches for new physics in such global fits. To demonstrate possible applications of AstroFit, a combined fit of the CMSSM has been performed with Fittino and AstroFit using results from direct, indirect and collider searches. The results and prospects from such a fit are illustrated. Moreover, it is shown how such a combination of data from complementary experiments and observations can constrain potential theoretical models even further.

Zusammenfassung

Diese Doktorarbeit beschreibt die Entwicklung und Anwendung des `AstroFit` Programms. Viele Studien weisen die Existenz von dunkler Materie (DM) nach. Hierbei handelt es sich um einen Massenbestandteil, der über achtzig Prozent der gesamten Masse des Universums ausmacht. Angefangen bei historischen astrophysikalischen Anzeichen bis hin zu Rekonstruktionen mit fortschrittlichen Methoden lassen sich die gravitativen Auswirkungen von DM darstellen, jedoch bleibt ihre Beschaffenheit unbekannt. Es gibt theoretische Erklärungen von DM, beispielsweise als schwach wechselwirkende massive Teilchen (WIMPs), innerhalb bestimmter Modelle. Die Mehrheit dieser Theorien erweitert das existierende Standardmodell der Teilchenphysik (SM), so dass neue Elementarteilchen den Kanon des SMs ergänzen. Eine dieser Theorien ist das 'constrained supersymmetric standard model' (CMSSM), welches in seinem Rahmen auf natürliche Weise ein geeignetes Teilchen einführt, das eine mögliche Erklärung für DM liefert.

Experimentell wird auf drei verschiedene Weisen nach DM gesucht. Erstens direkt durch sogenannte fixed-target Experimente, mit denen Wechselwirkungen zwischen WIMPs und Kernteilchen des Detektormaterials gemessen werden. Zweitens indirekt durch die Rekonstruktion von Signaturen dunkler Materie in Spektren bekannter Teilchen, welche mit Ballonexperimenten, Weltraumsatelliten oder bodengestützten Teleskopen beobachtet werden. Und drittens indirekt durch die Erzeugung von DM in Teilchenbeschleunigern wie dem Large Hadron Collider (LHC) und durch die Rekonstruktion der Energien, wobei fehlende transversale Energie den DM-Teilchen zugeordnet wird. Sogenannte 'global fit'-Programme ermitteln unter gleichzeitiger Berücksichtigung aller Parameter jene Parameterkonfigurationen einer Theorie jenseits des SM, die mit den gemessenen und beobachteten Daten übereinstimmen. So können theoretische Modelle erforscht und ihr Parameterraum zu beschränkt werden. Das Schnittstellenprogramm `AstroFit` wurde entwickelt, um alle vorhandenen Daten aus direkter und indirekter Suche nach DM sowie Daten über die Produktion neuer Teilchen in Teilchenbeschleunigern in solchen 'global fits' zu vereinen. Hierdurch wird zudem die Komplementarität auf dem Gebiet der DM-Forschung untersucht. Eine mögliche Verwendungsweise von `AstroFit` wird in einem kombinierten 'global fit' mit dem Programm `Fittino` gezeigt, in der Parametereinstellungen des CMSSMs mit experimentellen Daten aus direkter und indirekter Suche sowie Beschleunigerdaten ermittelt wurden. Ergebnisse und Perspektiven werden in dieser Arbeit dargestellt. Ferner wird gezeigt, auf welche Weise eine Kombination der Messdaten von komplementären Experimenten und Beobachtungen eine stärkere Einschränkung potentieller theoretischer Modelle ermöglicht.

Contents

Chapter 1

Introduction

Physics is a natural science that aims at describing all natural phenomena. Thus, the study of matter, the building blocks of the world surrounding us, has always been of great note. Astronomy, as one of the most ancient academical disciplines, has always been concerned with the formation and dynamics of the Universe. In parallel, the ancient Greek pre-Socratic philosophers such as Democritus had worked on a first description of particles building up its content. The first idea of smallest units of matter surrounded by empty space, i.e. vacuum, forming the world and all its substances, in other words the first atomic theory, was born.

Today, some two and a half centuries after Democritus, the understanding of matter has passed through many evolutions, eventually leading to the Standard Model of particles (SM) which has succeeded in describing most relevant phenomena in a broad energy range with a very high precision, proven in many experiments. New experiments continue to test the accuracy of the SM with increasingly precise measurements. Despite the great success of the SM in helping physics to achieve a deeper understanding of many processes of interaction and decay of matter, the SM fails to describe the physics of particles at very high energies. Furthermore, it is not a complete, neat and simple theory that can be reduced to fundamental principles, but remains a conglomerate of theorems.

Astronomy, as one of the disciplines of physics, has itself evolved in parallel to particle physics with ongoing observational instruments, enabling the survey of wide parts of outer space. These observations have identified one of the largest mysteries of the study of matter: "dark matter" (DM). This refers to a large amount of non-luminous and non-absorbing matter, accounting for over eighty percent of the entire matter in the Universe, that can be neither observed directly nor described within the SM of particle physics and whose nature remains presently unclear. Astroparticle physics, the union of astronomy and particle physics, has together with cosmology become a highly interesting field of research, addressing cosmic rays, gravitation and the nature of dark matter among many other topics. DM will be the main topic of investigation in this work. In the following, I will give a short outline of this thesis before describing the unique contribution of my work.

Chapter 2 will briefly explain how particles and particle interaction are described by the SM. If not stated otherwise, units are given in $\hbar = 1$ and $c = 1$ throughout this work. I will also address the shortcomings of the SM, not only in terms of explaining DM in terms of particles, but also the lack of explanation for phenomena such as gravity, neutrino masses and the hierarchy problem of particle physics. These unsolved limitations of the SM are a basis for the choice of the "Constraint Minimal Supersymmetric Standard Model" (CMSSM) as a theoretical framework. Subsequently, I will introduce the observational evidence for dark matter in Section 2.2, ranging from historical astrophysical observations to mass reconstructions from a method called gravitational lensing to latest cosmological measurements and simulations of structure formation with N-body simulations. All these indications form preconditions for particle DM candidates, which I list at the end of Section 2.2. Following these conditions, I will describe the methods for DM detection and observation via direct and indirect channels. Instruments for direct detection of DM particles are located underneath the Earth to minimize background events. Ground-based and space-based telescopes as well as balloon-borne experiments strive to detect secondary particles from DM annihilation, so that signatures of DM can be found in particle spectra. At particle colliders, a production of DM particles would be possible from the high-energy particle collision. DM particles would leave no direct trace, but could occur in the event reconstruction carrying away missing transverse energy. According to these observation opportunities, I will present a selection of theoretical models that address the DM problem. I will justify the choice of the CMSSM once more by showing that the DM particle candidate within the model, the neutralino as the lightest supersymmetric particle (LSP), is potentially detectable with state-of-the-art detection methods. This allows a complementary approach towards experimental observation and detection of such a particle. This work is singular in combining all three detection methods for DM, direct detection, indirect detection and collider production concurrently.

Section 3 proceeds with the introduction of global fits as a method to test a theoretical model by confronting it with data from experiments and observation. In global fits, model parameters of a model beyond the standard model of particle physics (BSM) are fit simultaneously to experimental data to find the best fit point of parameter space. The term 'model' is mistakable in this context, as both a BSM theory can be referred to as a model as well as a specific set of parameters of one such theory (as in 'benchmark models'). I will therefore use the word 'model' for BSM models, especially for the CMSSM, and refer to a specific set of parameters either as 'benchmark model' or 'point in parameter space' if it is not unquestionably clear from the context. I will also explain the relevant techniques of global fits in general and describe the specific methods used for this study.

An explicit description of `AstroFit`, the stand-alone program that I have developed together with Torsten Bringmann and Nils Plambeck, will be given in Section 3.4. `AstroFit` is a platform that brings together all astrophysical information that potentially constrain BSM models. As such, it is easy to extend the program and add new data. It is designed to easily interface with global fit programs, so that com-

parable studies are enabled. The design is user-friendly, so that the potential user can add astrophysical information from text files without interference with the underlying code. A release of the full program is planned for the future, once the functions for all currently relevant observation channels are implemented.

In Chapter 4, I will show and discuss the results from a combined fit with the fit program `Fittino` and `AstroFit` as an example for the usability of the latter. I will illuminate the CMSSM fit in terms of DM by pointing out the influence of individual observables and indicating the relation between particular ones, confirming the complementary behavior of observables from different detection methods and the potential by bringing together the whole set of available experimental and observational information. Finally, I will conclude with a summary of the results from the CMSSM fit with respect to the DM question in Chapter 5.

In the frame of this thesis, I have contributed significantly to the creation and development of `AstroFit` and coordinated the project. I have implemented the subroutines responsible for the calculations in the sector of direct and indirect detection within `AstroFit` as well as all data from experiments and observation currently usable by the program. I have also set up the interface between `AstroFit` and the global fit program `Fittino` as a first example how `AstroFit` can be used. In this context, I have tested the setup with respect to technical and physical aspects. Eventually, I have analyzed the results from a global fit of the CMSSM under DM relevant considerations, using `Fittino` and `AstroFit` in combination. The status of the `AstroFit` program is reported in Section 3.4, while the result of the fit in terms of DM is described in Chapter 4. My work is reported in Nguyen et al. [2012] and Bechtle et al. [2012].

The distinctive character of my work is manifested in two aspects. First, the creation of the `AstroFit` program is unique by itself. It is a program that facilitates the universal approach in DM research by offering a complete tool that adds astrophysical information to global fits without programming effort, as all programming steps are already done entirely within the `AstroFit` program. In this way, anyone working with global fits has the opportunity to include `AstroFit` and thereby extend the current set of observables of a global fit according to requirement. And secondly, I present an analysis of a CMSSM fit with combined information from direct and indirect searches for DM with astrophysical instruments and information from collider production, which has not been done before. The results show that the combination of information from different research areas connected to the study of DM or the extension of the SM is able to constrain the parameter space of the CMSSM even further, therefore demonstrating that such a complementary approach is trend-setting, meets future requirements for solving the DM problem, and helps constrain BSM models.

Chapter 2

Dark Matter from a Complementary Point of View

2.1 Quantum Field Theory and the Standard Model of Particles

Quantum mechanics revolutionized physics by delivering a complete theory to explain physical processes and states at atomic scales [$\sim O(10^{-10}$ m)] and taking physics from a deterministic discipline to a science of exact probabilities. Special relativity established an interpretation of particle behavior at high velocities, which is different from classical mechanics. It allows an understanding of the equivalence of matter and energy with the formula $E = mc^2$, thereby describing the behavior of particles and interactions of matter at high energy scales, with particles moving with a speed close to that of light ($c \approx 3 \times 10^8$ m/s). Quantum field theory (QFT) is the theoretical framework that combines both quantum mechanics and special relativity, striving for a thorough description of the physics of particles, their motions and interactions, at all energy scales (see e.g. Peskin and Schroeder [1995], Zee [2010]). In each field of physics, a formalism consisting of fundamental equations exists or is aspired, from which all motion equations can be derived. This formalism is given by the Lagrangian density in many frameworks and can be applied to the problems addressed in this thesis. Taking into account all known fundamental particles and their interactions, the knowledge of the Lagrangian is expressed in the standard model of particle physics (SM), as revised for example in Cottingham and Greenwood [2007]. It is an effective theory that precisely describes and predicts particle behavior, with some exceptions that mark its failure to be a complete theory of fundamental interactions. For example, the theory of general relativity, and therefore gravity, cannot be incorporated into the SM. Therefore, although all other fundamental interactions are explained in QFT, the SM falls short of explaining gravity. Despite its shortcomings, the SM remains the phenomenological basis of fundamental particle physics. A thorough review of particle physics is for example given in Beringer et al. [2012]. The short description below is based on Griffith [2010].

All particles can be uniquely characterized by their quantum numbers which provide information on their symmetry behavior. Particles with identical quantum num-

bers are indeed identical, that is to say indistinguishable. In the SM, there are in principle three kinds of elementary particles: leptons, quarks and mediators (i.e. gauge bosons). While leptons and quarks form fermions, matter of our daily life, mediators are bosons, quanta of an interaction field and force carriers.

Leptons (Greek: light particle), such as the electron, are particles with lepton number 1 and charge $\pm$ 1 or 0. They can be classified into three generations, in which case the lepton number can be divided into electron, muon and tau number. The electron and electron neutrino would have electron number 1, the muon and muon neutrino share muon number 1, and tau and tau neutrino have tau number 1. Their antiparticles are called antileptons and have the same quantum numbers sign-reversed. So as an electron would have charge -1 and electron number $+1$, the positron, its antiparticle, would have charge $+1$ and electron number -1.

Quarks are particles that only occur naturally in compounds of two or three. A compound of two quarks, or more precisely of a quark and its antiquark, is called a meson (Greek: particle of medium weight), whilst three Quarks add up to a baryon (Greek: heavy particle), e.g. the proton or the neutron. Quarks come in six different flavors and can also be separated into three generations. They have charge $-1/3$ or $+2/3$, and their antiparticles share the same number of charge, flavor and generation, only with opposite signs. Furthermore, each quark exists in three different color charges, making the total number of quarks 36.

The four fundamental forces that act between particles are the strong, weak, electromagnetic and gravitational force. In the concept of QFT, each force operates through an interaction field with force-carrier particles. These particles are called mediators and are classified as bosons. The mediators of the strong force are gluons, the mediators of the weak force are W and Z bosons. The electromagnetic force is mediated by photons, whereas for gravity the predicted mediator is the graviton which has not been found yet (see problems of the SM in Section 2.1.2). Bosons are particles of integer spin, the quantum number for the internal angular momentum of a particle, as opposed to leptons and quarks with half-integer spin. This difference leads to highly different behavior of the particle itself and in its theoretical description. The interactions between particles are described by fields in QFT. A figure of the SM particles is depicted in 2.1.

2.1.1 The Lagrangian

In classical mechanics, the equations of motion could be derived from the Lagrangian of a system.

$$L = T - V \,, \tag{2.1}$$

where T denotes the kinetic energy of a particle moving through a potential V. By formulating the Euler-Lagrange equations, the equations of motion of the particle can be derived. In the simplest case of one single particle moving in one dimension, the equation would give:

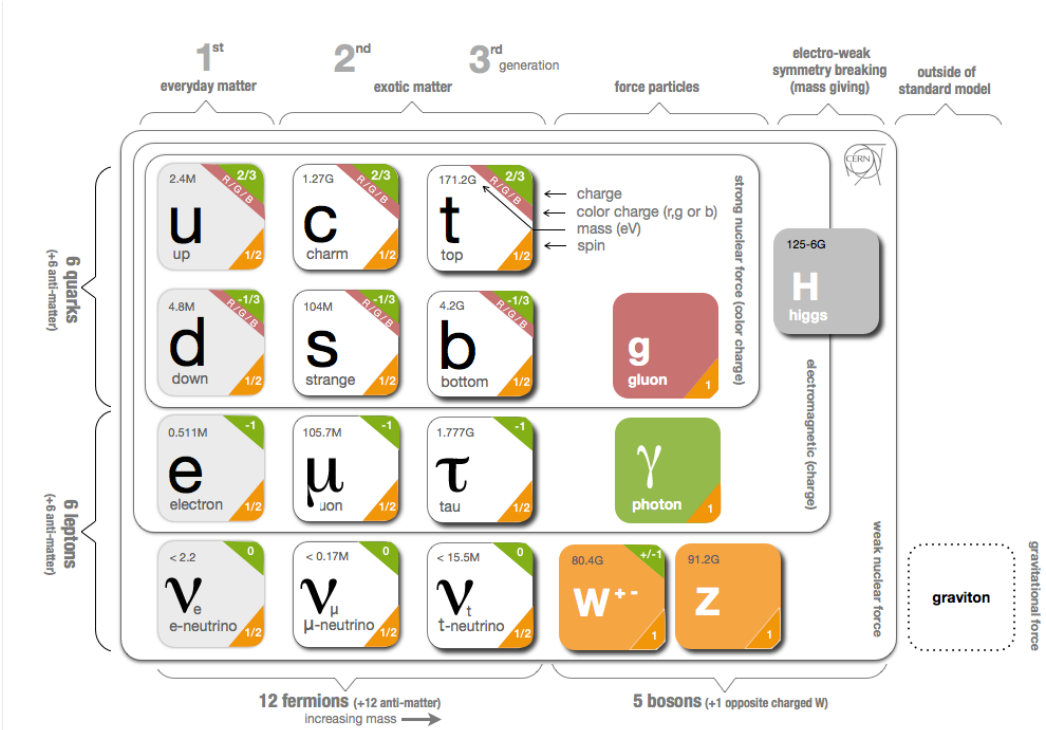

Figure 2.1: Particles of the SM and the predicted graviton and Higgs boson. The mass, spin, electric charge, color charge and interactions are given as labeled. The first-generation particles make up baryons, matter experienced in everyday life. Figure taken from iSGTW [2012].

$$\frac{\mathrm{d}}{\mathrm{d}t}\frac{\partial L}{\mathrm{d}\dot{x}} - \frac{\partial L}{\partial x} = 0\,. \tag{2.2}$$

The action is the integration of the Lagrangian with respect to time.

$$S = \int \mathrm{d}t L\,. \tag{2.3}$$

The action is always minimal, meaning that all other paths between initial and final position would result in a higher action. In QFT, as in any higher theory extending a classical one, these principles still hold and are applied to fields, which are functions of spacetime $\phi(x,t)$. In terms of fields, the Lagrangian density $\mathcal{L}$ is more often referred to. It is related to the Lagrangian in this way (see McMahon [2008]):

$$L = T - V = \int \mathcal{L}\mathrm{d}^3x\,, \tag{2.4}$$

with $\mathcal{L}$ depending usually on the fields and their first derivatives

$$\mathcal{L} = \mathcal{L}(\phi, \partial_\mu \phi)\,, \tag{2.5}$$

which makes the action

$$S = \int \mathrm{d}t L = \int \mathcal{L}\mathrm{d}^4x\,, \tag{2.6}$$

and the Euler-Lagrange equation of motion as a field equation for a field ϕ takes the form

$$\frac{\partial \mathcal{L}}{\partial \phi} - \partial_\mu \left(\frac{\partial \mathcal{L}}{\partial [\partial_\mu \phi]} \right) = 0 \, . \tag{2.7}$$

The Lagrangian is an important concept of both classical and quantum field theory, especially in the context of symmetries. If a symmetry is inherent to a system, transformations according to the particular symmetry leave its Lagrangian invariant. The Lagrangian of the strong interaction, quantum chromodynamics (QCD), remains invariant under local SU(3) color gauge group transformations. The electromagnetic and weak interaction, described by quantum electrodynamics (QED), remain invariant under SU(2) $\times$ U(1) group transformations, i.e. isospin and hypercharge gauge tranformations (see Ellis [2012]). The gauge group of the SM, which does not include gravitational interactions, is therefore SU(3)$\times$ SU(2) $\times$ U(1). A Lagrangian from which to derive all dynamics of quantum states and fundamental field needs to stay invariant under its gauge group transformations. The construction of a Lagrangian of the entire SM particles and their interactions requires kinetic terms defining the motions of particles, mass terms to represent the particle masses, and coupling terms typifying the couplings of each interaction field. A term with 18 free parameters would be necessary. An explicit description of the SM Lagrangian can be found in Peskin and Schroeder [1995].

One possible extension of the SM is supersymmetry (SUSY), a symmetry between the spin of particles, which will be introduced in Section 2.3. SUSY adds a new symmetry to the SM Lagrangian, creating a new set of particles identical to the SM particles save for their different spins. Adding a new symmetry is just one way of modifying the SM Lagrangian in order to solve existing weaknesses of the latter.

2.1.2 Shortcomings of the SM

Though the SM successfully and accurately describes physics at low energy scales, there are several problems that cannot be solved within the SM. First of all, there is no explanation for the Universe's entire DM amount in the SM. The only particles able to suit as a DM candidate by being stable, neutral and not coupling to photons are neutrinos. However, neutrinos do not fulfill the requirement of being non-relativistic in the early Universe, and they are not massive enough to match the relic abundance and make up the DM content of the Universe (Feng [2010]). Neutrinos may account for a hot dark matter component, but a different particle candidate is needed to explain the larger cold dark matter (CDM) content. This will be explained further in Section 2.2 and Section 2.3.

Furthermore, it is not clear why neutrinos should be massless as predicted from SM. In fact, neutrinos do have mass, as experiments with neutrino flavor oscillations indicate (see e.g. Beringer et al. [2012]). Nevertheless, their mass would need to be relatively small [$O(< 20\text{eV})$], compared to that of other SM particles due to many constraints, e.g. from cosmology. Yet within the SM, there is no mechanism giving

mass to neutrinos, and neutrino masses have never been measured directly.

Another problem concerning the mass of particles is the hierarchy problem. In general, hierarchy problems refer to the large divergence between fundamental parameters, i.e. masses or couplings, described by a Lagrangian and the measured value of these parameters. For example, the hierarchy problem is related to the question why the weak force is unnaturally stronger than gravity. Also, the cosmological constant deduced from the SM is too large and is not consistent with the cosmological ΛCDM model (see 2.21). In terms of the Higgs boson, the former bounds on its mass and the possibly measured value of $m_h \approx 126$ GeV at the LHC are far off the prediction of the Higgs mass having the magnitude of the Planck mass, which is

$$m_p = \sqrt{\frac{\hbar c}{G}} \approx 10^{19}\mathrm{GeV/c^2}\,, \tag{2.8}$$

with the reduced Planck constant $\hbar$, the speed of light c and the gravitation constant G. This is an enormously high mass of 22 μg, so that in comparison

$$m_h \ll m_p\,. \tag{2.9}$$

This gives rise to the question why the observed Higgs mass is so much smaller than the expected mass of Planck mass unit. The effect can be explained by self-energy, the particle's contribution to its effective mass due to interactions within a system (e.g. in electrostatics, self-energy is required to bring the charge from infinity). With renormalization, the total effective mass of a particle can be described. It differs from its vacuum mass or energy by the self-energy distribution and can be expressed with quantum corrections by virtual loops (see e.g. Feng [2010]).

$$m_h^2 = m_{h0}^2 + \Delta m_h^2\,, \text{ where} \tag{2.10}$$

$$\Delta m_h^2 \sim \frac{\lambda^2}{16\pi^2}\int^{\Lambda}\frac{\mathrm{d}^4 p}{p^2} \sim \frac{\lambda^2}{16\pi^2}\Lambda^2\,. \tag{2.11}$$

Even so, this leads to the question why the constants of nature are so incredibly fine-tuned to describe an effective Lagrangian, suggesting that there are mechanisms involved that have not been understood yet.

There are other problems with the SM that are however not directly related with the DM problematic of this study and therefore not mentioned in this work. In reminiscence, the most relevant deficiencies of the SM can be itemized:

- There is no quantum theory of gravity, although gravity is considered to be one of the four elementary forces. Nor has a particle been measured that could be the quantum of the gravitational field, i.e. the graviton. Even though QFT succeeds in unifying quantum mechanics and special relativity, it thereby fails to include Einstein's theory of general relativity.

- The process that gives mass to particles is not fully understood yet. It is assumed to be the Higgs mechanism, but whether there is only one Higgs boson or if the Higgs particle is just a compound of different states has yet to be experimentally proven. Additionally, neutrino masses remain unexplained in the SM.

- In QCD, no violation of the CP-symmetry (as commonly known for QED) has been found by experiment. However, the Lagrangian allows CP-violating terms in principle. This is a concept in some BSM models, one of them leading to propose particles called axions as DM candidates (see Section 2.3). This phenomenon is another fine-tuning problem in the SM.

- The origin of the difference between matter and antimatter, i.e. the domination of the Universe's matter content over its antimatter content, cannot be properly explained within the SM.

- The Lagrangian of the SM has 18 parameters, making it lengthy and therefore different from other fundamental equations, for instance the Maxwell equations of electromagnetism. This could hint that the SM lacks additional information to be a complete theory which would then resolve the inelegance of the SM Lagrangian.

- In accordance to the above, it remains unclear which exact number of elementary particles and species or families of particles exist in reality and how their mixing can be described.

- The unification of the fundamental interaction is not constituent in the SM. Grand Unification Theories (GUT) are not a necessity of nature, but rather a motivation to understand these interactions as manifestations of one underlying unitary force. Such a unification is thus predicted by many GUT theories and string theories, and an extrapolation of the three gauge couplings at LEP yielded a point at $\approx 2 \times 10^{16}$ GeV where the SM gauge couplings would meet (see Baer and List [2012]).

- And most important for this thesis, the SM does not offer a particle candidate that fulfills all criteria necessary from observations to explain DM in the Universe (see Section 2.2). Correspondingly, there is no explanation for the phenomenon of dark energy either.

In essence, these deficiencies of the SM lead to the assumption that the SM is an effective theory, yet there should be a more fundamental theory behind all matter and interactions in the Universe. For further reading on the SM and its discrepancies to the behavior of Nature, see Ellis [2012] and Shears [2012]. A complete BSM theory needs to be able to solve the problem of DM, and furthermore it should be able to address these problems in a clarifying way. From the DM point of view, supersymmetric extensions of the SM offer a satisfying solution. These will be described in Section 2.3.

2.2 Observational Evidence for Dark Matter

2.2.1 Historical Background

Throughout its history, the observational evidence for DM has grown progressively more precise, substantiating the fact that there must be some matter component not yet described by known particles with characteristics that made it evident to christen it 'dark matter'. Overviews are given in Einasto [2009], Bergstrom [2000], and Bertone et al. [2005], for example. In the 1920s, James Jeans and Jacobus Kapteyn studied the dynamics of the Milky Way galaxy with contradicting conclusions about the necessity of a DM component in order to explain the movement of stars near the galactic plane. When Fritz Zwicky reconstructed the velocity dispersion of galaxies in the Coma cluster in the 1930s, he demonstrated that a lot more mass would be needed to accomplish such behavior than the visible mass can supply. Following his work, other physicists reconstructed the rotation curves of spiral galaxies, again discovering that a much larger mass component would be necessary to achieve such flat rotation curves as observed (see Figure 2.2).

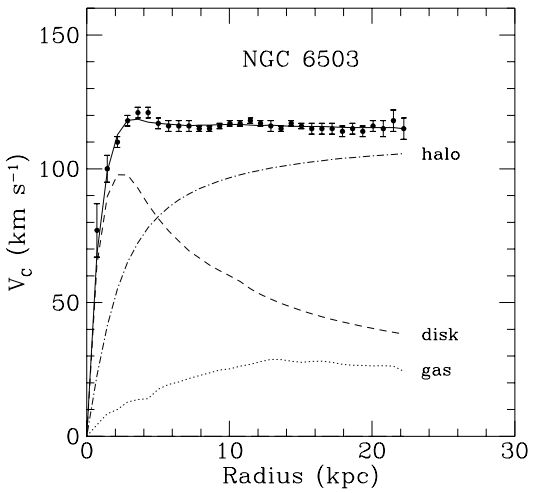

Figure 2.2: Rotation curve for the spiral galaxy NGC6503 as shown in Kamionkowski [1997]. While the solid line, points and error bars represent the circular rotation velocities as a function from the distance from the center of the galaxy as in fact measured, the dashed and dotted lines are the rotational velocity as theoretically expected from the inherent gas and disc. The dashed-dotted line shows the missing component which needs to be replenished by a DM component.

The rotation curve of a galaxy can be computed as the equation of the centrifugal force balancing the gravitational force:

$$\frac{mv^2}{r} = G\frac{m_1 m_2}{r^2}\,, \tag{2.12}$$

with the distance r from the center of the galaxy, the velocity component v, the Newton's constant of Gravity G, the masses involved in the center and at the point of

measurement, i.e. the halo m_1 and m_2, and the linear velocity magnitude derived from

$$v = \sqrt{\frac{Gm_1}{r}} \,. \tag{2.13}$$

Assuming the core of the galaxy to hold the majority of the galaxy mass, the speed at greater distance to the core would follow Newton's law and decrease with $v \sim r^{1/2}$. Instead, the speed was found to be constant even at high distances to the galaxy's center, suggesting that the halo of the galaxy adheres the majority of the galaxy's total mass. Since the luminous matter from the observed disk and gas does not suffice to achieve the measured rotation curves, a DM component was introduced to explain this unpredicted behavior.

2.2.2 Astrophysical Evidence from Gravitational Lensing

Gravitational lensing describes the effect that matter, i.e. energy density, has on light. The higher the mass density of a certain point in space, the greater the deflection of light in this area. Due to this effect, different optical phenomena can occur and be observed on Earth. The effects can be classified as strong lensing, weak lensing and microlensing. Strong gravitational lensing describes the effect that light of the same galaxy coming towards Earth is deflected by a high mass density between the galaxy and the Earth, enabling the observation of two or more images of the same galaxy. Microlensing is basically the same effect. The image of the ray of light, coming from a distant galaxy, is deflected. In this case, instead of multi-images occurring in the observed sky, the images are projected into a visibly indistinguishable part of the sky, so that the images overlay, making the source seem brighter than it would if the light had not been deflected. Weak gravitational lensing does not produce more than one image of the light coming from the galaxy, but it still has the effect of stretching or magnifying the image. A review on gravitational lensing in the context of DM is given in Challinor [2012].

Making use of this knowledge, the energy density lying between the Earth and the source of the light can be well estimated. The result strengthens the non-baryonic DM hypothesis. From the effect of gravitational lensing, in some regions a conspicuously higher mass is expected than is given by the available known baryonic mass. The most intriguing observation in connection with gravitational lensing is the observation of the galaxy cluster 1 E 0657-558, known as "the bullet cluster". Technically, the "bullet cluster" refers to one of the two colliding galaxies in this formation. In studies in the microwave regime, it can be shown that there is reason to assume that the two galaxies are DM dominated in order to collide in this particular way (see Clowe et al. [2006]). When reconstructing the event, it can be seen that most of the galaxy parts do not interact with one another at all. The small parts of baryonic matter interacting with each other can be seen in red in Figure 2.3, while the blue part resembles the DM content of the galaxies just passing through.

The "bullet cluster" has been used as DM laboratory for many studies under the assumption of the DM content. Even with a most conservative approach, not predict-

Figure 2.3: Image of the ”bullet cluster” as a reconstruction from observations with the Chandra X-ray telescope and the optical Magellan telescope and Hubble Space Telescope. The concentration of mass was determined with gravitational lensing. In this image, the baryonic matter part is shown in pink. It is slowed down by the impact of the collision. The higher distribution of matter, depicted in blue, is separated form the baryonic part, because it is not affected by the collision. As DM does not interact with gas and baryonic matter except via gravity, the blue part can be well interpreted as DM. Image taken from Chandra X-Ray Observatory [2009]. Credit: X-ray: NASA/CXC/CfA/M.Markevitch et al.; Optical: NASA/STScI; Magellan/U.Arizona/D.Clowe et al.; Lensing Map: NASA/STScI; ESO WFI; Magellan/U.Arizona/D.Clowe et al.

ing the content of DM, it is nonetheless a useful observation that can provide strong experimental limits. The DM hypothesis is strengthened by further observations of other galaxy clusters showing similar behavior, for example MACSJ0025.4-1222 (Bradac et al. [2008]) and “Pandora’s cluster”, Abell 2744 (Merten et al. [2011]).

2.2.3 Cosmological Evidence

Observations of anisotropies in the cosmic microwave background (CMB) radiation, large-scale structures of galaxies, baryon acoustic oscillations and type Ia supernovae add cosmological evidence for DM supplementary to the already mentioned astrophysical ones. These evidences are closely related to Big Bang theories and structure formation in the early Universe, which can be computed with N-body simulations. These lead to the ΛCDM model, the highly favored standard model of cosmology, which adds most relevant constraints on the particle nature of DM (see e.g. Bertone et al. [2005]). It infers the necessity of cold dark matter (CDM) and a cosmological constant Λ and gives explanation to cosmological phenomena, such as the expansion and specific structure of the Universe. Assuming a bottom-up scenario of the evolution of the Universe, the early Universe right after the Big Bang was largely homogeneous, yet already with small primordial radiation fluctuations, i.e. fluctuations of the energy density, which led to the development of small clumps first and galaxies and galaxy clusters with time, while the Universe expanded. A bottom-up scenario is in agreement with observations of large-scale structures. Redshifts from faraway galaxy clusters give exact information on the expansion of the Universe, visible for example with the Hubble Space Telescope. For this inflation theory to hold true and for structures to have formed in this manner, far more mass would have been necessary than the visible baryonic mass. With the COBE and the WMAP satellites (NASA [2011], Komatsu et al. [2011]), fluctuations of the cosmic microwave back-

ground can be measured. In N-body simulations, adding baryon acoustic oscillations from different sky surveys, e.g. SDSS (Skielboe et al. [2012]) to the measurement of WMAP, the structure formation of the Universe can be computed explicitly.

While astrophysical evidence for DM only introduces the necessity for additional mass in the Universe, these cosmological indications give rise to characteristic properties that DM particles must fulfill, making WIMP candidates more attractive than others (Jungman et al. [1996]).

In the early Universe with high thermal energies, DM particles could rapidly be created or destroyed in pairs. Two DM particles could therefore annihilate into SM particles, for example fermions or vice versa,

$$\chi\bar{\chi} \rightarrow f\bar{f} \,, \tag{2.14}$$

the bar denoting the according antiparticle. If the DM candidate is neutral, as in the CMSSM, it can be assumed that χ is a Majorana particle and therefore its own antiparticle. With the expansion and cooling of the Universe, the number density of DM particles decreased rapidly, until the particles were too dispersed to self-annihilate. They could no longer be created from two fermions, or in fact from any pair-production process either, because the thermal energies became too low, leaving the mass density of these particles freeze out at one point, meaning that there was no significant change in the number density hereafter. The relic abundance of a DM candidate can be obtained by solving the number density Boltzmann equation (e.g. Perkins [2003]):

$$\frac{\mathrm{d}n}{\mathrm{d}t} = -3\frac{\dot{R}}{R}n - \langle\sigma v\rangle(n^2 - n_0^2) \,. \tag{2.15}$$

According to WMAP measurements, the Universe is flat in Euclidean shape within small errors, and there is only a small window for the total mass density of the Universe, which can be expressed in the ratio

$$\Omega_{total} = \rho_{total}/\rho_{crit} \,, \tag{2.16}$$

with the critical density

$$\rho_{crit} = \frac{3H_0^2}{8\pi G_N} = h^2 \times 1.9 \cdot 10^{-29} \mathrm{g\ cm^{-3}} \,, \tag{2.17}$$

and the Hubble constant $H^0 = 70.4^{+1.3}_{-1.4}\,\mathrm{km/(Mpc\ s)}$ and the scale factor for the Hubble expansion rate $h = 0.704^{+0.013}_{-0.014}$ (see NASA [2011]). For a flat Universe, the energy content of the Universe needs to fulfill the following equation:

$$\Omega_{total} = \Omega_b + \Omega_{\mathrm{CDM}} + \Omega_\Lambda \approx 1 \,, \tag{2.18}$$

stating that the matter content of the Universe must be made up of baryonic matter, dark matter and dark energy. The latter is also referred to as the cosmological constant Ω_Λ, which is responsible for the acceleration of the expansion of the Universe.

Cosmology fits with latest WMAP7 data give the following parameter set for a spatially flat ΛCDM model (NASA [2011], Komatsu et al. [2011]), matching equation 2.18:

$$\Omega_b h^2 = 0.0225 \pm 0.0006 \tag{2.19}$$

$$\Omega_{\mathrm{CDM}} h^2 = 0.112 \pm 0.006 \tag{2.20}$$

$$\Omega_\Lambda = 0.73 \pm 0.03 \tag{2.21}$$

In addition to the information on the DM content of the Universe as in Equation 2.21, measurements and studies reproducing structure formation show that not just the DM content, but also the baryonic matter content is given a narrow window. Reconstructions using the abundances of helium, deuterium and lithium suggest that the baryonic matter fraction can only lie within a small bound as given by Equation 2.20. Therefore it can be concluded that the DM content needs to be non-baryonic and that baryonic DM candidates alone cannot fulfill the requirement to be the DM imposed by cosmology making up for the relic abundance of DM in the Universe, and that it needs a non-relativistic, non-baryonic, massive DM candidate. If structure formation can be explained as described, DM particles need to be thermal relics, and the abundance of DM today would be set by its annihilation cross-section $\langle \sigma v \rangle$ (Kuhlen [2010]).

$$\Omega_\chi h^2 = \frac{3 \times 10^{-27} \mathrm{cm}^3 \mathrm{s}^{-1}}{\langle \sigma v \rangle} \tag{2.22}$$

A candidate that would match this requirement is a weakly interacting massive particle (WIMP) with the properties of being neutral, stable, non-relativistic and only interacting via the weak and gravitational force (see e.g. Hooper and Baltz [2008], Jungman et al. [1996]). The dependence of the relic density of CDM on the WIMP annihilation cross-section $\langle \sigma v \rangle$ and the evolution of the early Universe is depicted in Figure 2.4. In thermal equilibrium, WIMPs could equally annihilate and be produced, so that the number of WIMP particles remains unchanged. As the Universe expanded, the temperature decreased, so that WIMPs could still self-annihilate, but could not be produced from other particles anymore, because the energy was no longer sufficient for such a production process. This resulted in the decrease of the total WIMP number. With the continuing expansion of the Universe, the WIMPs were finally so dispersed that self-annihilation did not occur any longer and the number of WIMPs remains basically unchanged. Depending on the self-annihilation cross-section $\langle \sigma v \rangle$ of such WIMPs, the relic density is higher if $\langle \sigma v \rangle$ is small and lower if $\langle \sigma v \rangle$ is larger.

Finally, criteria that a successful DM candidate must fulfill can be formulated (see also Bertone [2010]).

- It needs to be massive [O(100 GeV)] as to reproduce the necessary mass in the Universe and the observed amount of DM from experiments.
- Closely related to the last point, it needs to have an annihilation cross-section that naturally produces the correct relic density today.

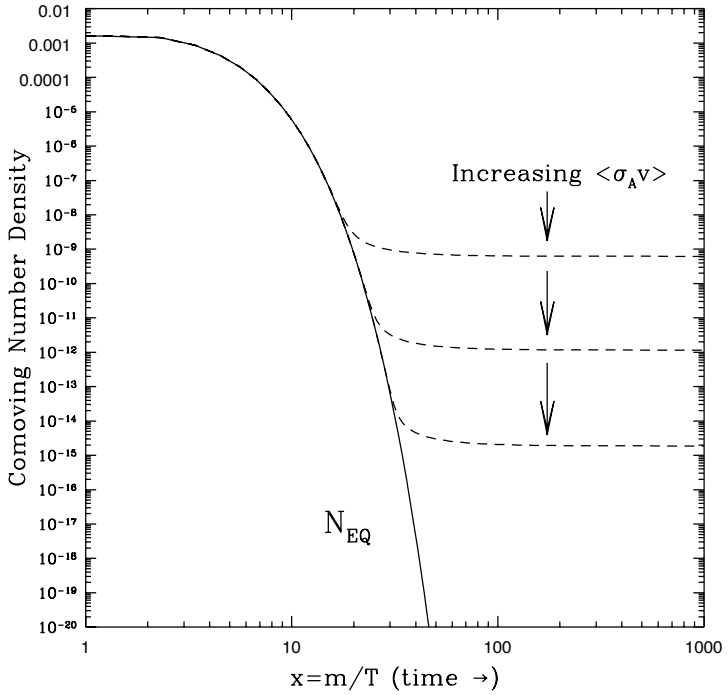

Figure 2.4: The comoving number density of WIMPs is shown on the y-axis, while the x-axis is an expression for progressing time in the early Universe in terms of mass per temperature, as time is inverse proportional to the energy density of the expanding Universe. The solid line depicts the decreasing number of WIMPs as a relic from the stage of thermal equilibrium until a WIMP freeze-out is reached, when WIMP self-annihilation ceases due to the high dispersion. The remaining number of WIMPs depends on the annihilation cross-section of the WIMPs. Further explanations are given in the text. Figure from (Jungman et al. [1996]).

- It needs to be dark, that is not coupling to photons, and hence not interactive via the electromagnetic force.
- It needs to be neutral likewise, so it does not interact with charged particles electrically and bind to nuclei.
- It needs to be non-baryonic, as the baryonic matter content cannot make up for the DM content in ΛCDM theories.
- It needs to be cold, i.e. not relativistic from the beginning of the Universe, for the observed structure formation.
- And eventually, it needs to be stable or long-lived with very weak interactions to have been produced at the Big Bang and in order to match the relic abundance.

Putting together these conditions, a WIMP would be a prospective DM candidate. In search for particle candidates that suit these requirements, both theories as well as restrictions from experiments have been taken into account. Theories are designed to offer solutions to the DM problem, ideally embedded in a model solving other

existing questions of particle physics in addition. Opposed to that, experiments are given the task to restrict those models gradually further until they can be safely ruled out, or in the best case, allow proof for a theory.

2.3 Dark Matter Models and Candidates

In Section 2.2, I have shown what conditions a DM candidate needs to suffice. While there are theoretical models, introducing a sole DM candidate without embedding it into a wider theory BSM, as in Maverick DM models (Beltran et al. [2010]), most theoretical DM candidates are part of a whole theory. Such models aim at modifying existing theories in one or more sectors and thereby solving puzzles of current models by introducing solutions via different particles, mechanisms, symmetries, dimensions or other modifications. To justify my choice of a supersymmetric extension of the SM of particles, I will introduce some of these theories, however only with a brief description that does not give justice to the full picture. Reviews of DM candidates are given for example in Bertone et al. [2005], Feng [2010] and Bergstrom [2012].

2.3.1 Overview of Dark Matter Models and Candidates

Mainly, theories concentrate on particle candidates outside the particles of the SM. Yet, there are theories that are motivated otherwise. From astrophysical motivations, massive compact halo objects (MACHOs) could account for some DM contributions (Paczynski [1986]), but if these objects exist, they could only make up some minor parts of the Universe's DM content, because they cannot explain structure formation from the early Universe. Neutrinos and sterile neutrinos are also possible DM candidates. As light particles with masses $m_\nu > 2$ eV, they do not fulfill the condition of being non-relativistic in the early Universe and can therefore not saturate structure formation and the measured CDM abundance if they were the only DM particles. Nevertheless, neutrinos and sterile neutrinos could constitute a hot or warm dark matter part, respectively (see Feng [2010]).

Without introducing a new particle physics model, one could assume that gravity has not been understood at very large scales, and a modification of Newton's law of gravity would adjust the present excess of currently unknown matter. Such theories of Modified Newtonian Dynamics, called MOND (Milgrom [1983] and Bekenstein [2004]), could explain the measured rotation curves, but they do not address to the set of other evidence for DM (see Scott [2011]). It is highly difficult to accommodate the cosmological evidence for DM and reconstruct phenomena as the "bullet cluster" or other gravitational lensing effects without introducing a new particle eventually.

Particle candidates that do address DM issues from particle and astroparticle physics as well as cosmology are therefore more attractive. Furthermore, there are theories that naturally contain a DM candidate. That is to say, these theories have not been constructed solely for the purpose of solving the DM problem, but are self-contained and conveniently offer a particle candidate for the DM. WIMPs and axions are particles that fall under this category (Kamionkowski [1997]). Therefore, I will list three theories with such a DM particle: the theory of Universal Extra Dimensions (UED), the Peccei-Quinn symmetry and the theory of supersymmetry (SUSY).

UED is a theory introducing another spatial dimension and a new conservation,

i.e. the conservation of the Kaluza-Klein parity (Cheng et al. [2002]). UED has been introduced independently from the DM motivation, yet it offers a WIMP candidate for DM with the lightest stable Kaluza-Klein particle (Servant and Tait [2003]). Unfortunately, detection prospects are rather bad, as these particles are impossible to observe directly (Melbeus et al. [2012]).

Axions, particles of $\sim 10^{-6}$ to 10^{-4} eV, as DM candidates are motivated by a different extra symmetry. By adding the Peccei-Quinn symmetry (Peccei and Quinn [1977]), the strong CP-problem of the Standard Model can be solved and, similar to the case of UED and SUSY, a DM particle is introduced inadvertently. The axion is a self-interacting CDM candidate that could have been produced at the Big Bang and that interacts with other particles very weakly. There are ongoing searches for axions (see e.g. Ehret et al. [2010], Chou et al. [2008], Sanchez-Conde et al. [2010]).

Indeed, the candidates best matching all evidence from DM observations with observation prospects are axions and supersymmetric DM. The latter will be explained in the following Section.

2.3.2 Supersymmetric Dark Matter Models

SUSY is a concept of another symmetry of the Lagrangian that links bosons to fermions, supposing that there are equal numbers of fermion and boson states. This would mean another set of particles equivalent to the existing SM particles, except with a spin different by $\frac{1}{2}$. A detailed SUSY review is given in Martin [1997], and SUSY DM is thoroughly described in Jungman et al. [1996]. The supersymmetric partner (hereafter superpartner) of a lepton would be a boson of same property, for example, the superpartner of a tau would have the same mass, electric charge and similar quantum numbers, but would have spin 1 instead of $\frac{1}{2}$ and would be called a stau. The convention is to call a superpartner to a lepton the same name as the latter except for an 's' as prefix and to call a superpartner of a boson, which would then be a fermion, the same name as the boson but with an '-ino' suffix (e.g. gluino). As these sparticles would have the same properties as their SM partners, it would be reasonable to assume that they were easy to detect and produce at colliders. For example, the selectron would be a particle of spin 1 with negative electric charge and about 511 keV mass. Yet up to now, such sparticles have not been found. To preserve the concept of supersymmetry, the symmetry needs to be broken, leading to higher masses for sparticles.

In a theoretical description, a supercharge operator Q is applied on bosonic or fermionic states to take one into the other.

$$Q|B\rangle = |F\rangle \tag{2.23}$$
$$Q|F\rangle = |B\rangle \tag{2.24}$$

If conservation of R-parity is assumed,

$$R = (-1)^{3B+L+2S}\,, \tag{2.25}$$

the lightest supersymmetric particle (LSP) is stable, seeing that it has no particle to decay to, without violating conservation laws. Coincidently, if neutral, the LSP is an ideal WIMP candidate. It is the lightest of the resulting four *neutralinos*, the linear combination of four neutral fermions: The bino $\tilde{B}$, as the U(1) supersymmetric partner of the photon, the wino $\tilde{W}^3$, which can be interpreted as the superpartner of the Z boson, and the two neutral Higgsinos $\tilde{H_1^0}$ and $\tilde{H_2^0}$, superpartners of the neutral Higgs bosons (Ellis [2011]).

$$\chi^0 = a\tilde{B} + b\tilde{W}^3 + c\tilde{H_1^0} + d\tilde{H_2^0} \tag{2.26}$$

With the new sparticle spectrum and a new complex scalar particle coupling to the Higgs, the self-energy contributions to the Higgs mass become zero, while the vacuum expectation value remains non-vanishing. With SUSY, the SM quantum corrections to the Higgs mass would extend to:

$$\Delta m_h^2 \sim \frac{\lambda^2}{16\pi^2}\int^{\Lambda}\frac{\mathrm{d}^4 p}{p^2}\bigg|_{\mathrm{SM}} - \frac{\lambda^2}{16\pi^2}\int^{\Lambda}\frac{\mathrm{d}^4 \pi}{p^2}\bigg|_{SUSY} \sim \frac{\lambda^2}{16\pi^2}(m_{\mathrm{SUSY}}^2 - m_{SM}^2)\ln\frac{\Lambda}{m_{\mathrm{SUSY}}}\,. \tag{2.27}$$

A problem that arises with the doubling of particle numbers and an unknown symmetry breaking mechanism is a loss of the simplicity of the Lagrangian, and the supersymmetric Lagrangian of a minimal supersymmetric standard model (MSSM) would consist of at least 124 field parameters of which 18 correspond to SM parameters. However, with a Grand Unified Theory (GUT) motivation, uniting the forces of nature at high energy scales, i.e. the GUT scale $M_{GUT} \approx 10^{16}$ GeV, a constrained minimal supersymmetric extension of the standard model (CMSSM) can reduce the number of effective parameters to five, additionally to the 18 SM parameters (Jungman et al. [1996]).

The CMSSM

The CMSSM has been considered a well-motivated SUSY extension of the SM for the last decades (Kane et al. [1994], Ellis and Olive [2012], Roszkowski et al. [2001]). It offers solutions to the hierarchy problem and the problem of fine-tuning (which is true for all supersymmetric models) and additionally delivers a solution for the unification of the strong and electroweak forces next to being a simple model with a limited number of parameters and therefore easy to compute as a first test scenario. Similar things can be said of the simplest non-universal model (NUHM1, for models with non-universal Higgs masses see Santoso [2003]) that has also been studied alongside, but will not be brought into more focus here.

In the CMSSM, the gauge couplings of the electroweak and strong interaction field unify. This leads to a universal soft SUSY breaking scalar mass M_0, gaug-

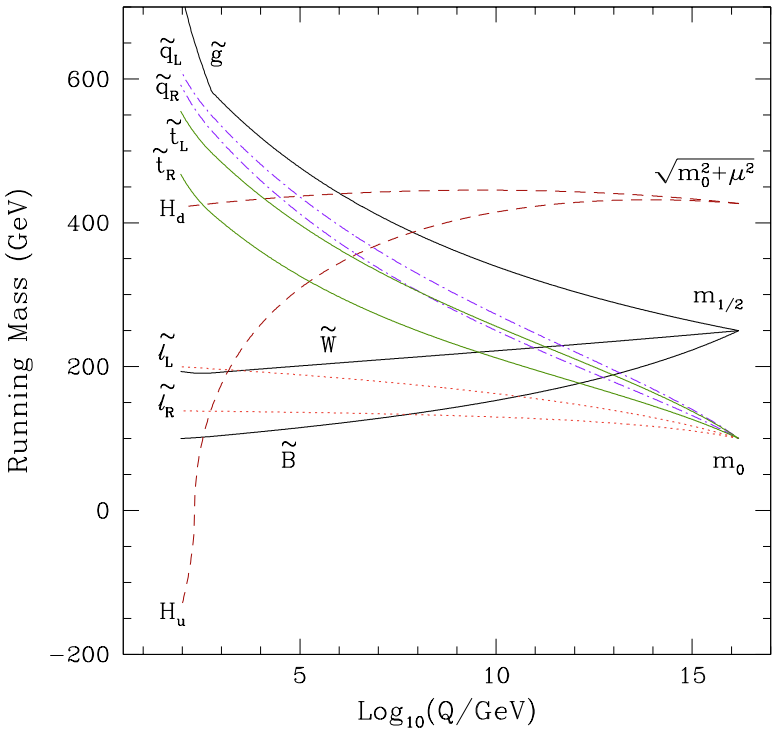

Figure 2.5: The evolution of the mass parameters up to the GUT energy scale for a CMSSM scenario. Figure from Ellis and Olive [2010], references therein.

ino mass $M_{1/2}$ and A-terms at GUT-scale. Thus, the five SUSY parameters in the CMSSM are:

- M_0 – common scalar mass
- $M_{1/2}$ – common gaugino mass
- A_0 – common trilinear scalar coupling
- $\tan\beta$ – ratio of the Higgs vacuum expectation value
- sign(μ) – sign of the Higgsino mass parameter

M_0, the universal scalar mass, is the mass of the Higgs bosons and all scalar particles like sleptons and squarks at GUT energy. $M_{1/2}$, the universal gaugino mass, is the mass all fermions have in common at GUT scale, i.e. the Higgsinos and the supersymmetric partners of the gauge bosons. A_0, the common trilinear coupling, unites the couplings of the Higgs bosons to quarks and leptons. $\tan\beta$ is the ratio of the vacuum expectation value of the two neutral Higgs fields, coupling to either right-handed or left-handed particles. Finally, sign (μ) is the sign of the Higgsino mass parameter (not to be confused with its magnitude), which can be either $+1$ or

-1. The CMSSM scenario up to GUT scale is demonstrated in Figure 2.5.

Advantages of the CMSSM

The attractiveness of SUSY models lies in the naturalness of their introductions. They have not been specially designed to explain DM, yet they offer a suitable DM candidate that fulfills all WIMP DM requirements and reproduces the CDM relic density very closely. Moreover, SUSY was introduced as a theory independent from the DM problem, but includes a particle candidate that has all properties to account for DM. Furthermore, SUSY models solve the hierarchy problem of the SM by canceling the quadratic divergences and thereby avoiding the blow-up of the Higgs mass due to self-energy (Martin [1997]). And eventually, SUSY can be joined with other theories, for instance string theory and axion models, most easily.

In spite of that, not so much the unbiased introduction and natural beauty have promoted the choice to study a SUSY model here. It is also the fact that most advanced experiments with a good approach for complementarity studies are able to provide data to investigate a SUSY model with a promising DM candidate. A neutralino WIMP can be searched with many state-of-the-art techniques, i.e. indirect and direct astrophysical searches, and indirect searches at particle colliders. Additional direct SUSY searches can be carried out at particle colliders, yielding either for detection of sparticles or upper limits on sparticle properties. Searching for other DM candidates with experiments is difficult when striving for complementarity. Although having designed experiments for the purpose of finding specific particles, they lack the opportunity to contrast results from different experiments simultaneously, or at least do not offer as many favorable occasions as the SUSY scenarios do. SUSY models can be investigated comprehensively by theory and experiment, so that they will evidently be proven or contradicted.

The CMSSM has been chosen from several existing SUSY models, as it is the least complex with few free parameters and serves ideally as a test object for BSM models. Thus, it is a good starting point for further studies. In addition, the CMSSM LSP is a neutralino of magnitude of some hundred GeV that annihilates with ideal attributes to match the relic density of CDM. Hence, it is also a prime opportunity for exploring BSM physics in general and DM in particular no matter the outcome, since the constraints will help further understanding of the subject in any case.

The CMSSM and Cold Dark Matter

To analyze the parameter space of the CMSSM, it is fortunate that not all regions of parameter space are relevant. Regions of interest can be defined from the theoretical understanding of what physical processes are, correlated with these particular regions and from restrictions already made by experiments. Most restrictions arise from the fact that the majority of the parameter space yields a too high relic density. Those regions that counteract a high relic density by channels of neutralino destruction, so

that the measured relic density can be achieved, are the regions of interest within the parameter space. These regions of interest (see also Baer et al. [2012], and Ellis and Olive [2012]) can be listed as:

- **The bulk region:** This region at low M_0 and low $M_{1/2}$ values contains light sparticles, leading to a light neutralino that annihilates mostly into $b\bar{b}$ and is mostly bino-like (Mohanty et al. [2012]).
- **The stau co-annihilation region:** A region at low M_0 near the excluded region, where the neutralino would not be the lightest supersymmetric particle anymore. This region refers to annihilations between neutralinos with the lightest $\tilde{\tau}$ in the early Universe with $m_\chi \approx m_{\tilde{\tau}}$, eventually leading to the right relic density. Here also, the neutralino is mostly bino dominated (Ellis et al. [1998] and Ellis et al. [2000]).
- **The funnel region:** This region at high $\tan\beta$ ties with annihilations dominantly taking place via direct-channel heavy Higgs boson H/A-resonances and where $m_A \approx 2m_\chi$ (Ellis et al. [2001] and Bringmann et al. [2008]).
- **The focus point region:** The strip at large M_0 ($M_0 \gg M_{1/2}$) and moderate to large $\tan\beta$ values corresponds to a neutralino that has mixed bino and higgsino contributions with thus relatively large couplings and enhanced annihilation into WW, ZZ or Zh (Baer et al. [1999]).
- **The stop co-annihilation region:** In the region of large negative A_0 values, $m_\chi \approx m_{\tilde{t}}$ and co-annihilations of neutralinos with the lighter stop particle are high in the early Universe (Ciuchini et al. [1998]).
- **The h-pole region:** In this band at low $M_{1/2}$, near the excluded region by electro-weak symmetry breaking, neutralinos have an enhanced annihilation rate in the s-channel h resonance (Djouadi et al. [2005]).

In SUSY phenomenology, it is the goal to constrain these parameter regions by measurements from experiments. Large restraints even among these regions already exist from various experiments and observation. In this study, a global approach is made to exclude further parts of the parameter space and thus the regions of interest while understanding the origin of the limitation and the conclusion that can be drawn from it. In the frame of this work, latest complementary experimental data was used to put further constraints to the parameter space of the CMSSM. Further elaborations on this topic will follow in both Chapter 3 and Chapter 4.

In Figure 2.6, the relevant regions of the CMSSM are shown in a typical M_0 – $M_{1/2}$ plane. This is a conventional way of showing, for instance, experimental results in a CMSSM context, since of all five parameters, M_0 and $M_{1/2}$ are the two parameters with the most impact on collider and DM phenomenology (see Feng [2010]). In this Figure, benchmark models are shown. In these, all parameters except for two, in this case M_0 and $M_{1/2}$, are kept fixed. Therefore, it needs to be treated with care, as deductions can only be made for the particular case of each benchmark scenario.

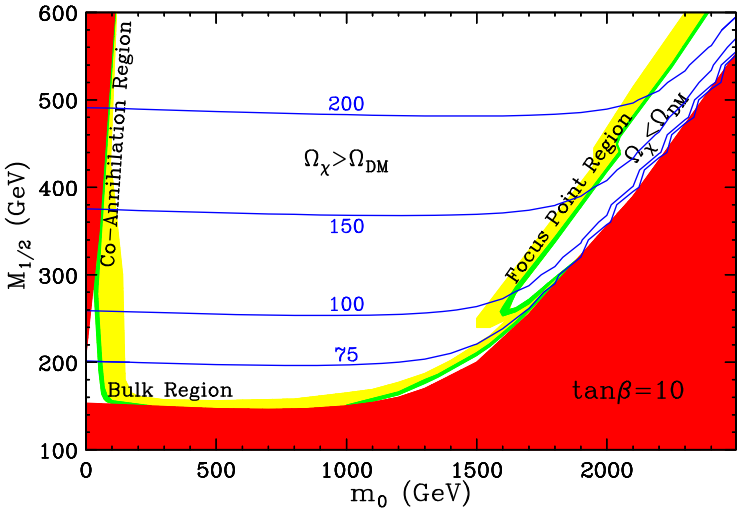

Figure 2.6: Regions of the CMSSM parameter space shown in the M_0–$M_{1/2}$ plane for $A_0 = 0$, $\tan\beta = 10$ and $\mu > 0$. The bulk region at low M_0 and $M_{1/2}$, the stau co-annihilation band at low M_0 and the focus point region at large M_0, while $M_0 \gg M_{1/2}$, are marked. The funnel and stop-coannihilation region cannot be shown, as they depend on A_0 which is fixed to be 0 in this figure. The h-pole region is not shown, because it is not favored by cosmology. The region at low M_0 values next to the stau co-annihilation region is excluded, as not the neutralino, but a charged particle would be the LSP. The other red region in the lower right is excluded by collider bounds on chargino masses. Figure from Feng [2010].

This method can help understand the theory of SUSY models and forming predictions. For an interpretation of the CMSSM in accordance to experimental data, it is necessary to consider all parameters at the same time. A solution how to treat all parameters simultaneously is given with global fits (see Chapter 3).

2.4 Search for Dark Matter

In principle, there are three ways to detect DM (see also Hooper and Baltz [2008]). The first and somewhat straightforward way is via direct detection, which means that a particle detector records signals from a DM particle distinguishable by the immediate response of the target material. Another established method to look for unknown particles is to produce these particles in a particle accelerator and search for traces not expected from SM particles. A more subtle, yet powerful method is the indirect search for DM, where secondary particles from DM interaction are surveyed and investigated in order to understand the underlying processes. All of these methods have their advantages and their difficulties in distinguishing a real DM signal. Even in the case of a claimed detection it would still be sensible to cross-check the signal with experiments of similar approach, and with other detection methods. These three methods shall be explained in more detail below.

2.4.1 Indirect Searches

In indirect searches for DM, observations from ground-based, balloon-borne or space-based instruments are studied in order to reconstruct processes tracing back to DM self-interaction or interaction with other particles. DM processes are expected to leave signatures in particle spectra. Therefore, DM interactions can be observed as signatures or features in the spectrum of gamma-rays, neutrinos or antimatter such as antiprotons, antideuterons or positrons. The disadvantage of an indirect approach towards DM searches lies in the difficulty to interpret the observed data correctly. It is always necessary to assume models to describe the behavior of DM in the according processes without observing the DM particle itself and without knowledge of the source, respectively. Therefore, all other explanations for such cosmic-ray signals, such as astrophysical origins from nearby pulsars or supernovae, need to be excluded first, before assuming a DM scenario. The advantage, however, lies in the opportunity to study DM in a holistic context. DM studies can be carried out not only locally in a selective environment, but globally, i.e. with an entire Galactic or even cosmological (see Bringmann et al. [2012]) framework. Furthermore, as many experiments observe the same sky region at the same time, a large amount of data, both in the same particle channel as well as in different observation channels, is available for thorough study and cross-checks. The final state SM particles from a possible DM annihilation or decay is shown in Table 2.1.

Gamma-Ray Searches

Gamma-rays are observed with both space telescopes and Cherenkov telescopes, covering different energy regimes with an overlap that permits cross-checks between the yielded results. Ground-based Imaging Air Cherenkov Telescopes (IACTs) are effective instruments to measure gamma-rays and cosmic rays by imaging atmospheric air showers from Cherenkov light. Latest IACT techniques enable to measure air showers with a high effective area, low energy threshold and low background. The high effective area is a specific feature of IACTs as the atmosphere is made use of as

Final state particles	Dominant detection signal
$W^{\pm}, Z, g, q$	$\pi, p, \bar{p}, D, \bar{D}, e^{\pm}, \gamma, \nu$
e	$e\pm$
μ	$e_{\pm}, \nu$
τ	$\gamma, e_{\pm}, \nu$
γ	γ
ν	ν

Table 2.1: Final-state SM particles from dark matter annihilation and scattering and their dominant detection signals. Table based on Porter et al. [2011]. The πs decay further to either $e^{\pm}$ or photons.

a calorimeter. This advantage can be used to observe specific sky regions or objects in great detail. The most relevant IACTs operating in the field of DM research are the MAGIC experiment (Albert et al. [2008]) on the La Palma island and the VERITAS observatory (Weekes et al. [2002]) in Arizona on the northern hemisphere, and the H.E.S.S. telescope array (Aharonian et al. [2006b]) in Namibia on the southern hemisphere. IACTs do not measure photons specifically. Instead the entire air shower is recorded, from which the energy of the primary particle needs to be reconstructed with sophisticated techniques (see Aharonian et al. [2006b], for example). Cherenkov telescopes cover photon-induced air-showers in the energy regime of ~ 50 GeV up to ranges of several TeV, with large improvements to widen the ranges in both directions even further, e.g. with the Cherenkov Telescope Array (CTA, Doro and consortium [2011], Doro et al. [2012]).

One of the space telescopes measuring gamma-ray data is the Fermi satellite (Atwood et al. [2009]) with the Fermi Large Area Telescope (Fermi-LAT) detector. It is a pair-conversion telescope and tracks gamma-rays as well as electrons and positrons. A calorimeter obtains the energy of the electromagnetic shower. The energy band covered with Fermi-LAT and comparable experiments ranges from 20-300 GeV. Higher energies cannot be reached due to limitations on the effective area with this technique. The advantage of satellites is the large field of view (2.4 sr with Fermi-LAT) and the possibility of all sky surveys with a coverage of nearly 20 % of the entire sky at every instant (Porter et al. [2011]). IATCs and telescope searches have an overlap at around 100 GeV, enabling combined efforts in this energy range.

DM signatures in gamma-rays can have three different shapes (Kuhlen [2010]). First, and mostly referred to as a smoking-gun signal for DM, a sharp line-signal would be seen in a case of self-interacting DM, creating two photons from two DM particles.

$$E_{\gamma} = m_{\chi} \text{ , for the process } \chi\chi \to \gamma\gamma \tag{2.28}$$

A still distinguished line, albeit somewhat broader would be seen in case the DM self-interaction produces one photon and one Z-boson.

$$E_{\gamma} = \left(1 - \frac{m_{Z^0}^2}{m_{\chi}^2}\right) \text{ , for the process } \chi\chi \to \gamma Z \tag{2.29}$$

χ being the DM particle, γ the produced photon, E_γ the energy of the resulting photons, and m_{Z^0} and m_χ the mass of the Z boson and DM particle, respectively. These processes are loop-suppressed, but if found they would be strongly distinguishable due to their unique spectral feature. The photons would have the exact energy of the DM particle in the case of annihilation into two photons.

$$\frac{\mathrm{d}N_{\gamma\gamma}}{\mathrm{d}E} = \quad 2\delta(E - m_\chi) \tag{2.30}$$

$$\frac{\mathrm{d}N_{Z\gamma}}{\mathrm{d}E} = \quad \delta(E - m_\chi + \tfrac{m_Z^2}{4m_\chi}) \tag{2.31}$$

At energies higher than 100 MeV, a process called Internal Bremsstrahlung (IB) is increasingly taking place, leading to the process $\chi\chi \to f^+f^-\gamma$, where f^+f^- denotes a light fermion pair. In case of DM co-annihilation, virtual π^0 -particles are created, e.g. from a quark-antiquark pair, which decay into to gammas. All three processes are demonstrated in Figure 2.7.

An observation of gamma-ray spectra may show such signatures of DM annihilation. Therefore, recorded spectra are reconstructed to find traces in form of a continuous spectrum, an IB spectrum or a line feature that could stem from DM annihilation and that would differ from spectra produced by known particles. Recently, there have been studies discussing indications for a gamma-ray line of 130 GeV measured with the Fermi-LAT instrument with respect to DM. It is still at dispute whether or not a DM signal has been observed. This topic is addressed in Bringmann et al. [2012], Weniger [2012], Su and Finkbeiner [2012], Tempel et al. [2012], Hektor et al. [2012], for example. The debate is currently ongoing. A monochromatic line signal from DM annihilation would be remarkably distinctive. However, this is a rare, loop-suppressed process and it is therefore more likely to observe a DM signal in a continuous gamma-ray spectrum. Such a spectrum is the result of DM co-annihilation producing charged cosmic rays that scatter on the interstellar medium (ISM), as shown in Bringmann et al. [2008], for the case of an mSUGRA (a model closely related to the CMSSM) scenario. A DM signal would lead to a harder gamma-ray spectrum than expected from photon signals resulting from SM production processes and can therefore be discriminated carefully (Kuhlen [2010]) from an astrophysical signal origin. For further distinction, it is possible to consult additional information, e.g. from neutrino measurements or informations from photons of radio energies.

The photon flux, and in fact the flux of any particular final state particle d, resulting from a DM annihilation, can be described as

$$\Phi_\gamma(E, \Omega) = \Phi_\gamma(E) \times J(\psi), \tag{2.32}$$

This equation can be divided into a two parts. The particle physics component $\Phi_\gamma(E)$ contains the information about the involved particles and their interactions, while the astrophysical component $J(\psi)$ can be described as the integral over the

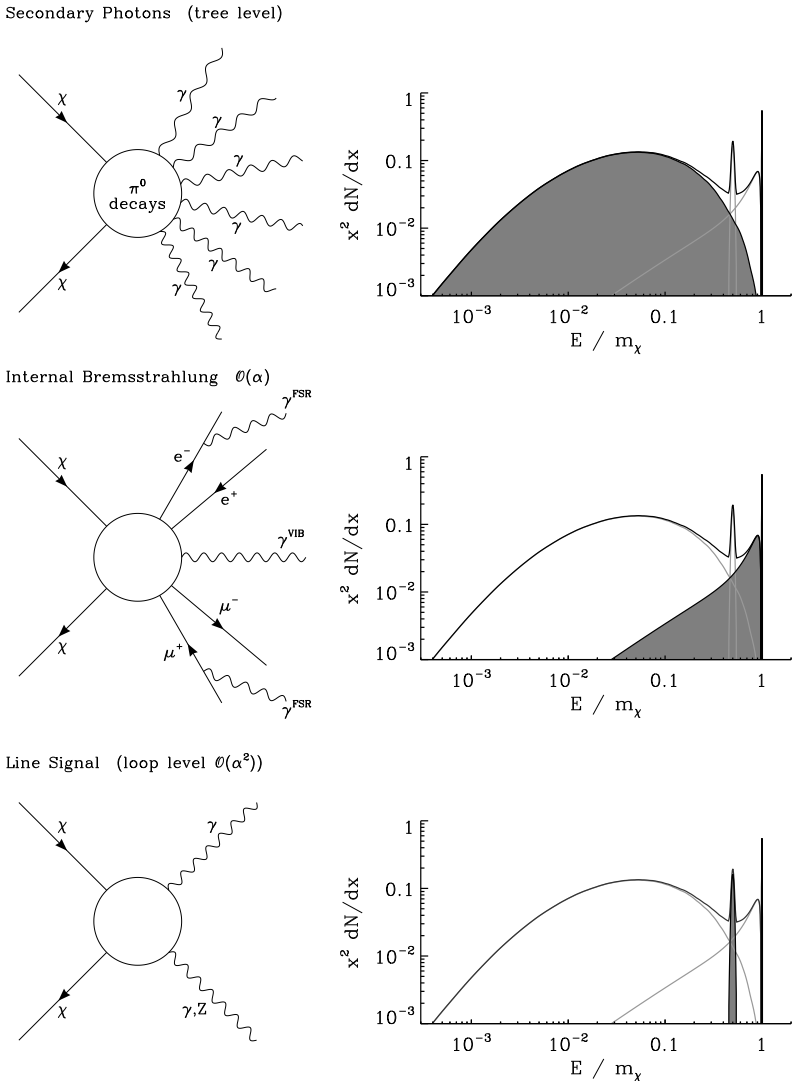

Figure 2.7: DM signatures in gamma-ray spectra, shown in Kuhlen [2010]. Above: Gamma-rays from co-annihilation of DM with other particles. Middle: Gamma-rays from IB. Below: Monochromatic line-signatures from DM self-annihilation (loop-level). The whole observable gamma-ray spectrum from DM self-annihilation and secondary annihilation is the overlap of all three spectra.

DM density along the line of sight in the ψ direction.

$$\Phi_\gamma(E) = \frac{1}{4\pi}\frac{\langle\sigma v\rangle}{2m_\chi^2}\sum_f \frac{dN_f}{dE}B_f \tag{2.33}$$

$$J(\psi) = \int_{l.o.s.} \rho^2(l)dl \tag{2.34}$$

The particle physics equation consists of the mass of the DM particle m_χ, the thermally averaged velocity-weighted cross-section of the DM particle $\langle\sigma v\rangle$, the yield of particles f per energy dN_f/dE per annihilation and B_f, the branching ratio for the final state f. This equation is valid for all final state particles. To determine the photon

flux, specifically, the equation needs to be adjusted to the branching ratio and final state of photons.

For comparable and model-independent results from different instruments, it is common to express the photon flux or photon flux upper limits in terms of more general final states. In the case of gamma-ray and cosmic-ray detectors, $\bar{b}b$ final states are often given for the gamma-ray line both for the flux and for the $\langle \sigma v \rangle$ value of the measured flux and flux upper limit, respectively. The $\bar{b}b$ limit is often chosen, because it can be applied to all supersymmetric models, and because it is one of the leading tree-level channels (see Porter et al. [2011]). Other common final states are $\tau^+\tau^-$, W^+W^- and $\mu^+\mu^-$.This work proceeds with the $\bar{b}b$ treatment, as it is the most conservative choice and therefore appropriate for the first series of global fits with this setup. The way this is done will be shown in Chapter 3.

Searches for Antimatter

The dominance of matter over antimatter in the Universe remains a mystery. In interactions and decays of baryonic matter, the dominant proportion of the result is matter compared to antimatter. In case of DM decay, matter and antimatter are produced likewise. Hence, an abundance of antimatter in the Universe could be the result of DM activity and should thus be investigated critically, regarding all possibilities that could be the source of such an antimatter excess.

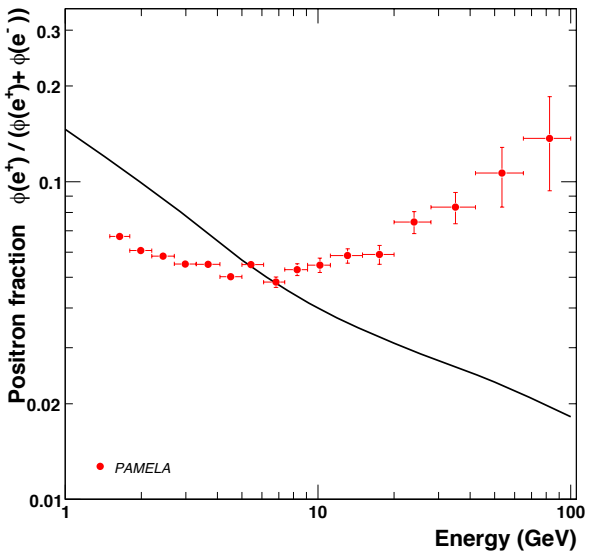

Figure 2.8: Positron flux over the full electron-positron flux. The solid line represents the theoretical expectation for purely secondary production of positrons, calculated in Moskalenko and Strong [1998]. Figure from Adriani et al. [2009] and references therein.

High-energy cosmic-rays (CRs) interact with the ISM. With center of mass energies high enough, they can create new particles during the collision of the CRs with the interstellar gas. Amongst these new particles are antiprotons, positrons and electrons. These particles contribute to the background radiation as secondary background (Simon [2012]). An unusual bump or excess in the full background can be a sign for primordial antimatter or WIMP annihilation. If such a signature were found, a suitable background model would have to be carefully applied and the possibility for being a WIMP signal could be computed.

Instruments looking for such antimatter signals in CRs are e.g. the PAMELA apparatus (Picozza et al. [2007]), the Anti Matter Spectrometer (AMS-02) (Battiston [2009]), the BESS-Polar (Abe et al. [2008]) and the CAPRICE (Papini et al. [2004]) balloon-borne experiments. In 2008, the PAMELA collaboration reported the results of positron measurements in the energy range of 1.5 - 100 GeV (Adriani et al. [2009]). The Fermi-LAT experiment has observed an increasing flux in the energy band from 20-200 GeV consistent with the PAMELA measurement (Abdo et al. [2009]). Possible explanations have been discussed (Grasso et al. [2009]).

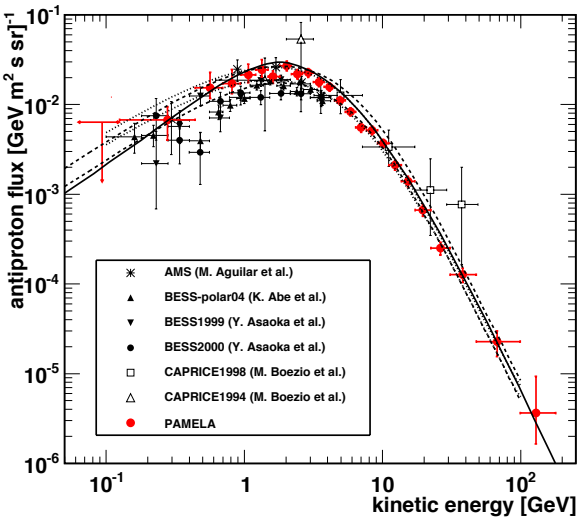

Figure 2.9: Antiproton fluxes from the AMS, BESS, CAPRICE and PAMELA experiments are shown as points with error bars. The lines show predictions for secondary antiproton production. Adriani et al. [2010] and references therein.

This excess can be explained by nearby pulsars or interactions of CRs with giant molecular clouds. An additional excess in the antiprotron flux in combination with the positron excess would make a DM scenario sounder. So far, no primary antiprotons from DM pair-annihilation have been found by experiment. The observed antiproton spectra are in consensus interpreted as secondary antiprotons from cosmic-ray propagation in the galaxy (Adriani et al. [2010] Kappl and Winkler [2012]). Antimatter fluxes are important measurements in the search for DM and should ideally be taken into account in further investigations.

Neutrino Searches

As WIMPs pass the Sun or Earth, they can be slowed down below escape velocity by elastic scattering, producing high-energy neutrinos that differ from otherwise produced neutrinos (Munoz [2012]). These neutrino signatures from WIMP scattering can be detected with specially designed experiments. The underground Super-Kamiokande experiment (Tanaka et al. [2011]) in Japan uses destilled water, the IceCube (Arguelles and Kopp [2012]) experiment at the South Pole uses a large volume of ice and the ANTARES experiment (Zornoza [2012]) in the Mediterranean Sea uses water as detector material. So far, no distinct signal of high-energy neutrinos has been found. Even though no DM signal has been found, the upper limits from these experiments set restrictions for other searches and are of substantial importance for DM research. For instance, they provide additional information on both the spin-dependent and spin-independent WIMP-nucleon cross-section for direct searches, which will be discussed in the following Section.

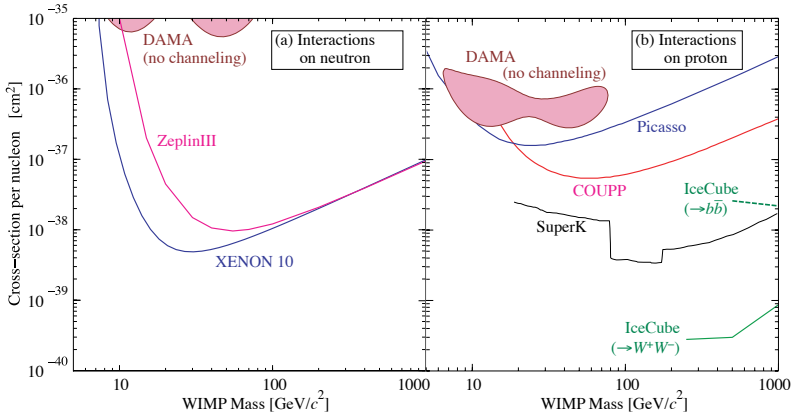

Figure 2.10: Spin-dependent cross section of WIMPS with nucleon particles, i.e. neutrons on the left and protons on the right. Constraints on WIMP-annihilation from the neutrino experiments SuperK and IceCube (for different annihilation channels) are shown for proton scattering. Figure from Beringer et al. [2012] and references therein.

2.4.2 Direct Searches

In direct searches for DM, underground laboratories are constructed to detect a WIMP signal with the target material from WIMPs reaching the Earth. Due to the low cross-section, these signals are rare. Despite that, the Milky Way galaxy is assumed to be a region of very high DM density. and DM signals can be distinguished by shielding them as well as possible from other particles reaching the detector. Hence the location of these detectors is underground, filtrating baryonic interaction with the target material through the ground, yielding a very low background. Most experiments also aim for a low energy threshold to get hold of even faint signals and a high fiducial mass for WIMP scattering. Signals can then be measured by energy deposition when the WIMP particle scatters off nuclei of the detector. Depending on the target material, these signals can be detected in three ways.

1. Via scintillation and the detection of light. Ideal target materials for scintillation are noble liquids like Xenon (Xe), Argon (Ar) and Neon (Ne) or compounds like NaI and CaF_2.

2. Via ionization and thus electric current. Common target materials for ionization are Germanium (Ge) and Silicon (Si).

3. Via phonons and the measurement of emitted heat. For measuring heat with bolometers, target materials as Ge and Si are used as well as compounds like TeO_2 or Al_2O_3.

All direct detection instruments use one or two of these techniques for WIMP searches. A table of current direct detection experiments and their detection methods can be seen below (2.2). Notwithstanding that there are other most recent experiments, this is simply a choice of experiments from which spin-independent WIMP-nucleon cross-sections have been derived that are either used in AstroFit already or are considered to be used in the near future.

Experiment	Reference	Target material	Detection method
DAMA/LIBRA	Bernabei et al. [2010]	NaI	Scintillation
CoGeNT	Aalseth et al. [2012]	Ge	Ionization
CRESST II	Angloher et al. [2012]	$CaWO_4$	Scintillation, Phonons
CDMS II	Ahmed et al. [2010]	Ge, Si	Ionization, Phonons
EDELWEISS II	Armengaud et al. [2010]	Ge, Si	Ionization, Phonons
Xenon100	Aprile et al. [2010]	Xe	Scintillation, Ionisation

Table 2.2: Selected list of current DM direct detection experiments with target material and detection methods. References are given in the second column. Therein, the detection method and the setup of the stated experiment are described in more detail.

Search for Annual Modulation

During the Earth's revolution around the Sun, there is a point in time when the velocity of the Earth and the DM particles from the Galaxy coming towards the Earth due to the velocity of the solar system sum up. At this point, the underground direct detection laboratories should be able to measure a peak of the event rate. Correspondingly, the Earth crosses a smaller flux of DM particles when the velocities of the Galaxy and the Earth subtract. As the Earth is constantly moving through the Galaxy, a perpetual rise and fall in the signal rate can be expected with a significant peak around June 2^{nd} and a minimum around December 2^{nd} (Bernabei et al. [2008]). The differential event rate can be described as

$$\frac{dR}{dE_R} = \frac{\rho_0}{m_\chi m_N} \int_{v_{min}}^{v_{esc}} v f(\vec{v}) \frac{d\sigma_{\chi N}}{dE_R} d^3\vec{v}. \tag{2.35}$$

showing the differential rate of events over the nuclear-recoil energy E_R being equal to the quotient of the local WIMP density ρ_0 over the mass of the target nucleon and the WIMP particle, respectively, times the integral over the velocity-weighted differential WIMP-nucleon cross-section $d\sigma_{\chi N}$ per recoil energy. v is the velocity of the WIMP with the velocity distribution function $f(v)$. m_χ and m_N denote the mass of the WIMP and the nucleus, respectively. The minimum of the integral is the velocity necessary for the WIMP to interact with the target, while the maximum is naturally the escape velocity with which the WIMP would not be captured by the Earth.

An annual modulation can be described as a contribution to the counting rate. Supposing R_{k0} to be the constant part of a signal, then a modulation amplitude R_{km} can be added to the total signal rate R_k with the k-th energy as follows:

$$R_k = R_{k0} + R_{km} \cos \omega (t - t_0) \ , \tag{2.36}$$

with $\omega = 2\pi/T$, T being the period and t_0 being the phase. Consecutively, a modulation in form of a cosine function with maximal amplitude in June and minimal in December with the period of one year can be assumed. In Figure 2.11, the residuals on the annual modulation are shown to contrast the results from the CDMS II experiment and the CoGeNT measurement. Residuals show the difference between a measured value x_i and its theoretical prediction $\langle x \rangle$. To demonstrate the signal strength of a possible annual modulation, the best fit for an unmodulated rate is subtracted from the measurement.

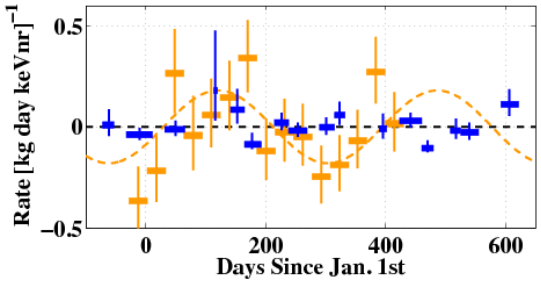

Figure 2.11: Contrast between the CDMS II and the CoGeNT annual modulation in the $5.0 - 11.9\,\mathrm{keV}_{nr}$ range (the index *nr* standing for nuclear recoil), after subtracting the best fit unmodulated rate for each detector. The blue points show the rate of the CDMS II nuclear-recoil band, starting in late 2007. The orange points show the derived CoGeNT rate for nuclear recoils, starting in 2009. The orange dashed line shows the maximum-likelihood modulation model for the corresponding energy range. The CDMS II band is consistent with no modulation while the CoGeNT collaboration has reported a modulation in the electron-recoil band. Figure from Ahmed et al. [2012] and references therein.

In fact, the DAMA/LIBRA and CoGeNT collaboration claim to have measured such an annual modulation. The combined DAMA/LIBRA and DAMA/NaI data result in a signal of 8.2σ confidence level (Bernabei et al. [2008]). The CoGeNT collaboration has also published indications for an annual modulation of 2.7σ with phase, period and amplitude consistent with a DM signal from a light WIMP of 4.5 - 12 GeV (Hooper and Kelso [2011], Aalseth et al. [2011]). From theory, a WIMP is expected to be in the order of magnitude of 100-1000 GeV. That being the case, DM interpretations from the measurements on the WIMP mass and scattering cross-section from

DAMA/LIBRA and CoGeNT clash severely with upper limits from other direct detection experiments. This discrepency between collaborational researches has been an extraordinary opportunity for DM discussions.

Direct Detection of WIMP-Nucleus Cross-Section

The cross-section of a WIMP scattering on a target nucleus can be divided into two components, the spin-independent and the spin-dependent term. The former refers the coupling to the mass of the nucleus, while the latter refers to the coupling to its spin (De Jesus [2004]). For massive target nuclei, the spin-independent cross section is dominant and has been chosen to be utilized in this study. Both have been explored by various instruments in this area of research. In Figure 2.12, most recent signals or upper limits derived from measurements with different experiments are shown. As mentioned in the last section, there is a disagreement between the resulting signal regions for WIMP detection from DAMA/LIBRA and CoGeNT, and the absence of such a signal from other collaborations, most prominently Xenon100. In the latest publication, the Xenon100 collaboration show even lower upper limits on the spin-independent cross-section (Aprile et al. [2012]) and were confident to predict even lower bounds when taking data with the future instrument Xenon1T, standing for a fiducial mass of one ton, if no signal was found.

The total WIMP-nucleus scattering cross-section per recoil energy E_R can be written as the sum of the spin-independent and the spin-dependent cross-section per recoil energy, respectively:

$$\frac{\mathrm{d}\sigma_{\mathrm{WN}}}{\mathrm{d}E_R} = \left(\frac{\mathrm{d}\sigma_{\mathrm{WN}}}{\mathrm{d}E_R}\right)_{SI} + \left(\frac{\mathrm{d}\sigma_{\mathrm{WN}}}{\mathrm{d}E_R}\right)_{SD} \tag{2.37}$$

The total zero-momentum transfer cross-section with its spin-independent (SI) and spin-dependent (SD) parts can be written as:

$$\sigma_{0\mathrm{WN}} = \frac{4\mu_N^2}{\pi}\left[Zf_{\mathrm{p}} + (A-Z)f_{\mathrm{n}}\right]^2 + \frac{32G_{\mathrm{F}}^2\mu_N^2}{\pi}\frac{J+1}{J}(a_{\mathrm{p}}\langle S_{\mathrm{p}}\rangle + a_{\mathrm{n}}\langle S_{\mathrm{n}}\rangle) \tag{2.38}$$

with the WIMP-nucleus reduced mass $\mu_N = M_\chi M_N/(M_\chi + M_N)$, the spin-independent and spin-dependent reduced couplingsf_{p},f_{n}, a_{p} and a_{n} to the proton and neutron, respectively, the atomic and mass number Z and A of the target element, Fermi's constant G_F, the total nuclear spin J and the expectation values of the proton and neutron spin within the nucleus $\langle S_{\mathrm{p}}\rangle$ and $\langle S_{\mathrm{n}}\rangle$ (see Schnee [2011]). As most direct detection experiments use different target materials, it is practical to derive the cross-section of a WIMP with a nucleon inside the target nucleus for reasons of comparison.

In the frame of this thesis, both signal regions from DAMA/LIBRA and CoGeNT as well as upper limits from Xenon100 have been used for the analysis (see 4).

2.4.3 Collider Searches

In collider searches for DM today, only indirect searches are likely to be possible, as a neutralino DM particle being neutral and stable would leave no final state to be

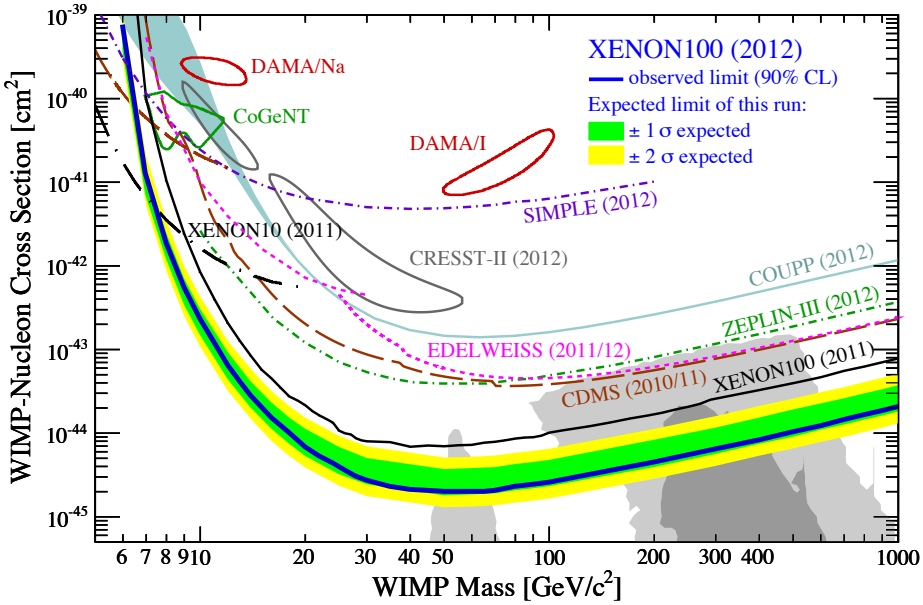

Figure 2.12: Derived spin-independent WIMP-nucleon scattering cross-sections for various experiments. Figure from Aprile et al. [2012] and references therein.

triggered. Thus, for DM searches at colliders it is of vital importance to produce other matter states associated with new physics and detect their SM final states (Nath et al. [2010]). Hence at the LHC, DM searches concentrate on searches for SUSY particles and unusual events. Since the LSP would leave no trace in the detectors, jets with missing transverse energy (E_T^{miss}) are prospected. If all processes in the jets from SM particles can be reconstructed, leaving parts of the reconstruction in question, e.g. by a missing component in the energy reconstruction, it can be assumed that an unknown neutral particle, as a neutralino LSP would be, carries this missing energy. These reconstructions are made with sophisticated methods, taking into account all SM background processes and grouping jets with isolated leptons, e.g. one or three leptons, and opposite sign or same-sign dileptons. Searches are carried out for jets + E_T^{miss} (Baer [2011]), to trace back possible DM signals. The $\tilde{g}$ and $\tilde{q}$ decay reconstruction is done with event generator programs, with a probabalistic event generation for expected SUSY events.

Apart from jets + E_T searches, the lookout for heavy Higgs bosons H,A is an important quest for SUSY indications. Also, the rare decay $B_s \to \mu^+\mu^-$ is observed closely, as it is a massive constraint on neutralino DM with R-parity conservation (Buchmueller et al. [2012]).

2.5 The Importance of Complementarity

While many experimental approaches to finding DM are made, it becomes even more important to assemble and combine them. Not only is it helpful to gain a wider view on the subject of study and extend the understanding of it. Combining complemen-

tary approaches helps mitigate uncertainties of each single approach and puts the results together in a framework where the influence they have on each other can be clearly seen. In this way, that agreements and contradictions in the findings can be investigated, closing in on the best solution and excluding formerly regarded options that might be ruled out by a more complete viewing.

In indirect searches for DM, thorough studies on both astronomical as well as cosmological scales are made possible. However, uncertainties must be taken into account from the method, as it does not find the dark matter particle itself, but its interaction products. The reconstruction of events and the assumed model of the dark matter density in the observation target can lead to errors in the outcome of signal interpretations.

In direct searches, DM particles can be detected directly, and their cross section with the target material can be described. Nevertheless, there is no information on the theory of the particle and its interactions with other particles, and background estimations can lead to false signal claims or the failure to detect one as such.

In particle collider experiments, the runs of the experiment can be adjusted and studies of collisions can be made available at any time. Yet, even with a missing transverse energy/momentum component, it remains unclear what this missing energy is concerned with. Other particles, for example charged particles, can be detected and described due to their activation of certain particle detectors within the collider, giving understanding to their interactions which makes it easier to catalog them. As opposed to that, with DM particles, there is no such catalog and no detection except via indirect channels due to the unexpected behavior of other particles and the missing of transverse energy. Again, there is nothing to be said about the particle causing these phenomena.

For each evidence of DM, there is always another explanation if considered independently. Astrophysical evidences can be explained if a lack of understanding gravity is assumed. The bullet cluster can be seen as the one exemplary evidence for DM, but it leads to questions, why there is only one such galaxy interaction that could be observed and no other collisions likewise. Excesses in antimatter in cosmic rays can be a sign for DM. However, they can also be explained astrophysically by nearby objects like pulsars. Production or even measurement of a possible candidate cannot give conclusion on whether or not all necessary criteria are met for being a DM particle that matches all conditions stated at 2.2.3. For example, only the confirmation with indirect DM searches can answer the question if the particle is stable on cosmological scales (Munoz [2012]). Many recent measurements of possible DM evidence so long are at some point questionable, in some cases with possible other explanations to the phenomena like detector artifacts or astrophysical objects (Bergstrom [2012]).

By combining all methods and their results and confronting them with different theoretical models, it could be possible to either pinpoint the regions of interest within

the parameter space of the model or to discuss contradictions and pursue a different theoretical model to tackle the description of DM in a conclusive theory. It is also a way to gain a greater picture of questions and answers towards the DM entity. In all cases, the complementary approach offers an unprepossessed way to study DM in a global context.

Chapter 3

Global Fits with AstroFit

Global fits have been a distinctive method in particle physics to comprehensively probe BSM models with given data from particle physics experiments. As particles are not only observed in collider experiments, but also astrophysically, and as solving the DM question remains a task to which both fields, particle physics and astrophysics, commit exceedingly, it is vital to include astrophysical observations into global fits to gain more knowledge about particle physics BSM in general and DM in particular.

In the frame of this thesis, it has been the goal to develop a self-contained program that adds astrophysical and cosmological data and observation to global fits. Therefore, I have created the `AstroFit` tool (Nguyen et al. [2012]) in collaboration with Torsten Bringmann. The overall approach with `AstroFit` is to combine astrophysical observations into global fits by creating a platform in semblance of an independent interface program that includes all relevant astrophysical data and neatly delivers the information to the minimization process of a chosen fit program to use. The crucial points are provision of as much information as possible and the minimal effort in integrating it into a fit program. In the progress of my work, I have developed this tool further, implemented data from experiment and observation, i.e. data from direct detection experiments and indirect searches, and tested the technical and physical properties of the setup. Subsequently, I have written an interface to the `Fittino` global fit program and done operational and efficiency tests of the interface. Eventually, a combined study of the CMSSM with `Fittino` and `AstroFit` has been obtained (Bechtle et al. [2012]), for which the setup, analysis and report on the DM related topics are all part of this work.

In the following, I comment on the aims and methods of global fits in general, before explaining the techniques and input that were used for this thesis. Then I describe the `AstroFit` interface program in particular, starting with the structure and functionality of the program, continuing with the specific observables and how they are calculated within `AstroFit`. The calculation of the $\Delta\chi^2$ contributions, needed for the minimization process in `Fittino`, is explained separately. Thereafter, I will demonstrate the results from the testing of these tools with some examples before I conclude this Chapter with an outlook and future prospects for `AstroFit`.

3.1 Global Fits

In this Section, I describe the techniques of global fits used in this study. Global fits are an important tool of particle phenomenology. In Sections 2.1.2, I have shown that there is rising need for new models to explain BSM phenomena in particle physics, one of these phenomena being DM. Since these models are primarily represented by a large theoretical framework, usually comprising many parameters, a comprehensive study of such models is necessary. In the reciprocation between theory and experiment, there is presently a plethora of theories to be probed by a small capacity of experiments. It is thus important to confront these models with all experimental data available, in order to constrain or exclude any such model. In global fits, this is done under statistical consideration of all relevant parameters involved. Benchmark models, in which all except two parameters of a BSM model are fixed to a theoretically motivated value, enable an in-depth study of specific interrelations between two parameters (e.g. Battaglia et al. [2004]). When studying the CMSSM globally, and confronting the SUSY model with actual data, not so much information can be gained by a two-dimensional projection into e.g. the M_0–$M_{1/2}$-plane, as there is no knowledge of the other parameters or the interplay of all parameters. Collapsing the CMSSM to a two-dimensional model while arbitrarily fixing the other parameters can be highly ambiguous. Global fits are therefore a method to understand a BSM model in total by taking into account all model parameters. By doing so, global fits provide statistical means to depict the goodness of a fit, that is the extent to which observed data match the values expected by theory. The interpretation remains, needless to say, intricate.

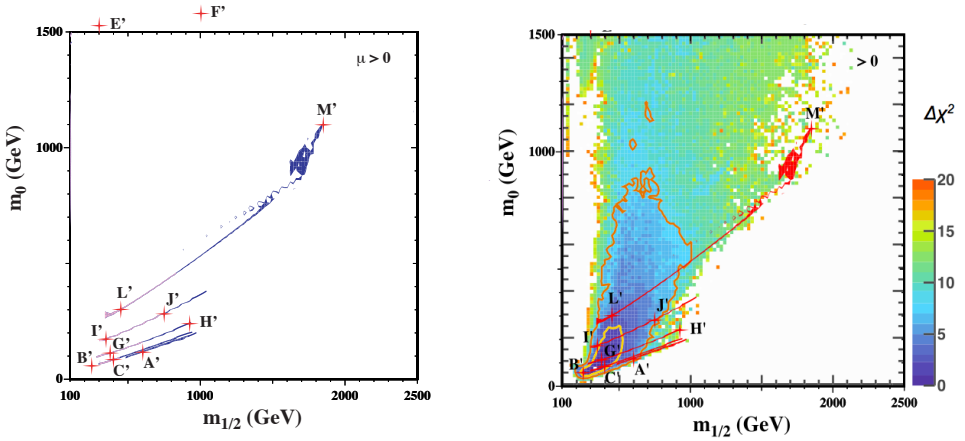

Figure 3.1: Left: Figure showing the influence of the WMAP-measured relic density on the $(m_0, m_{1/2})$-plane of the CMSSM from 2003 as a two-dimensional projection and varying but fixed $tan\beta$ ranging from 5 to 50 (Battaglia et al. [2004]), $A_0 = 0$ and $sign(\mu) > 0$. Benchmark points formerly corresponding to the bulk, funnel and focus-point region, with a specific set of all parameter values each, are denoted with letters from A to K. Battaglia et al. [2004] mention the option of more thorough scans of the parameter space for a better understanding. Right: Results from a global fit of all CMSSM parameters from 2012 with the according χ^2-value for each point indicated by a color scale. Confidence regions are shown in yellow and orange. To demonstrate the distinct contrast, the WMAP strips from the left Figure have been drawn in. Figure entirely from Buchmueller [2012].

3.1.1 Bayesian and Frequentist Approach towards Global Fits

In general, there are two different approaches to global fits. Their common aim is to fit the parameter space of a theoretical model beyond the SM by confronting these models with input data from experiments. They are called global, because all parameters are fit simultaneously in order to find the best fit values for all of them in interdependence rather than keeping most of them fixed to some estimated value and trying to fit one or two parameters. The goal is to find the overall global minimum of the model parameter space, that is the point where all, i.e. four in this study, parameters reach their common most significant values in accordance with the input data.

There are two philosophies of how this global minimum in parameter space can be found. One is the Bayesian approach, the other one is the frequentist approach (see Trotta and Cranmer [2011]). A Bayesian interpretation of a probability from a global fit represents the degree of belief in a prior after confronting it with data. A frequentist interpretation of a global fit has no prior, but the probability states the proportion to which extend the parameter set is fit around a certain region of parameter space.

Bayesian Interpretation

In a Bayesian interpretation, Bayes' theorem is applied which generally states

$$P(A|B) = \frac{P(B|A)P(A)}{P(B)} \tag{3.1}$$

with the following meaning:
$P(A)$ and $P(B)$ are the a priori probability for event A or B respectively. $P(A|B)$ is the a posteriori probability of A, taking into account B. $P(B|A)$ is the probability for event B to occur under the condition that event A has taken place, and $P(B|A)/P(B)$ is the support B provides for A.

In terms of global fits of the CMSSM, Bayes' theorem can be formulated as

$$P(\theta|d) = \frac{P(d|\theta)P(\theta)}{P(d)} \, . \tag{3.2}$$

Here, $P(\theta)$ is the prior distribution of parameters before knowledge of the data d. $P(\theta|d)$ is the posterior distribution of parameters after taking account observations. Finally, $P(d)$ represents the Bayesian evidence or model likelihood, which accounts for the constraining power of the data. Not only the parameters of a BSM model can be considered in the set of parameters θ, but also nuisance parameters ψ, which have formerly shown to have high influence on the CMSSM predictions. In case of a CMSSM fit, for instance, the set of parameters would be $\phi = (M_0, M_{1/2}, A_0, \tan\beta, sign(\mu))$ and the nuisance parameters could be $\psi = (m_t, m_b, \alpha_s, \alpha_{em})$ with the mass of the top and the bottom quark and the strong and electromagnetic coupling constant within the SM, as in former fits with `SuperBayeS`, e.g. in Martinez et al. [2009a], so that

$\theta = \{\psi, \phi\}$ would be the vector of parameters for the fit. Applying Bayes' theorem (see Equation 3.2), the likelihood function can be obtained from the posterior distribution function $P(\theta|d)$. As $P(d)$ is a constant to the fit, the likelihood function can be defined as $P(d|\theta) \equiv \mathcal{L}(\theta)$ with $P(d|\theta)$ as a function of θ for the observed data d (see also Trotta et al. [2011], Trotta et al. [2008], de Austri et al. [2006]).

Summarizing the Bayesian approach of global fits, the Bayesian interpretation makes use of the definition of probability density functions and regions of interest for the fit that are based on prior information, e.g. from former experiments. The likelihood function is concluded from the prior by applying Bayes' theorem. The advantage of this method lies in the high precision of the fit, as parameter scans are performed with focus to the preferred parameter regions, under the condition that the prior is appropriate. In spite of this advantage, this method will more likely fail to find a global minimum that lies considerably far away from the prior assumptions of the model to fit. Choosing priors also weakens the potential of a conclusion for the model fit in total, as the latter would only be tested very specifically. A goodness of the fit can only be stated for the given priors. No statement can be made otherwise. With such a high number of theoretical models explaining BSM phenomena, a more unbiased approach, even with a weak goodness of fit, permits a more general conclusion and unexpected outcomes. It also offers a strong possibility to contrast different theoretical BSM models by comparing the outcome of the fits.

Frequentist Interpretation

The second approach is the frequentist method. Here, no a priori assumption of the parameter model is made, allowing the global minimum to be anywhere in parameter space. Scanning an infinite parameter space not only needs very high statistics and frequent evaluation of the method. It also needs an algorithm that will eventually prefer regions of higher significance over those with low significance. Therefore, in the fit process according to the frequentist interpretation, a likelihood function without prior assumptions is used for the parameter scan, in order to find the most probable set of parameters. The scan of the parameter space depends solely on the likelihood function and the χ^2(chi-squared)-value associated with the likelihood of a specific point in parameter space, which corresponds to particular values for each parameter of the fit. I will roughly illustrate the connection between the likelihood function and the χ^2 as in Press et al. [2007]. In general, a likelihood of a data set can be defined as the product of the probability of each point in an interval Δy.

$$\mathcal{L} = \prod_{i=1}^{N} \left\{ \exp\left[-\frac{1}{2} \left(\frac{O_i - T_i}{\sigma_i} \right)^2 \right] \Delta y \right\} , \tag{3.3}$$

O_i being the measured data, T_i the theoretical prediction, and σ_i the error on the measured value. The point of maximum likelihood corresponds to the parameter set with maximal probability. The function that needs to be minimized within the likelihood function is called χ^2-function.

$$\chi^2 = \sum_{i=1}^{n} \left(\frac{O_i - T_i}{\sigma_i} \right)^2 \tag{3.4}$$

Divided by the number of degrees of freedom (ndf), the reduced χ^2 is given, which represents the goodness of fit for the specified parameter set that should be close to 1 for a good fit.

$$\chi^2_{red} = \chi^2/ndf \text{ , quantity for the goodness of fit} \tag{3.5}$$

The advantage of this method is clearly the impartial position towards the outcome of the fit and thus the opportunity to find the global minimum anywhere within the parameter space, even in unpredicted areas. Moreover, the necessary thorough scan of parameter space provides a wide statistical understanding of the fit. A parameter scan can be informative and meaningful, no matter how the fit behaves towards new experimental data. The effect of the data leaves its immediate unbiased imprint on the result, which then has to be interpreted carefully. However, there are disadvantages, also. While the Bayesian approach may find the best fit regions in a defined parameter space more accurately, the frequentist method might fail to find the absolute minimum and resulting in finding a local minimum that is close to being the global minimum. Even with an ideal number of test runs of many steps, all tests could end up finding the same, in this case, wrong result. The higher the number of parameters of the model to fit, the more careful one has to be with this method. Still, it is more a question of philosophy than a dominance of one method over the other. In most cases, it will always be a mixture of the two methods to some extend, as it will always be the goal to scan a large parameter space in an unbiased way, and as there is always the human mind behind each method to judge the correctness of the results, tracing sources of error and accounting for the exposition of the outcome. Scans from both methods are an ideal cross-check. If both yield the same result, it can be a confirmation that there was minimal fault in the execution of the fit. If there are conflicts, it is a chance to look into the scans more carefully. And in any case, it is also important to keep in mind that predictions from theory codes and the application of statistical and systematic errors in the global fit can also be a source of error, be it the false understanding of nature or the computing of the theoretical estimation for a certain value.

Within `Fittino`, the fit program used for the global scans in this work, both the frequentist as well as the Bayesian methods can be used. For all studies, both methods have been applied so that comparisons between both were possible. The emphasis of this work lies in the question, which parameter regions of the CMSSM are still in good agreement with latest experimental data. In this study, the overall compatibility of the CMSSM model with the combined input of data from latest direct, indirect and collider searches is investigated. Therefore, I will focus on the result from the frequentist interpretation only, describing the techniques in more detail. Nonetheless, cross-checks have been made with the Bayesian method also, as shown in Bechtle et al. [2012]. From the results, follow-up studies can be designed.

3.2 Techniques

In the following, I will describe the minimization technique as well as the method used to derive the confidence regions used for the analysis part of this thesis.

3.2.1 Minimization Process

In `Fittino`, three techniques for the parameter estimation are available: MINUIT, Simulated Annealing and Markov Chain Monte Carlo (MCMC). For the analysis described here, the MCMC has been used for a global scan of the parameter space, as it is best suited for fitting a multi-parameter space and has the advantage of delivering an efficient scan around the minima (see Bechtle et al. [2010]). For the minimization process, a Metropolis algorithm is used. The χ^2 value of each CMSSM model, i.e. point in parameter space, represents the agreement between the theoretical values of the parameters at that point with the given data set. The best fit point is directly defined by the χ^2_{min}, the lowest total χ^2 of the fit or equivalently as the point with the largest likelihood. The designed minimization process utilizes a likelihood function that is only dependent on the χ^2 of each parameter point and not on any prior assumption of parameter values. In accordance to the likelihood function described above, the MCMC minimization process can be described as follows: A sequence of points x_i, $(i = 1, 2, ..., n)$ following a designed algorithm, is created with an associated likelihood $\mathcal{L}(x_i)$ to each point. The likelihood function can be written as

$$\mathcal{L} = \exp(-\frac{\chi^2}{2}) \,. \tag{3.6}$$

The Markov chain is computed to start at a random point of the parameter space. New points x_{n+1} are chosen arbitrarily without direct connection to the point x_n before, following these rules: In order to find the best fit minimum of the parameter set to fit while avoiding confusions with local minima, a new point is added to the chain when it leads to an improvement of the associated likelihood with

$$\mathcal{L}(x_{n+1}) > \mathcal{L}(x_n), \tag{3.7}$$

or in other respects, it will still be accepted with a probability of

$$\mathcal{L}(x_{n+1})/\mathcal{L}(x_n). \tag{3.8}$$

So if the likelihood of a new point is relatively small, an acceptance to the chain is less likely than for a point with a greater likelihood. With this algorithm, the chain progresses in the direction of the best likelihood but can recover from local minima that do not resemble the global minimum. If the new point x_{n+1} is accepted, it is added to the sequence. If it is declined, the old point x_n is added to the chain once more. With a statistics of many million points and defined step widths, the best fit region can be securely found. To make the chains as independent of the starting point as possible, twenty Markov chains with two million accepted points each are started with a random generator, defining the starting point of each individual chain which are eventually stacked to have a most thorough scan of the entire parameter space.

Approximately 138 million steps of a χ^2 of 30 or lower have been used in the analysis of this work. The minimization process is demonstrated in Figure 3.2.

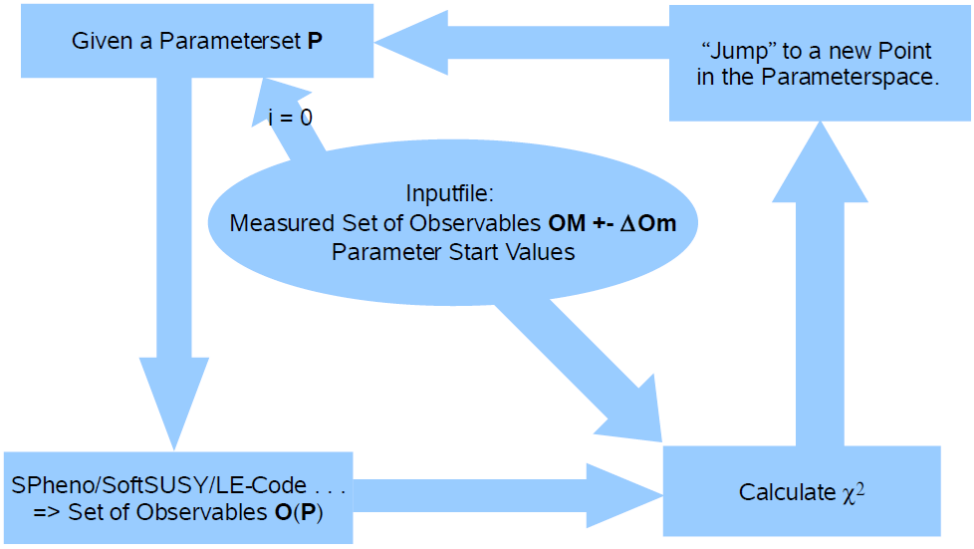

Figure 3.2: Chart from Matthias Hamer (Fittino Collaboration) demonstrating the minimization process. Experimental data with corresponding statistical uncertainties are stored in the `Fittino` input file (labeled as OM and +- ΔOm). Starting parameters are estimated within `Fittino`. From this set of starting parameters, a set of observables is calculated which is then compared to the input. A χ^2 is calculated for the parameter set by comparing the observables from the prediction to the experimental data. After that, a new point in parameter space is used for the calculation and added to the chain according to the algorithm described in the text.

3.2.2 Best Fit Point and Confidence Regions

The best fit point of a fit is the point with the miminal χ^2-value. In the analysis Chapter of this thesis (Chapter 4), resulting confidence regions of the fit are shown in a two-dimensional projection. These are obtained by taking into account all points from the fit that match the conditions for a certain confidence interval. These condition are defined by

$$\Delta\chi^2 = \chi^2 - \chi^2_{min}\,, \tag{3.9}$$

with χ^2_{min} being the point with the lowest χ^2 of the fit. The value of $\Delta\chi^2$ for a confidence level is given in Table 3.1, depending on the percentage of confidence interval and the number of parameters (see e.g. Press et al. [2007] for reference).

The 1σ and 2σ regions are approximated with the 68% and 95% containment region, respectively. The points are selected by a scanning technique that takes into account the point density of all points satisfying the conditions in each region of parameter space. If the spacial distribution of points is of high enough density, a smooth surface is drawn across all accepted points. Plots in this work are usually shown as

p (%)	m=1	m=2	m=3
68.27	1.00	2.30	3.53
90.	2.71	4.61	6.25
95	3.84	5.99	7.82
95.45	4.00	6.18	8.03
99	6.63	9.21	11.34
99.73	9.00	11.83	14.16

Table 3.1: Depending on the coverage probability of the confidence region in percentage, the $\Delta\chi^2$ is given for a number m of parameters. In the two parameter projections used in this work, $\Delta\chi^2 = 2.3$ and $\Delta\chi^2 = 5.99$ have been used to approximate the 1σ and 2σ confidence regions.

an overlay of two different sets of input data, so that the results from the two sets are comparable. In this case, the confidence regions are distinguished by solid and dashed lines, and lighter and darker shades of color, respectively. This is demonstrated in Figure 3.3, where a data set without Xenon100 upper limits and a data set with these limits have been used in comparison.

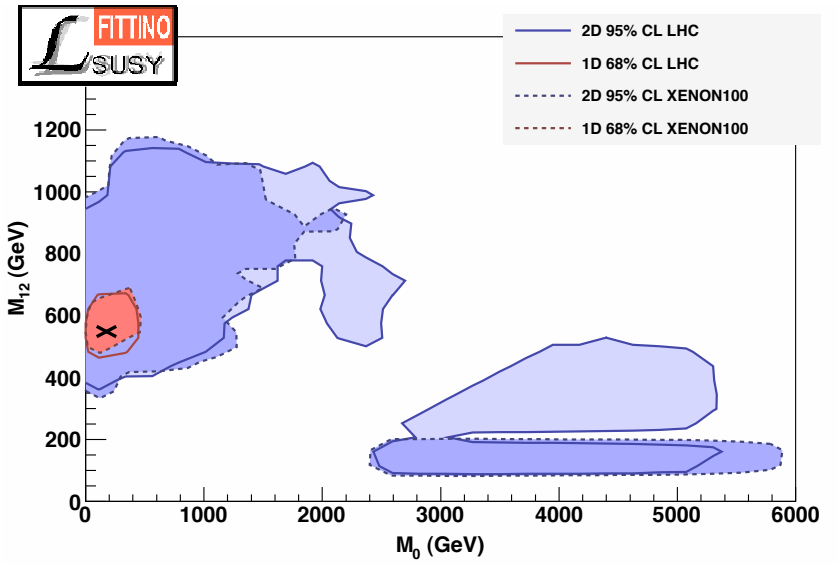

Figure 3.3: The two-dimensional M_0–$M_{1/2}$ plane from an earlier fit with and without the Xenon100 upper limit (Aprile et al. [2011]) is shown as an example to demonstrate the technique. Here, the 1σ and 2σ region are depicted as areas within the solid red and blue line for the fit without Xenon100 upper limit. The cross represents the best fit point, which is the point of the global minimum, χ^2_{min}, of the fit. All hidden dimensions are profiled, so that even though the result of the fit is projected into the M_0–$M_{1/2}$ plane, all parameters are taken into account.

This method has been used for all two-dimensional figures shown in Chapter 4. In order to monitor this technique, scatter plots have been made directly from the saved ROOT n-tuple file as a result from the Markov chain for comparison. These tests are shown later in Section 3.4.4. All figures of this manner resemble a fit of

all four model parameters. The two-dimensional representation is only a projection into the two dimensions of study interest. The best fit point, if given, is the point of the overall χ^2 minimum of the fit. The results of the global fits with `Fittino` and `AstroFit` are shown in Chapter 4.

3.3 Input from Particle Physics

In the analysis part of this thesis, input from particle physics, astrophysics and cosmology have been used. Since the implementation of the information from astrophysics and cosmology are a main part of this thesis and a major contribution from this work, they will be explained in the Section on `AstroFit` (Section 3.4) with a more detailed description of the choice of the observables and the technical devices. Here, I will specify the observables from particle physics that have been used for this study and the analysis within this thesis. They are provided within `Fittino` and are relatively similar to information from other global fit programs. For a better overview, all observables in total will be summarized once more at the beginning of the analysis Chapter (4). The observables contributed from particle physics are:

- Rare decays from B-mesons
- The anomalous magnetic moment of the muon
- Electroweak precision data from LEP, SLC and Tevatron
- Sparticle searches from LEP and LHC
- Mass limits on the Higgs mass or the measured Higgs mass from ATLAS, respectively

B-physics The study of flavor physics can deliver strong constraints to the CMSSM and other BSM models from the rare decay of B-mesons. For example, the decay $b \to s\gamma$ within $B \to X_s\gamma$ decays as a flavor changing neutral current (FCNC) process is highly suppressed in the SM. If branching ratios deviated from the SM prediction, it would be a clue for BSM physics where these processes could be enhanced. The LHCb experiment has acquired upper limits on the branching ratio of the $B_s \to \mu^+\mu^-$ processes from LHC runs with a total luminosity of 1.0 fb^{-1} (Aaij et al. [2012b]) that have been used in this analysis next to precision measurements on the branching ratios for $B \to \tau\nu$ and the $\text{BR}(b \to s\gamma)$ therein from the Heavy Flavor Averaging Group (Asner et al. [2010]). Another important constraint comes from B_s oscillations, a process where the meson changes into its antiparticle and back. New data is available from the LHCb experiment for the $B_s \to \mu^+\mu^-$ process that was not yet published at the beginning of this study (Aaij et al. [2012a]).

The anomalous magnetic moment of the muon The magnetic moment of the muon is defined as

BR($b \to s\gamma$)	$(3.55 \pm 0.34) \times 10^{-4}$
BR($B_s \to \mu^+\mu^-$)	$< 4.5 \times 10^{-9}$
BR($B \to \tau\nu$)	$(1.67 \pm 0.39) \times 10^{-4}$
Δm_{B_s}	$17.78 \pm 5.2\ \mathrm{ps}^{-1}$

Table 3.2: Measurements and bounds from branching ratios of rare B-decays and the $B_s\bar{B}_s$ oscillation frequency Δm_{B_s} as in Asner et al. [2010] and Aaij et al. [2012b], respectively.

$$\vec{\mu}_\mu = g_\mu \left(\frac{q}{2m} \vec{S} \right) \tag{3.10}$$

where m, q and $\vec{S}$ are the mass, charge and spin of the muon and g_μ is the gyromagnetic ratio. For muons and electrons as structureless spin-$\frac{1}{2}$ particles with charge $\pm e$, it is expected that $g_\mu = 2$. Due to radiative corrections where the particle is coupled to virtual fields, an anomalous magnetic moment can be defined as

$$a_\mu = \frac{1}{2}(g-2)_\mu \tag{3.11}$$

and is usually given in units of parts per million (ppm) (see Bennett et al. [2006]). Within the SM, the anomalous magnetic moment of the electron and muon can be predicted and probed with precision measurements as have been carried out by the LEP and TEVATRON experiments. The results of the measurements differ from the prediction (see Table 3.3), which can be interpreted as a sign for new physics and is thus included in global fits. The deviation of the anomalous magnetic moment of the muon from its SM prediction is most sensitive to new physics, exploring the energy range above 100 GeV. Furthermore, a_μ is correlated to the branching ratio BR($B_s \to \mu^+\mu^-$) in the CMSSM (Dedes et al. [2001]). In the fits, the deviation of the experimentally measured (exp) and the theoretically within the SM expected (SM) anomalous expected moment of the muon, $a_\mu^{exp} - a_\mu^{SM}$, has been used as input. It will be referred to as the $(g-2)_\mu$ observable or constraint hereafter. While the measurement of a_μ is unproblematic, there has been a debate on the accuracy of the SM prediction. Discrepancies occur in the interpretation of τ data compared to e^+e^- data (Davier et al. [2010]). As the latter have been argued to be theoretically better motivated, these have been used in the fit. Comparison tests have been made by leaving out the $(g-2)_\mu$ observable completely. The $(g-2)_\mu$ constraint disfavors the focus point region of the CMSSM and is therefore an important input.

Electroweak precision data Other low energy observables have been used in form of electroweak observables. As former fits with `Fittino` Z physics data have not shown any influence on the fit, they are not included here. Together with the SM gauge couplings and the mass of the top, bottom and charm quark as well as the τ-lepton, the Z mass has been used as a fixed input in the fit (see Bechtle et al. [2012]). Only formerly shown relevant constraints have been taken into account as observables, namely the measurement of the W-boson mass and the effective weak mixing

angle $\sin^2\theta_{\text{eff}}$. An overview over particle physics precision data is given in Beringer et al. [2012]. Table 3.3 replenishes the observable input from B physics in Table 3.2.

$a_\mu^{exp} - a_\mu^{SM}$	$(28.7 \pm 8.2) \times 10^{-10}$
m_W	(80.385 ± 0.015) GeV
$\sin^2\theta_{\text{eff}}$	(0.23113 ± 0.00021)

Table 3.3: Electroweak precision data used in all fits of this work. For all precision data, see Beringer et al. [2012].

Searches for sparticles Direct searches for supersymmetric particles at the LHC via jets + E_T^{miss} (as described in Section 2.4.3) can provide evidence for the existence of BSM particles. Most illuminating, both for SUSY and DM searches, are squark and gluino channels with a neutralino as stable particle, carrying away the missing energy.

$$\tilde{q} \to q\tilde{\chi}_1^0 \tag{3.12}$$

$$\tilde{g} \to qq\tilde{\chi}_1^0 \tag{3.13}$$

First results from LHC searches with no measurements of new particles provide important limits, i.e. limits in the squark–gluino plane (Aad et al. [2012]), that correspond to an exclusion of the h-resonance region and a restriction of large parts of both the co-annihilation regions and, most important, the funnel region and therefore the preferred lower region of the M_0–$M_{1/2}$ plane in the CMSSM framework. Upper limits have been derived from SUSY searches at the LHC from jets + E_T^{miss}.

Also included in the fit are limits on chargino masses and limits on the neutral and charged Higgs boson masses from LEP and Tevatron observations as well as upper limits on the lightest chargino from LEP (Abdallah et al. [2003]).

Bounds and measurements on the Higgs boson mass During the first setup for the study described in this thesis, there had not been significant signs of a Higgs boson from the LHC yet. The information for evidence of a neutral boson of mass ≈ 126 GeV found at the LHC arose during the first runs of the global fits for this work and has then been adopted. Later on, the signal of such a boson, assumed to be the lightest neutral Higgs boson and referred to in this work as such, has been confirmed with both the ATLAS and the CMS experiment (see ATLAS Collaboration [2012] and CMS Collaboration [2012]) with

$$m_h = 126.0 \pm 0.4(\text{stat}) \pm 0.4(\text{sys}) \text{ GeV, from the ATLAS Collaboration} \tag{3.14}$$

$$m_h = 125.3 \pm 0.4(\text{stat}) \pm 0.5(\text{sys}) \text{ GeV, from the CMS Collaboration} \tag{3.15}$$

Therefore, runs with both bounds on the Higgs mass as well as the observed mass from the ATLAS experiment have been performed. Since the information on

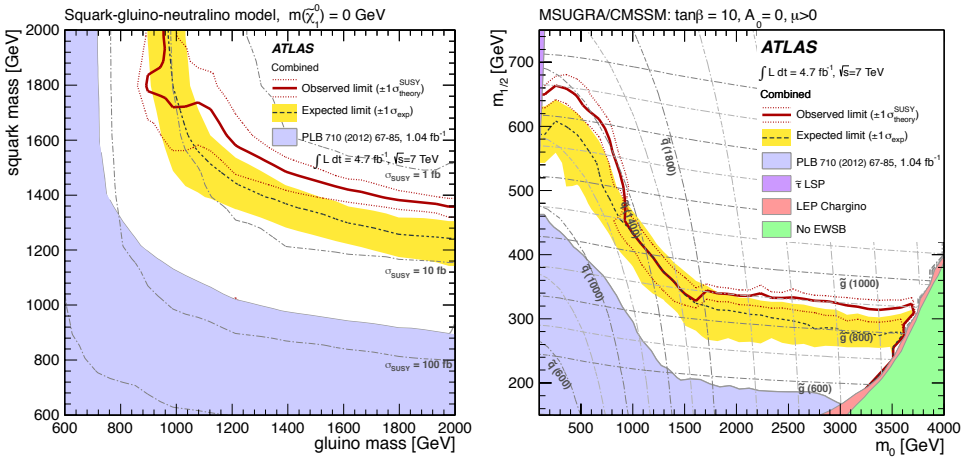

Figure 3.4: Limits on the squark-gluino plane from ATLAS searches and the corresponding regions in the M_0–$M_{1/2}$ plane of the CMSSM for a fixed $\tan\beta = 10$, $A_0 = 0$ and $sign\ (\mu) > 0$. Figures from Aad et al. [2012]. The limits are evaluated from LHC runs with an integrated luminosity of 4.7 fb$^-$1 and a center-of-mass energy of $\sqrt{s} = 7$ TeV. Information on present and former limits and exclusions are given directly in the Figures. The limits are also given coherently in terms of cross-sections of SUSY particles to give an estimate of the SUSY detectability at the LHC.

the Higgs boson had not been as well studied at the time of the setup, preliminary information from the ATLAS Collaboration of $m_h = 126 \pm 3$ GeV has been used. Bounds on the Higgs mass have been calculated with `HiggsBounds` (Bechtle et al. [2011]). With an algorithm inside `HiggsBounds`, the value for the 95% bound, i.e. upper and lower limit, is calculated individually for each model, which on the whole lies in the range of $114.5 < m_h < 130.5$ GeV.

Beside the information on the Higgs boson, the decay channels and branching ratios of the detection can give another important testimony to BSM physics if varying from the SM prediction significantly. First evidences on the Higgs boson existed from the $H \to ZZ \to 4l$-channel and the $H \to \gamma\gamma$-channel, and later on also from the $H \to WW \to e\nu_e\mu\nu_\mu$-channel. For example, the branching ratio of the $\gamma\gamma$-channel had been higher than expected, leaving to study whether this occurrence lies within the uncertainty range or may in fact be a sign for new physics. Thus, new runs with `Fittino` and `AstroFit` including the branching ratios and decay channels of the Higgs are already in progress.

3.4 AstroFit

AstroFit (Nguyen et al. [2012]), the core of this work, is an independent interface program to include astrophysical and cosmological information into global fits. In this way, AstroFit provides all necessary data autonomously, so that it can easily be taken into operation. In the creation process of the tool, two approaches seemed possible: One way could have been an inclusion of astrophysical data into one global fit program by extending the capacity of an existing global fit program with additional functions. In the close collaboration to the Fittino project, it was an idea that came to mind. However, in progress, it became evident that a self-contained tool would be much more expedient for many reasons. First, it was easier to deal with the technical implementation when working independently from the fit program. In this manner, a structure close to the program package DarkSUSY, from which many functions have been included for theoretical calculations, could be initiated. Also, the coordination of the project became easier, as consultations were kept within a smaller working group. Secondly, such a tool would be usable not only by Fittino, but could provide for a larger community working on BSM models, DM phenomenology and global fits. As a result, thirdly, this approach leads to an enhancement of discussion on observations, statistical methods, implementations and steps in the analysis of the outcome of a fit. The result of this is a unique and so far unrivaled tool which is easy to use and extend and constantly maintained. Alongside Fittino, there are other designated programs for global fits that fit particle data information to BSM models, such as Mastercode, GFitter, SuperBayeS, or BayesFITS. Recent studies of the CMSSM with these tools have been published, e.g. Buchmueller et al. [2012], Ludwig [2010], Martinez et al. [2009b], and Fowlie et al. [2012]. AstroFit therefore offers a complete and independent software that adds astrophysical components of BSM searches to the fit process of these programs.

As a long-term goal for the AstroFit project, the tool is developed to provide all available information from astrophysical and cosmological observation and experiments. As a first prospect, it has been utilized for a global fit with the global fit program Fittino, adding data from direct and indirect DM searches as well as the relic density observable from cosmology. All observables that are to be included in AstroFit are listed below:

- The WIMP-nucleon cross-section as well as constraints from underground DM direct detection experiments (e.g. Aprile et al. [2012], Aalseth et al. [2011], Ahmed et al. [2010], etc.)
- Information on high-energy photon fluxes from the Galactic center and Galactic halo region (e.g. Aharonian et al. [2006a] and Abramowski et al. [2011b])
- Photon flux upper limits from faint satellites and dwarf spheroidal galaxies (e.g. Ackermann et al. [2011], Abramowski et al. [2011a], Abramowski et al. [2012])
- Survey of the photon emission from different energy bands, ranging from radio emission to ultra-high energies (Zechlin and Horns [2012])

- Data on the positron flux or electron-positron flux and positron ratio from satellites, balloon-borne and ground-based instruments (e.g. Abdo et al. [2009])
- Antiproton spectra, for example measured with PAMELA (Adriani et al. [2010])
- High-energy neutrino data from neutrino experiments and limits from low-energy neutrinos (e.g. Mangano [2012])
- The relic density of CDM from WMAP (Komatsu et al. [2011])

In a first setup with `Fittino`, `AstroFit` has been tested with a few of these input parameters. The results on the DM study are shown and discussed in Chapter 4. Other results from the fit can be found in the publication (Bechtle et al. [2012]).

3.4.1 Structure and Functionality

Here, I will explain the structure and functionality of the program and its development. The structure of `AstroFit` is held as simple as possible for further extensions and potential users. It is written in FORTRAN code due to its close relation to the `DarkSUSY` package (Gondolo et al. [2002], Gondolo et al. [2004], Gondolo et al. [2010]), a library of functions covering a wide range of relevant theoretical calculations concerned with DM, for example all sorts of particle spectra and Ωh^2. Alternatively, the code could have been developed in C++, matching the `Fittino` program. However, since the interface to the fit program is held as punctual as possible in order to facilitate the stand-alone development of `AstroFit` and the bonding into the fit program, there were stronger arguments for using FORTRAN code. Moreover, other fit programs do not necessarily have to be written in C++, while the usage of `DarkSUSY` for calculating theoretical predictions will remain the first choice within `AstroFit` for its completeness in model-independent DM calculation and its constant maintenance, documentation and available support. Alternatively, functions from `MicrOmegas` (Belanger et al. [2010]) could be used for cross-checking results. In any case, due to the handling of particle spectra for SUSY model calculations via the SUSY Les Houches Accord (SLHA, Skands et al. [2004]), a cross-language management between FORTRAN and C++ becomes straightforward. The SLHA file contains all necessary information on models, masses and couplings and can be included into FORTRAN and C-based code alike.

Figure 3.5 illustrates the setup of `AstroFit`. On the left side, the program for the global fit, in this case `Fittino`, is shown. In each step of the minimization process, the spectrum file with the information on the predicted SUSY parameters is handed to `AstroFit` via SLHA files. From the given spectrum file, subroutines within `AstroFit` have been designed to calculate the theoretical prediction for astrophysical observables with the usage of various `DarkSUSY` functions. A $\Delta\chi^2$ value for each observable is calculated with special functions in `AstroFit` for the cases of data points, signal regions and upper limits, using experimental data stored in simple ASCII files in a designed location. In the following, the `AstroFit` program will be explained in more detail.

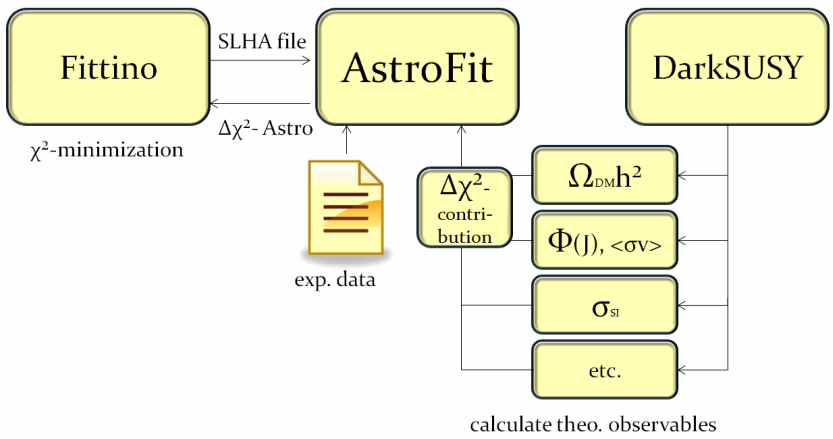

Figure 3.5: Flowchart of the `AstroFit` interface program. On the left side, the program for the global fit, in this case `Fittino`, is depicted. The SLHA file is handed to `AstroFit` with the information on the particle spectrum. The theoretical value for each observable is calculated in the according `AstroFit` subroutine with the use of various `DarkSUSY` functions from the SLHA file. The theoretical prediction is then compared with the experimental value stored in the data file in order to calculate the $\Delta\chi^2$- contribution from each observable. The result is handed to the fit program in each step of the minimization process.

Storage of Experimental Data

The experimental data is stored in data files of ASCII format in one designated directory, simplifying the augmentation of the data pool without the need of programming effort. The data is accessed by the assigned subroutines and functions via another function, named `afreaddatafile` that is computed to read out the data from the files, removing blanks and comments and identifying the physical information. The read-in function recognizes keywords and the following data. For cases where the structure of the data file has been violated, error messages occur in the test program. In this manner, it is easy to add further experimental data into a similar ASCII file without knowledge of the code itself, and anyone working with `AstroFit` can add or update information from experiments without interfering with the actual program. The difficulty when using ASCII files instead of FORTRAN files to manage the storage of data lies in the possible errors that could occur at very late notice. If the structure of the data file is kept correctly in terms of the keywords, but the number of blanks does not match the precise prescription, it takes some effort to notice an error, which is only possible by evaluating the test result. It then takes additional effort to find the source of the miscalculation. This has occurred a few times before special attention was brought to this matter, so that all data files are now carefully tested immediately after their introduction. An example of an `AstroFit` data file is given in the Appendix.

Input File

The input file is the steering file for `AstroFit` in which the information to use and the way of calculating the theoretical predictions is defined by the user. It is divided

into three parts:

1. Relic density
2. Indirect searches
3. Direct detection

For each section, there are flags (labeled as FLAG) to activate the calculation. For instance, the relic density calculation, which can take up to a few seconds per calculation if done with the highest accuracy, can be left out. In this case, the flag for the relic density would simply be enabled, so that only the $\Delta\chi^2$ contributions from direct and indirect detection are calculated. In each section, additional flags can be put, for example to decide which contributions from indirect detection should be taken into account, or in case of direct detection whether to use the information from the spin-dependent or spin-independent elastic WIMP-nucleon scattering cross-section. Some of these are already implemented, others planned for the near future.

Relic density options	Comments
FLAG relic	Determines whether the calculation of the relic density is activated
HOW relic	Options between 1 and 3. The default (1) is a fast calculation including co-annihilations, while option (2) is fastest, leaving out co-annihilations. Option (3) takes the longest time but is the most accurate, considering all co-annihilations in the calculation.
DATA	States the measurement of the relic density with experimental errors directly and can be changed in the input file.

Table 3.4: Options how to calculate the relic density in `AstroFit`

Furthermore, there are additional options called HOW that address the way in which the theoretical prediction for the according observable is to be calculated. As mentioned, the relic density calculation can take relatively long if calculating all co-annihilations accurately. In `DarkSUSY`, there are several options for the speed of the calculation at the expense of the fidelity. By the number following the HOW, the calculation option is appointed, with the default being the next to best, that is most precise, option.

In each part, experimental data can be chosen by the option DATA which addresses the corresponding data file from storage. For example, the standard input file contains the data options using data from the WMAP measurement of the relic density, the photon flux upper limits from the Fermi-LAT joint likelihood analysis of ten dwarf spheroidals and ultra-faint satellites in the $b\bar{b}$-channel, and the upper limits on the spin-independent elastic scattering cross-section σ_{SI} from the Xenon100 collaboration from the 2012 data (for more information on the input observables, see 3.4.2). All fully and partially implemented options are listed in Tables 3.4, 3.5 and 3.6. An example of the `AstroFit` input file can be found in the Appendix.

Indirect detection options	Comments
FLAG nu	Activates neutrino-related calculations. This option is not fully implemented yet.
FLAG pbar	Activates positron flux calculations. This option is not fully implemented yet.
FLAG photon	Activates the calculation of photon fluxes and upper limits in general.
FLAG photon_gc	Takes into account photon flux information from the Galactic center region.
FLAG photon_gh	Takes into account photon flux information from the Galactic halo.
FLAG photon_dSph	Takes into account photon flux information from dwarf spheroidal galaxies and ultra-faint satellites.
FLAG photon_sv	Activates the stand-alone calculation of the thermally averaged velocity-weighted WIMP annihilation cross-section $\langle \sigma v \rangle$, as this is the form in which many papers on indirect detection choose to present their results.
HOW photon_sv	Options between 0 and 4. The default (0) calculates all photon flux final states, while (1) calculates annihilation into $b\bar{b}$, (2) into $\tau^+\tau^-$ and (3) into W^+W^-. Other final states can be included if necessary. Currently, this HOW option is still named HOW photon_dSph, but as it actually concerns only the final states and not the observation object, this will be changed shortly.
DATA	Currently, data files with photon flux upper limits and $\langle \sigma v \rangle$ from dwarf spheoridal galaxies observed with the H.E.S.S. and Fermi-LAT instruments with different final states and the stacked analysis from Fermi-LAT can be included to the user's choice.

Table 3.5: Options for calculations towards indirect searches in `AstroFit`. The options for neutrino, antiproton and positron fluxes are still to be added.

Direct detection options	Comments
FLAG direct	Activates the subroutine for direct detection calculation.
DATA	For the moment, information on σ_{SI} are available from the experiments DAMA/LIBRA, CoGeNT, CRESST and Xenon100.

Table 3.6: Options for calculations towards direct DM detection in `AstroFit`. Spin-dependent cross-section calculations could be a next extension in this sector.

Fittino Interface

As mentioned above, the interface is handled as uncomplicated as possible with minimal contact points, so as to have clear task areas and avoid any confusion. Hence, all calculations and processes are contained in `AstroFit`. Eventually, both the result

on the theoretically calculated values and the $\Delta\chi^2$-contributions from each observable are written into a text output file in the desired manner. An example of such an output file is given in the Appendix. In `Fittino`, the output can be read out and used in the minimization process by adding the $\Delta\chi^2$-contributions from each astrophysical observable to the fit process and store the information on the theoretical prediction for each model in the ntuple-file (Fittino storage file for a fit). Independently from the flags set in `AstroFit`, flag options have also been created for the `Fittino` input file. This precaution allows a higher flexibility, so that even though all available calculations are addressed in `AstroFit` and the information is made entirely available in `Fittino`, not all observables necessarily have to be used in the fit. For example, the information from indirect detection could be left out in the fit and hence have no influence to the result, while the output for the calculation is still stored in the ntuple-file and can be used in the analysis and for other tests.

3.4.2 Observables from Astrophysics and Cosmology

Here, I will refer to the DM-related observables used in `AstroFit`. The data for the observables come from DM experiments and are taken from the cited publications. The way of calculating the theoretical prediction is described for each observable. For all input information, a specially designed subroutine called `afreadinputfile` is in charge for handling the information from the data file, the theoretical calculation, and passing the results to the output file. The $\Delta\chi^2$-calculation is accomplished by discrete functions addressed in these subroutines and will be explained later.

Relic Density

As described in Section 2.3.2, the relic density of CDM is the most constraining observable from astrophysical and cosmological observation and is calculated in the subroutine `afchi2relic`.

The measurement of the relic density excludes large parameter regions of the CMSSM and constrains the relevant regions of interest to the bulk region, the focus point region, the co-annihilation region and the funnel region. The theoretical prediction in `AstroFit` is calculated directly by calling the specified `DarkSUSY` function `dsrdomega`. The experimental value is written into the input file, and with the according χ^2-function, the χ^2 is calculated, and both the $\Delta\chi^2$-contribution as well as the theoretical prediction of Ωh^2 for the according model spectrum are written into the output file. For this study, the information of the observed relic density from Komatsu et al. [2011] provided by NASA [2011] has been used:

$$\Omega h^2 = 0.1123 \pm 0.0035 \tag{3.16}$$

This value corresponds to observations from WMAP with additional BAO angular diameter distance measurement and local measurement of the Hubble constant.

Photon Fluxes

As discussed in Section 2.4, photon fluxes and upper limits on photon fluxes can add important constraints to DM models. For model independent comparison, it is also customary to give upper limits on the velocity-weighted DM particle annihilation cross-section $\langle \sigma v \rangle$. Enhancing effects could make these fluxes effectively higher, e.g. the Sommerfeld effect (e.g. van den Aarssen et al. [2012], Kuhlen [2010]), Internal Bremsstrahlung (e.g. Bringmann et al. [2012]), and clumps in the DM distribution (e.g. Zechlin et al. [2012]). These effects will not be considered here, but the option of enhancement factors and their effects has been tested in `AstroFit`. There are different observation regions for photon fluxes from DM annihilation. The Galactic Center is a region favored for observation due to its proximity and supposedly high DM density with the disadvantage of a high gamma-ray background (Aharonian et al. [2006a]. The Galactic Halo region can be observed to lower the background without too much loss of the high-density advantage (Abramowski et al. [2011b]. Promising observation targets for gamma-ray searches from DM annihilation are also dwarf spheroidal galaxies and ultra-faint satellites (both referred to as dSPhs in this work). They benefit from a low astrophysical gamma-ray background and a high mass-to-light ratio of order 100-1000 from the absence or near absence of active star formation and gas content (Scott et al. [2010]). Located in the Milky Way, they are in reasonably good observation distance. As dSPh had been the most intriguing and among the most discussed objects for DM observation at the beginning of this study and provided the best model-independent flux upper limits, observations from dSphs have been implemented in `AstroFit`, changing in time to match the most recent experimental results. This study has been conducted with the H.E.S.S. observation of the Carina and Sculptor dSphs (Abramowski et al. [2011a]) and the at that time available Fermi-LAT observations of fourteen dSphs (Abdo et al. [2010]). To choose the most conservative approach, the derived photon flux upper limits for a branching ratio of purely $b\bar{b}$ final states has been used. The lowest derived flux for a dSPh was chosen respectively from both publications, which was the derived flux from the Carina dSph from the H.E.S.S. observation and the derived flux from the Ursa Minor dSPh from the Fermi-LAT observation.

The most constraining upper limits at the beginning of the analysis had been on the velocity averaged pair annihilation cross-section in the $b\bar{b}$-channel from Fermi-LAT observations on the controversial dSPh Segue 1 (Scott et al. [2010]), which had been used at the beginning. In the process of this study, more recent upper limits have been provided by a joint-likelihood analysis of the Fermi-LAT collaboration, combining the observations from ten different dSphs (Ackermann et al. [2011]), which have since then been used additionally.

All photon-related calculations are taken care of in the subroutine `afchi2photon`. For calculating the flux upper limits, the formula from 2.4 is specified to processes resulting in photons from DM annihilation and used in the photon flux subroutine of `AstroFit`, so that

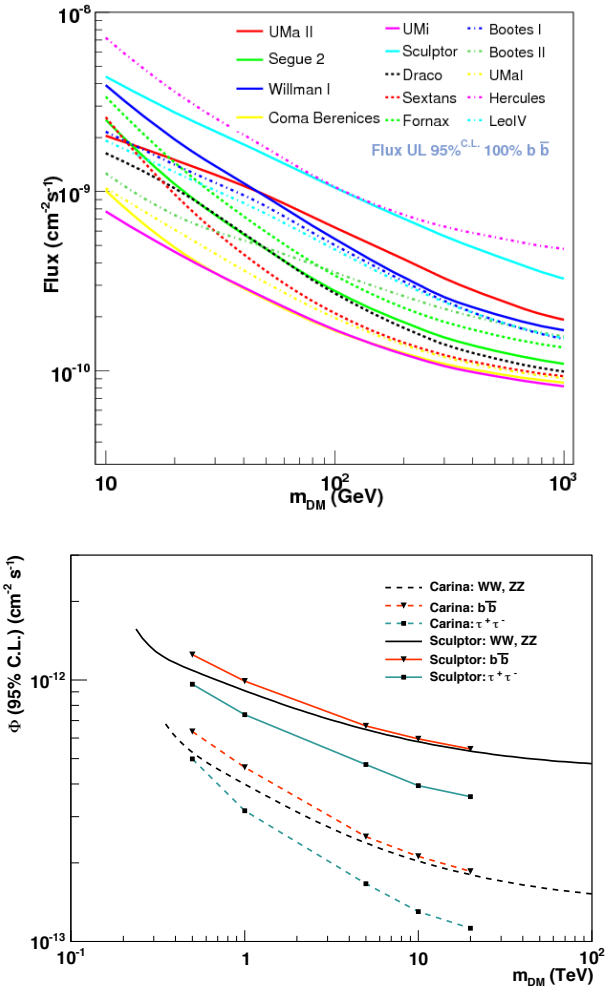

Figure 3.6: Above: Derived photon flux upper limits as function of the WIMP mass from Fermi-LAT observation of 14 dSPhs, assuming a branching ratio of 100% into $b\bar{b}$ (Abdo et al. [2010]). Below: Photon flux upper limits as function of the WIMP mass for different decay channels derived from observations of the Carina and Sculptor dwarf galaxies with the H.E.S.S. IACTs as in Abramowski et al. [2011a] are shown on the left side. Note the different scales on the abscissa, complementing each other. The fluxes derived from Fermi-LAT observaton are well in the GeV range while the derived fluxes from H.E.S.S. observation begin in the regime of hundreds of GeV and reach into tens of TeV.

$$\frac{\mathrm{d}\Phi(E_\gamma \Delta\Omega)}{\mathrm{d}E_\gamma} = \frac{\mathrm{BF}}{4\pi} \frac{\langle \sigma_f v \rangle}{2m_\chi^2} \frac{\mathrm{d}N_\gamma}{\mathrm{d}E_\gamma} \times J(\Delta\omega)\Delta\Omega \tag{3.17}$$

where J is

$$J(\Delta\Omega) = \frac{1}{\Delta\Omega} \int_{\Delta\Omega} \mathrm{d}\Omega \int_{l.o.s.} \rho_\chi^2(l)\mathrm{d}l \tag{3.18}$$

with a possible boost factor BF which is per default set to BF = 1. This equation has been computed in `AstroFit` using several different `DarkSUSY` functions and additional input. While the thermally-averaged cross-section for various final states $\langle \sigma_f v \rangle$ (e.g. for $f = b\bar{b}$, $\tau^+\tau^-$, W^+W_- or γs in general) and the differential number

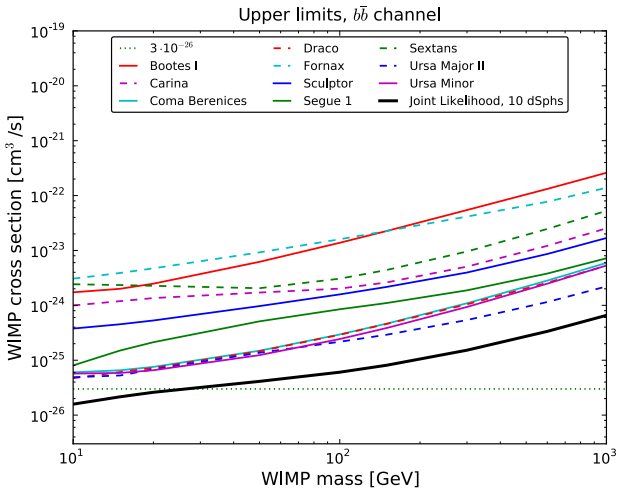

Figure 3.7: Derived WIMP cross-section from the joint-likelihood analysis of ten observed dwarf spheroidals (Ackermann et al. [2011]) as function of the WIMP mass.

of photons produced per annihilation and energy $\mathrm{d}N_\gamma/\mathrm{d}E_\gamma$ can be calculated with the separate `DarkSUSY` functions `dshaloyield` and `dssigmav`, the mass of the neutralino m_χ can be directly taken as a variable from `DarkSUSY`. Finally, the J-factor with the model-dependent DM density ρ_χ^2 along the line of sight and the solid angle is used directly according to the publications and is stored as such in the data file. As the H.E.S.S. upper limits have been set to be comparable to the Fermi upper limits, the same profile and J-factor have been used (Abdo et al. [2010], Abramowski et al. [2011a]).

Using the `DarkSUSY` function, the total photon spectrum is calculated as the sum of all three described processes from Section 2.4.1, i.e. secondary photons, photons from IB and photons from the loop-suppressed annihilation of two neutralinos resulting in a line spectrum.

$$\frac{\mathrm{d}N^{\gamma,total}}{\mathrm{d}x} = \sum_f B_f \left(\frac{dN_f^{\gamma,sec}}{\mathrm{x}} + \frac{dN_f^{\gamma,IB}}{\mathrm{x}} + \frac{dN_f^{\gamma,line}}{\mathrm{x}} \right) \tag{3.19}$$

with the branching ratios B_f into the annihilation channel f, $x = 2E_\gamma/\sqrt{s} = E_\gamma/m_\chi$ and the center of mass energy s (Bringmann et al. [2008], Gondolo et al. [2004]). As the IB contribution to the total flux is only of consequence at higher energies ($E \geq 1/100\, m_\chi$) and takes more time to calculate at $E < 1/100\, m_\chi$ without notable contribution, the default version in `AstroFit` takes into account the entire calculation with all three contributions only for the cases where $E \geq 1/100\, m_\chi$. In cases of $E < 1/100\, m_\chi$, the IB contribution is left out in order to speed up the calculation.

The flux upper limits and the upper limits on the velocity-averaged pair-annihilation cross-section are stored in an `AstroFit` data file and have been addressed from the input file. Results on the calculated fluxes and the $\Delta\chi^2$-contributions are stored in the output file.

Direct Detection Signals

The spin-independent cross-section for a WIMP-nucleon scattering σ_{SI} is derived within the `AstroFit` subroutine `afchi2direct`. Recalling the equations from Section 2.4.2, it is shown that the spin-independent part for the cross-section per nucleus can be expressed as

$$\sigma_{\mathrm{SI},N} = \frac{4\mu_N^2}{\pi}\left[Zf_{\mathrm{p}} + (A-Z)f_{\mathrm{n}}\right]^2 . \tag{3.20}$$

To derive the cross-section for a nucleon within the nucleus, the approximation $f_{\mathrm{p}} \approx f_{\mathrm{n}}$ is made, as in Cerdeno and Green [2010] and Schnee [2011], so that

$$\sigma_{\mathrm{SI},x} = \frac{4\mu_x^2}{\pi} f_x^2 , \tag{3.21}$$

where x is either a proton or a neutron, μ_x is the derived mass for a WIMP-nucleon system and f_x is the form factor for a nucleon, which can then be expressed as

$$f_x = \pm\sqrt{\frac{\pi}{4}\sigma_x}\frac{1}{\mu_x} . \tag{3.22}$$

Making use of this relation and the relation between a nucleon and the entire nucleus so that

$$\sigma_{\mathrm{SI},N} = \sigma_x \frac{\mu_N^2}{\mu_x^2} A^2 \tag{3.23}$$

the equation above can be expressed as:

$$\sigma_{\mathrm{SI},N} = \mu_N^2\left[Z\sqrt{\sigma_{\mathrm{p}}}\frac{1}{\mu_{\mathrm{p}}} \pm (A-Z)\sqrt{\sigma_{\mathrm{n}}}\frac{1}{\mu_{\mathrm{n}}}\right]^2 . \tag{3.24}$$

The spin-independent cross-section per nucleon recoil in form of

$$\sigma_{\mathrm{SI},x} = \frac{\mu_x^2}{\mu_N^2}\frac{1}{A^2}\sigma_N \tag{3.25}$$

can finally be converted into the form

$$\sigma_{\mathrm{SI,nucleon}} = \frac{\left(Z\sqrt{\sigma_{\mathrm{p}}} \pm (A-Z)\sqrt{\sigma_{\mathrm{n}}}\right)^2}{A^2} \tag{3.26}$$

with the elastic-scattering cross-section of a WIMP with a proton σ_{p} or neutron σ_{n}, respectively. These can be calculated directly with the designated `DarkSUSY` functions. Note that the $\pm$ could stand in front of the $Z\sqrt{\sigma_{\mathrm{p}}}$ part as well, with a plus sign between the two expressions, so that both adding or subtracting the two expressions is a possible solution. There are other ways to express the spin-independent scattering cross-section per nucleon, but this form is easiest to compute with `DarkSUSY`. A cross-check has been made using equations as suggested in Cerdeno and Green [2010] with similar results.

To allocate the correct atomic and mass number Z and A of the target material, which could also be a compound, the information on the material is stored in the data

file, and a function within `AstroFit` computes the right combination and number of Z and A of a target material before attending to the calculation of the cross-section. The equation is computed by using the information on Z and A and the `DarkSUSY` function `dsddgpgn` for the calculation of the WIMP scattering cross-section on a nucleon. The same function also calculates the spin-dependent elastic scattering cross-section and could be used for calculating the latter within `AstroFit` in future.

Both signal regions from DAMA/LIBRA (Bernabei et al. [2010]) and CoGeNT (Aalseth et al. [2011]) and upper limits on σ_{SI} from Xenon100 (Aprile et al. [2011]) have been used in this study. Predictions for later Xenon100 phases with longer run times (referred to as Xenongoal) and a higher fiducial mass of one ton (Xenon1T) (see Aprile et al. [2012]) have also been included. Formerly declared signal regions from the CRESST collaboration (Angloher et al. [2012]) have also been added optionally in `AstroFit`, but have not been taken into account in the analysis, since the results are not significant any longer. A WIMP of mass $O(10\,\mathrm{GeV})$ would be aberrant from the CMSSM expectation of $O(100\,\mathrm{GeV})$, but possible in other SUSY models (Fitzpatrick et al. [2010]).

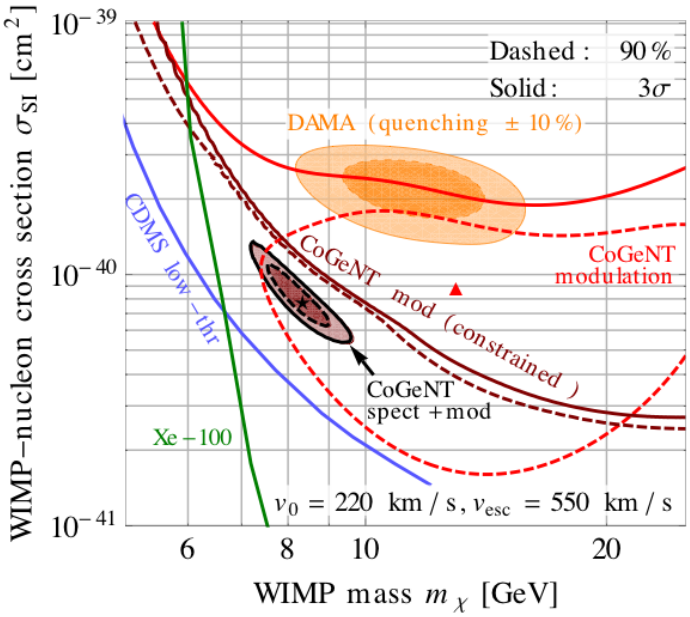

Figure 3.8: Figure showing the 3σ and 90% c.l. interpretation of signal regions from DAMA/LIBRA and CoGeNT for the WIMP-nucleon spin-independent scattering cross-section in terms of the WIMP mass due to anomalies in the observed data. Regions occur for WIMP masses of $\sim$ 10 GeV at cross-sections of $O(10^{-40})$ cm^2. Figure from Fox et al. [2012] and references therein. These signal regions stand in contradiction to the upper limits procured by CDMS and Xenon100 (as shown in Aprile et al. [2012]).

The scattering cross-section is highly complementary. Future gamma-ray constraints in the TeV range, e.g. from IACTs like CTA or upper limits on sparticle masses at the LHC, can put constraints on the detection regions of direct detection instruments or explore parameter regions beyond. Regions in parameter space attain-

able by all three detection methods can be tested thoroughly likewise.

In the calculation of σ_{SI}, large systematic uncertainties of $\sim 20\%$ are possible and stem from the QCD pion-nucleon sigma-term, $\Sigma_{\pi N}$ (Pavan et al. [2002]). A justified treatment of these theoretical uncertainties is therefore necessary. This has been attended to by adding such an uncertainty directly to the `DarkSUSY` calculation of the form factor, as this is the quantity that is affected by the uncertainty and thus impacts the calculation of the cross-section. The effect on the σ_{SI} calculation resulted in an uncertainty of up to 50% which has been taken into account in the analysis. The calculated theoretical prediction for the scattering cross-section is stored in the output file with the according $\Delta\chi^2$.

3.4.3 Calculation of Chi-Squared

The $\Delta\chi^2$-contribution from each observable is calculated according to the form of the observable. In general, there are different types of provided measurements. The relic density for example is an observable with a measured value and a given statistical uncertainty on the measurement. Some flux spectra from indirect detection could also be given as data points with uncertainties. Measurements from direct detection are usually given in contours of containment regions, for example 1σ and 2σ, or in confidence levels, for example 90% and 95%. Sometimes a best fit point in the inner region is given additionally. If no measurement has been found in a survey, bounds in form of upper or lower limits or both, respectively, can be set for an observable. These bounds are also usually given in terms of the standard deviation σ from a Gaussian distribution or in terms of percentage of confidence level. In DM-related searches, upper limits are for instance given on photon fluxes or on the spin-independent elastic scattering cross-section in direct searches. As observables are usually given in one or the other of these three forms, it is practical to have a separate sector in `AstroFit` that takes care of the corresponding $\Delta\chi^2$ and that is used in each subroutine when according to need. For all three cases,

1. measured values with uncertainties
2. given confidence intervals
3. upper limits on observables,

a function has been designed to handle the χ^2-calculation individually. The development of the χ^2-functions in `AstroFit` with statistical background is thoroughly covered in the bachelor thesis of Nils Plambeck (Plambeck [2011]).

Treatment of Data Points

Data points, for example the relic density of CDM, are observables that can be directly measured and have a distinct value with possibly a given statistical uncertainty to the measurement or a systematic uncertainty to the prediction. Momentarily, only the relic density of CDM is treated as a data point observable. In future, measured particle fluxes also fall under the category of data points. These are calculated with

the same formula as shown in Chapter 3. For better narration, I will refer to the measured values from observation and experiments as O_{obs} and to the theoretical predictions for the same quantities computed with `AstroFit` as O_{theo}.

$$\chi^2 = \sum_{i=1} \left(\frac{O_{obs,i} - O_{theo,i}}{\sigma_{exp,i}} \right)$$

The treatment of a data point is straightforward. The observed value is taken from the according `AstroFit` data file. The uncertainty is also given there. The calculation for the theoretical value is done within the according subroutine from the information of the spectrum file.

Treatment of Confidence Intervals and Upper Limits

When applying the χ^2-statistics to upper limits or confidence intervals, a Feldman and Cousins (Feldman and Cousins [1998]) approach is applied in `AstroFit`. Upper limits can be given in percentage or in terms of σ, based on the Gaussian distribution. A Gaussian (or normal) distribution is a continuous probability distribution that accounts for the description of numerous distributions of real measurements and follows a bell-shaped curve. From the probability density function

$$f(x,\mu,\sigma^2) = \frac{1}{\sigma\sqrt{2\pi}} e^{-\frac{1}{2}(\frac{x-\mu}{\sigma})^2} , \tag{3.27}$$

the integral of the normal distribution is given by

$$F(x) = \int_{-\infty}^{x} f(x',\mu,\sigma^2)\mathrm{d}x' . \tag{3.28}$$

with the mean or expectation value μ and the standard deviation σ. For a standard (or unit normal) distribution with $\mu = 0$ and $\sigma = 1$ for a variate X (Arens et al. [2008]), it takes the form:

$$f(x) = \frac{1}{\sqrt{2\pi}} e^{-\frac{x^2}{2}} \text{ for } X \sim \mathcal{N}(0;1). \tag{3.29}$$

The factor $\frac{1}{\sqrt{2\pi}}$ acts as an integration constant, so that the area under the bell curve equals 1. The density function for a standard distribution is commonly denoted as $\varphi(x)$, while the distribution function is betokened $\Phi(x)$. For each x, the surface area is conventionally computable in many programs, and tables are available. For a general calculation of the χ^2 from any given upper limit, an `AstroFit` function based on the incomplete gamma function (shown below) is in charge for computing the right σ value for each given confidence level. This function is called `afigamma`. If the confidence limit is given in terms of σ already, the function is not needed. If a confidence limit is given in percentage, it converts the value so that it takes the general form of $X\sigma$. The incomplete gamma function within `AstroFit` has been implemented according to Press et al. [1992]. A gamma function is defined as

$$\Gamma(x) = \int_{0}^{\infty} t^{x-1} e^{t} \mathrm{d}t . \tag{3.30}$$

If choosing limits from x to infinity, an upper incomplete function is sufficient:

$$\Gamma(a,x) = \int_x^\infty t^{a-1} e^t \mathrm{d}t \ . \tag{3.31}$$

With the Γ value, in relation to the σ of a standard deviation, the χ^2-calculation can be done, assuming the measurements follow a Gaussian distribution or a Poisson distribution with sufficiently large data samples. Astrophysical events may follow a Poisson distribution instead of a Gaussian distribution. A Possion distribution can be expressed as

$$P(X = k) = \frac{\lambda^k}{k!} e^{-\lambda} \ , \tag{3.32}$$

with the variable X parameter λ. For large numbers of λ of $O = (10)$, a Gaussian distribution can be approximated, so that the calculation within `AstroFit` still applies.

$X\sigma$ standard deviation	Percentage of confidence level	c_i for $n = 1$	c_i for $n = 2$
1 σ	68.27%	1	1
1.645 σ	90%	2.70	4.6
1.960 σ	95%	3.84	6.0
2 σ	95.45%	4	6.18
2.576 σ	99%	6.64	9.2
3 σ	99.73%	9	11.83

Table 3.7: Table with confidence levels given in terms of σ as calculated from the `afigamma` function. The according percentage of confidence level is shown in the second column. The corresponding c_i-values, necessary for the $\Delta\chi^2$-calculation within `AstroFit` is given in the third column for one parameter ($n = 1$) and in the fourth column for two parameters ($n = 2$). Further explanation is given in the text.

Table 3.7 shows the calculation within the `afigamma` function. While in cases of data points, the χ^2- calculation is simple, for upper limits and signal regions the `afigamma` function is needed as an intermediate step to compute the $\Delta\chi^2$-contribution from an observable. From here, the calculation can be done with the regular subroutine in `AstroFit` that is in charge of the χ^2-calculation. How this is done is described in the next to paragraphs for both cases of upper limits and confidence regions.

Treatment of upper limits If an upper limit is given, this corresponds to a non-detection. Thus, the expected value of the observable is 0. The given confidence level indicates the probability of the statement that there has been no observation to be true. Hence the $\Delta\chi^2$ calculation can be written as

$$\Delta\chi^2 = \left(\frac{0 - O_{theo}}{\sigma}\right)^2 = \left(\frac{O_{theo}}{\frac{X_{c.l.}}{\sqrt{c_0}}}\right)^2 = c_0 \left(\frac{O_{theo}}{X_{c.l.}}\right)^2 \ . \tag{3.33}$$

$X_{c.l.}$ being a point on the given upper limit on the same orthogonal line to the x-axis as the theoretical prediction for the observable O_{theo}, and c_0 being a specific

value depending on the confidence level or the standard deviation σ corresponding to the upper limit which can be taken from Table 3.7, where c_i for $n = 1$ resembles the c_0 from the equation. It can be easily noted that c_0 takes the number of $(X\sigma)^2$. The `afigamma` function has been implemented to calculate the c_0-value for any percentage, therefore a very exact χ^2 for any given form of confidence level from the experimental result or observation can be computed. This method of handling upper limits is more appropriate than the treatment as a step function at early stages of `AstroFit`, as it deploys the proper χ^2-distribution and makes its conduct consistent with that of other observables. In Figure 3.9, as a generic example, the quadratical increase of $\Delta\chi^2$ is shown in comparison to the behavior of a step function.

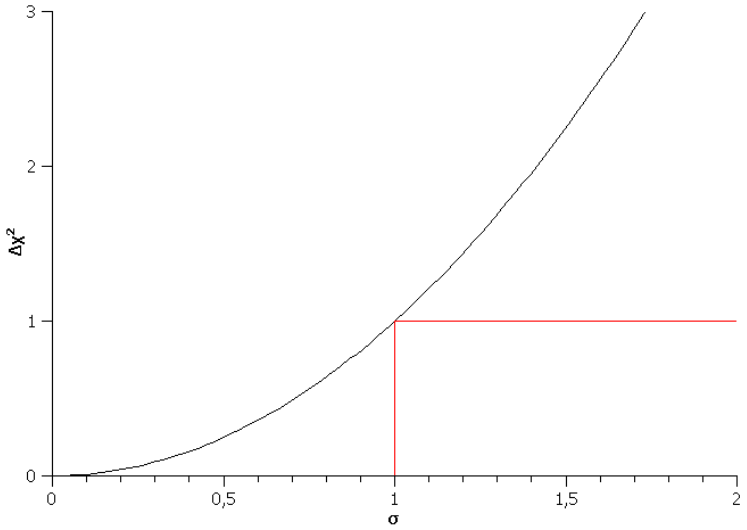

Figure 3.9: Appropriate treatment of quadratically increasing $\Delta\chi^2$-contribution compared to a step function at early stages of `AstroFit`.

In the calculation of a $\Delta\chi^2$-contribution from an upper limit observable, first the theoretical value is computed as described above. Points of the upper limit are stored in the data file. As the points do not necessarily match the x-value of the theoretical calculation exactly, yet the points are given in very close proximity from one another, an interpolation is made with a simple 'min-med-max' function. Once the right x-value is found, it is checked whether the point is above or below the limit. If the point is directly on the limit, the right χ^2 is given by the percentage of the limit. If the point is above, the correct $\Delta\chi^2$-value is found by quadratically extrapolating from the given limit with reference to zero on the axis. If the point lies below the limit, it is either possible to assign a χ^2 of zero, arguing that anything below the limit can be counted as background and therefore no measurement, or to interpolate and take the according $X\sigma$ value. A visual example is given in Figure 3.10. As an example, the upper limit from latest Xenon100 data (Aprile et al. [2012]) has been used. If the calculated value lies above the limit in the σ_{SI}–m_χ plane (with m_χ being the WIMP mass), the $\Delta\chi^2$ is calculated as demonstrated in Figure 3.10. The c_0-value at the

90% confident level (marked a circle) is calculated by the `afigamma` function within `AstroFit`. From the x-axis, where the $\Delta\chi^2$ would be zero, to the upper limit, a line is drawn. The line is elongated from the upper limit to the point from the theoretical prediction. As the c_0-value is known and therefore the $\Delta\chi^2$-value at the limit, the $\Delta\chi^2$ for the theoretical point can be calculated by using the ratios of the two lines.

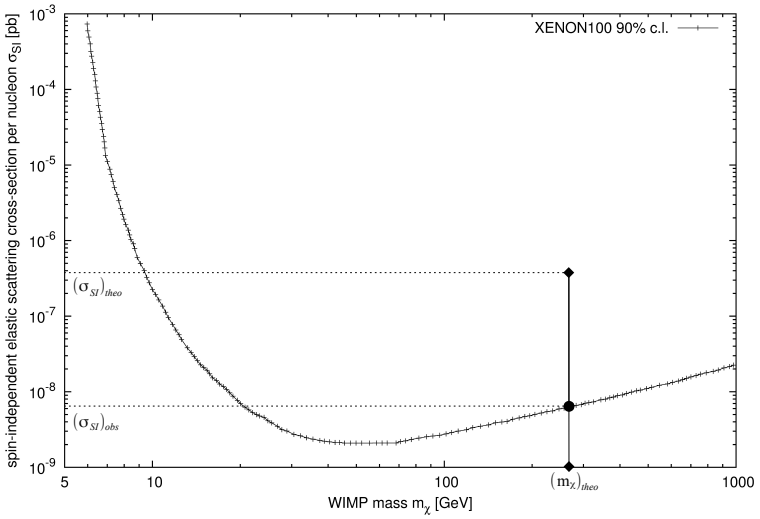

Figure 3.10: Figure demonstrating the $\Delta\chi^2$-calculation for upper limits. $(\sigma_{\mathrm{SI}})_{theo}$ is the theoretically predicted value for σ_{SI} for a given WIMP mass $(m_\chi)_{theo}$, while $(\sigma_{\mathrm{SI}})_{obs}$ is the value from the experimental upper limit according to this WIMP mass. Further explanation is given in the text.

Treatment of confidence intervals Confidence intervals (or signal regions) are evaluated analogically to upper limits. For two given confidence regions, the c_i-values (similar to the c_0-value of upper limits, but describing a confidence interval of a signal) are calculated with the `afigamma` function. The calculated theoretical value for the observable can be

1. inside the inner containment region,
2. in between the two given containment regions,
3. outside the two containment regions or
4. exactly on one of the borders of the given confidence interval.

In the last case, it is easy to attribute the corresponding $\Delta\chi^2$, as it is analog to the case of upper limits, where the upper limit relates to a certain c_0-value and the according $\Delta\chi^2$-contribution. The c_0-value determines the confidence level on the

border of a given containment region. In the case of signal regions, one merely needs to mind the fact that it is a two-dimensional scenario instead of a one-dimensional case, so that $c_i, i = 0,1$ is given in Table 3.7 in the fourth column for $n = 2$. The χ^2-calculation then takes the form

$$\Delta\chi^2_n = \left(\sqrt{c_0} + (\sqrt{c_1} - \sqrt{c_0})\frac{d_{01}}{d_{12}}\right)^2 , \tag{3.34}$$

summing over the two components of the plane (for instance the spin-independent scattering cross-section σ_{SI} and the WIMP-mass m_χ in the direct detection plane) expressed in the theoretical observable with $n = 2$ for the two-dimensional scenario, while the observed value is replaced by c_i and $X_{c.l.}$. c_i would take the value for two parameters.

In case the theoretical point O_{theo} lies outside both regions, a line is drawn perpendicular to the inner region, thereby crossing the outer region. The two values c_0 and c_1 from the given confidence intervals are known and thus also the χ^2 along the borders. The line between the two borders is used to quadratically extrapolate the $\Delta\chi^2$-value at the theoretical point. If O_{theo} happens to lie between the given confidence intervals, the $\Delta\chi^2$ is interpolated along the line between the regions. If O_{theo} lies within the inner region and no best fit point is given, it is assigned a $\Delta\chi^2$-contribution of zero. If there is a best fit point, an option in the data file is given, so that the user can choose whether to use this point as a reference rather than the inner confidence interval. In this case, the shortest line from O_{theo} is drawn to the best fit point with references towards the borders of the confidence intervals. In the innermost region, the $\Delta\chi^2$ may be interpolated if desired and would be zero if O_{theo} was exactly on the best fit point. This is optional, and if a best fit point is either not given or should not ne taken into account in the calculation, it can simply be left out in the data file. The method is depicted in Figure 3.11.

In case a best fit point is given and the theoretically predicted point lies within the inner region, the shortest line is drawn to the best fit point, and the $\Delta\chi^2$ takes the form

$$\Delta\chi^2_m = c_0 \left(\frac{d_{m,\mathrm{bfp}}}{d_{0,\mathrm{bfp}}}\right)^2 . \tag{3.35}$$

In spite of the intelligible approach, the technical implementation of signal regions has proved to be rather extensive. I will not elaborate on the programming particularities, as it would go beyond the scope of this work, but would like to point to the more detailed account given in Plambeck [2011].

3.4.4 Transitional Tests

`AstroFit` has been tested under many aspects, both separately and in interaction with `Fittino`. In the following paragraphs, I will summarize the built-in test utility of `AstroFit`, give examples from a functionality test for the $\Delta\chi^2$-contribution of an

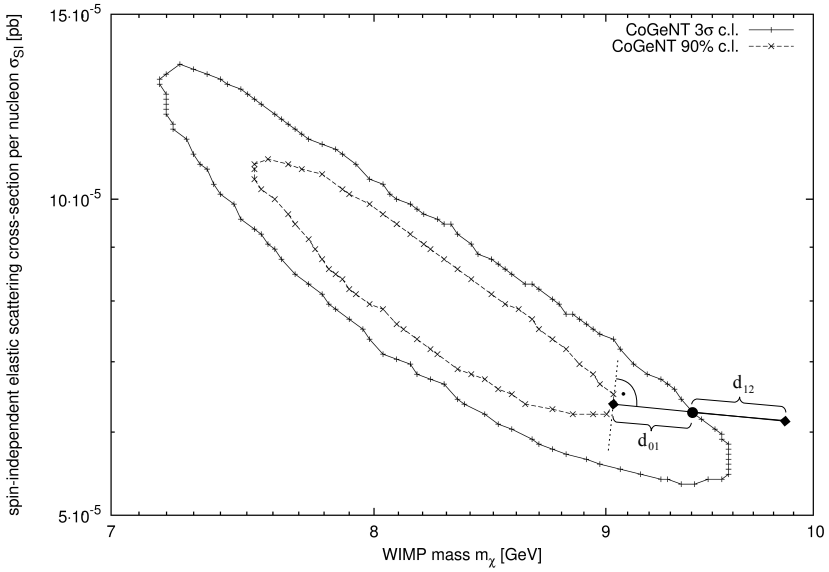

Figure 3.11: Figure demonstrating the $\Delta\chi^2$-calculation for signal regions as an example. From a theoretical point in the plane, a perpendicular line to the inner region is drawn. From there, the distance d_{01} is drawn between the inner and the outer region. From the c_0 and c_1 value, the correct $\Delta\chi^2$-value is known. By drawing a line from the point on the outer region towards the theoretically predicted point and comparing the length of the two distances d_{02} and d_{12}, the according $\Delta\chi^2_n$ is calculated. The containment regions in this Figure match the signal from Fox et al. [2012].

`AstroFit` observable in the interplay with `Fittino` and demonstrate a consistency check for the macros from which the figures shown in Chapter 4 resulted.

Test program in AstroFit A test program has been created within `AstroFit`. This program calls every function within `AstroFit` and returns

1. all theoretically calculated observable values for a given spectrum file,
2. the corresponding $\Delta\chi^2$-contribution from each observable,
3. the time needed for each process.

This way, all the steps can be overseen, and new features can be tested without interference with the core of the setup. Also, theoretical values can be estimated or calculated manually and compared to the outcome of the test program. The test program can use any given SLHA model input file which enables testing specific points of the fit process individually. Storing different model files that correspond to the best fit point, a low overall χ^2 or a very high total χ^2, respectively, can be helpful when testing their sensitivity to changes or expansions in `AstroFit` and give a first estimation.

Consistency check with colored scatter plots When setting up the interface with `Fittino`, a consistency check of the $\Delta\chi^2$-calculation has been made in order to ensure that the right value was written into the ntuple file. For example, in Figures 3.12 and 3.13, the $\Delta\chi^2$-contribution from the `afchi2direct` subroutine that is in charge of the calculations calculation from direct detection is demonstrated in transitional scatter plots. The color scales show the increase in $\Delta\chi^2$ in distance to the upper limit. For visions of clarity, a cut has been applied so that only $\Delta\chi^2 < 50$ are depicted.

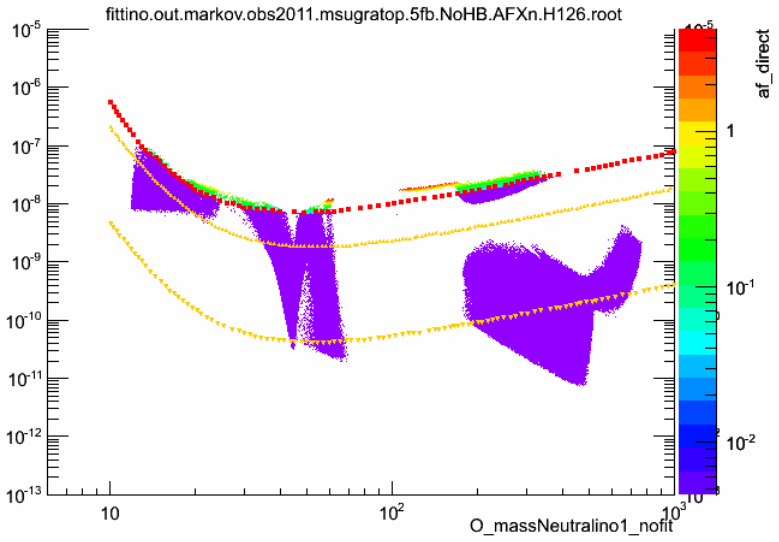

Figure 3.12: Colored scatter plot as consistency check for the $\Delta\chi^2$-calculation with direct detection, showing that the contribution is zero below the upper limit, in this case the Xenon100 upper limit, and rises quadratically above.

Scatter plots for 1σ and 2σ regions In the analysis, another type of scatter plots has been made on the raw data from the ntuple files. To secure the correctness in the application of the macros drawing the 1σ and 2σ regions into the final plots for public use, the regions have been drawn manually. All models meeting the conditions described in Equation 3.9 from Section 3.2.2 have been taken into account. The 1σ region is marked with red points for each model, and the 2σ region for the standard fit is marked black. In Figures 3.14 and 3.15, the 2σ regions for a fit using the Xenongoal and Xenon1T data, respectively, are also shown in dark and light purple as an overlay after evaluating each one separately. In general, numerous consistency checks for all observables have carefully been made directly from the ntuple files.

3.4.5 Discussion and Future Prospects

So far, astrophysical input has successfully been implemented in form of the relic density of CDM, photon flux upper limits and both signals and limits on the WIMP-nucleon cross-section from direct detection instruments. Still a lot more data from

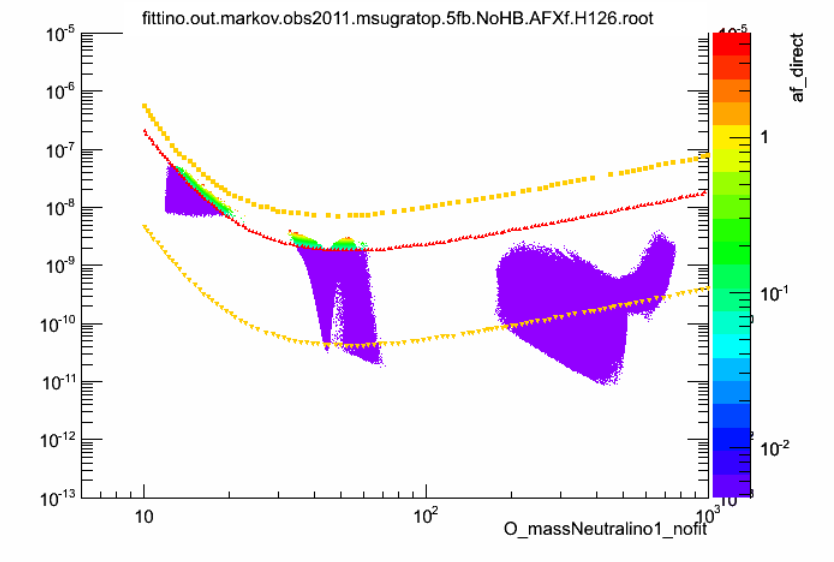

Figure 3.13: Colored scatter plot as consistency check for the $\Delta\chi^2$-calculation with direct detetcion as in Figure 3.12, but with the Xenongoal upper limit.

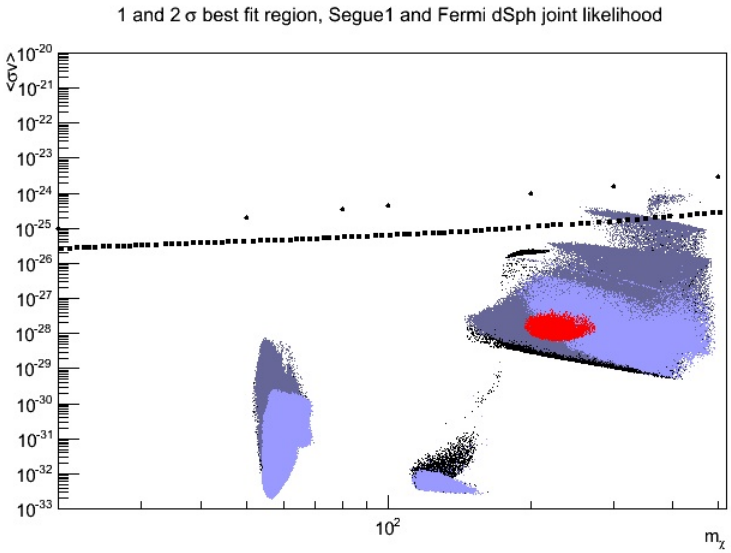

Figure 3.14: Overlay scatter plot for the standard fit in relation of the neutralino mass to the indirect detection velocity-averaged WIMP annihilation cross-section.

astrophysical observation is available, as shown at the beginning of this Section, and should hence be included into the framework.

In order to contribute to global fits in general, it would be desirable to use `AstroFit` with other fit programs while extending the usage of `AstroFit` in combination with `Fittino`. To simplify matters, the first action could be to include `AstroFit` into the `Mastercode` fit program (Buchmueller et al. [2012]) which is closely related to

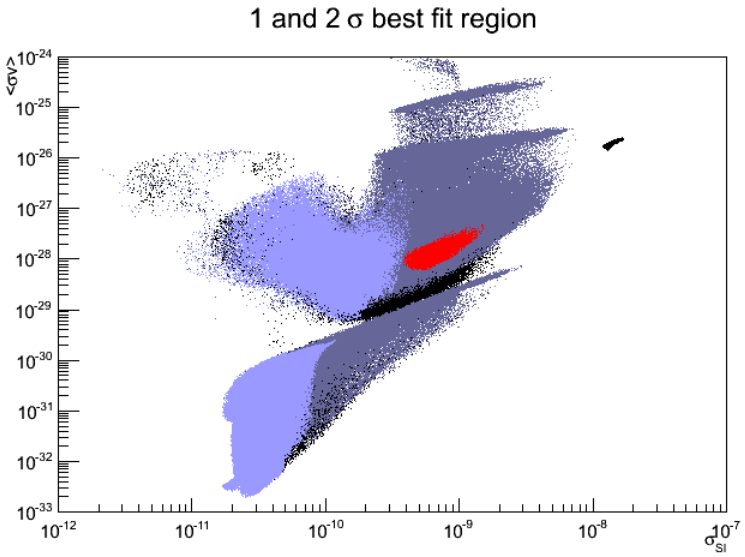

Figure 3.15: Overlay scatter plot for the direct and indirect detection plane with Xenon100, Xenongoal and Xenon1T.

`Fittino` due to its frequentist approach. Nonetheless, it would be also valuable to provide an interface to fit programs using a Bayesian interpretation eventually in order to compare the results. As only the `AstroFit` function that takes care of the χ^2 calculation needs to be changed to match a Bayesian approach while the base frame remains the same, an implementation is not much more difficult than for a global fit program with a frequentist approach.

The treatment of systematic uncertainties is an issue that should be addressed. To reduce the influence of model estimations and uncertainties commensurate with these calculations, it should always be aimed at using the astrophysical data that has the least theoretical dependence, e.g. the flux rates instead of particle counts, and the event rate instead of the confidence level on upper limits. Using information from plots, published by collaborations of specific experiments, can be ambiguous. For example, the spin-independent elastic WIMP-nucleon scattering cross-section leads to a false sense of comparability when limits and signals from miscellaneous experiments are shown in the same diagram. These limits and signal regions come from studies using different target materials, detection signals, background estimation and statistical methods for the derivation of confidence intervals. The precision within `AstroFit` can only be as accurate as the published data.

Furthermore, data used in the fit should remain universal to suit the requirements for a global fit. Certainly, more specific data or scenarios can be tested in `AstroFit` by saving the SLHA file of the best-fit point of a fit. This can later on be used to give an estimation of the impact of a hypothesis, such as the gamma-ray line discussed in Weniger [2012].

The choice of which information to use in the fit other than the latest results from particle physics is not an evident one, but has to be executed with care. Nevertheless, it should be the goal to use as much generic information as possible. Information already available at this time that should be incorporated into `AstroFit` was listed at the beginning of this Chapter, as there are photon flux information from the galactic center and galactic halo region, positron fluxes or combined positron and electron fluxes, antiproton fluxes, upper limits on neutrino fluxes from the Sun and Earth and the spin-dependent WIMP-nucleon cross-section. These additions will be made one step at a time, depending on the manpower of the project. In the following Chapter, I will present the results from the analysis of the setup described above.

Chapter 4

Analysis

In this Chapter, I present the outcome of the combined `Fittino` and `AstroFit` global fits for the frequentist interpretation with focus on DM-relevant results. In order to indicate the influence of particular observables, various fit scenarios have been probed. Initially, I will illustrate the general features of the fit with all established observables, which I will refer to as the "standard fit" or "standard fit scenario". All other scenarios are compared to this reliable standard fit. Subsequently, I will focus on the contribution from individual observables and fit scenarios differing from the standard fit by either leaving out particular observables or varying observables, for instance by using predicted experimental data instead of real measurements. I will discuss the preferred parameter regions for each scenario, the difference to the standard fit and the interrelations between discrete observables.

Since in global fits the minimum and best fit regions are obtained from the minimum of a combined total χ^2 of all input observables as shown in Section 3.2.2, the influence of one particular observable has to be interpreted in a global context. The interrelations between all contributing observables need to be considered. Nonetheless, the contributions of individual observables can be exhibited in ratios, which can give hints to tensions between two or more observables. Moreover, they can give insight to limits soon reached by pushing a certain observable to its border within the allowed parameter space. From a global prospect, the combined outcome is of particular interest, as only the combination of all observables can reflect the interrelations within a theoretical model in the context of most recent experimental measurements. The general outcome of the fit using all available complementary channels is an indication for how well the model represents given experimental behavior. It is reasonable to contrast different cases where one particular observable is varied or left out, to demonstrate its impact on the overall fit. Furthermore, the results of the fit provide opportunities to reflect on tensions or agreements between two or more observables, which I shall attend to at the end of this Chapter.

4.1 Introduction to the Standard Fit Scenario

In the following, I will summarize the input and methods used for the standard fit and the results acquired from it. The observables gained from direct or indirect observations and experimental measurements that potentially contributed to the overall χ^2 of the fit are listed in Table 4.1.

#	Observable
1	Anomalous magnetic moment of the muon $a_\mu - a_\mu^{\mathrm{SM}}$
2	Branching ratio BR($b \to s\gamma$)
3	Branching ratio BR($B_s \to \mu^+\mu^-$)
4	Branching ratio BR($B \to \tau\nu$)
5	B_S oscillation Δm_{B_s}
6	Mass of the W boson m_W
7	Effective weak mixing angle $\sin^2\theta^2_{\mathrm{eff}}$
8	Mass of the lightest neutral Higgs boson m_{h^0} or bounds on m_{h^0}
9	CDM relic density $\Omega_{\mathrm{CDM}}h^2$
10	Spin-independent elastic WIMP-nucleon scattering cross-section or upper limits
11	Limits from direct SUSY searches for jets $+E_T^{miss}$ at the LHC
12	Gamma-ray flux upper limits from indirect DM searches
13	Chargino bounds from LEP

Table 4.1: List of all observables contributing to the number of degrees of freedom in the standard fit scenario. To derive the number of degrees of freedom, the fit parameters have to be subtracted from the number of observables. Thus, the ndf in the standard fit is $ndf = n_{obs} - n_{para} = 13 - 4 = 9$.

Using these observables as input, a global fit has been performed as described in Chapter 3, fitting the observables to the CMSSM. The best fit values for the parameters M_0, $M_{1/2}$, A_0 and $\tan\beta$ have been obtained while fixing the sign of the Higgs/Higgsino mass parameter μ to positive values, which it is most agreeable with the $(g-2)_\mu$ observable. In Table 4.2, the outcome of the standard fit is shown, labeled as "LHC". Other fit scenarios have been investigated to acquire the impact of specific observables, which I will explain marginally for a better comprehension of the setup of the global fits. For the standard fit, all observables from Table 4.1 have been used. In the case of the Higgs boson, bounds have been used with `HiggsBounds`, instead of an explicit mass. In the case of direct detection, upper limits from Xenon100 are included in the standard fit.

To study the impact of the SUSY searches at the LHC with 5 fb^{-1} integrated luminosity, the standard fit is compared to a fit scenario referred to as "LEO" ("low energy observables"). In the "LEO" fit, the direct searches for sparticles at the LHC are not included, reducing the ndf to eight. Save for this one observable, the input remains the same. The scenario named LHC+XENON1T is again similar to the standard fit, except for one particular change. Instead of using up-to-date upper limits from direct DM searches with the Xenon100 experiment, the presumed data for the Xenon1T experiment is used. In this case, the upper limit on σ_{SI} from an experiment

with a fiducial target mass of one ton would be lower than the current bound from Xenon100. The discovery of a boson of mass approximately 126 GeV or 125 GeV from the ATLAS and CMS experiment, respectively, can be interpreted in view of the lightest neutral Higgs boson. The Higgs boson is already predicted for the SM and does not necessarily have to be a SUSY particle, but if it were construed in a SUSY context rather than in the SM one, it would have significant impact on the fit. In the LHC $+m_h = 126$ GeV scenario, therefore, a Higgs mass of $m_{h^0} = 126 \pm 3$ GeV as obtained at the time of the conduct of the fit is used. This fit scenario differs from the standard fit only by the explicit Higgs mass.

Despite this classification of scenarios, I will not arrange my objects of discussion along this line. Instead I will take into consideration the following points that can be discussed with respect to DM:

- The knowledge that can be acquired from the standard fit
- The effect of the relic density constraint
- The impact of the LHC searches
- The impact of $m_{h^0} \approx 126$ GeV on the CMSSM and neutralino DM
- The influence of the spin-independent WIMP-nucleon cross-section, considering the conflict of detection regions compared to a non-detection and future prospects from this observable
- The relevance of indirect searches

Fit	M_0 [GeV]	$M_{1/2}$ [GeV]	$\tan\beta$	A_0	χ^2/ndf
LEO	$84.4^{+144.6}_{-28.1}$	$375.4^{+174.5}_{-87.5}$	$14.9^{+16.5}_{-7.2}$	$186.3^{+831.4}_{-843.7}$	10.3/8
LHC	$304.4^{+373.7}_{-185.2}$	$664.6^{+138.3}_{-70.9}$	$34.4^{+10.9}_{-21.3}$	$884.8^{+1178.0}_{-974.9}$	13.1/9
LHC+XENON1T	$296.1^{+1366.8}_{-150}$	$747.4^{+303.4}_{-143.5}$	$28.3^{+21.2}_{-17.8}$	$-518.7^{+5266.3}_{-2166.1}$	15.0/9
LHC+$m_h = 126$ GeV	$1163.2^{+1185.3}_{-985.7}$	$1167.4^{+594.0}_{-513.0}$	$39.3^{+16.7}_{-32.7}$	$-2969.1^{+6297.8}_{-1234.9}$	18.4/9

Table 4.2: Summary of the results for various CMSSM fits with different sets of input observables. The names of the fits and the observables included are explained in the text. The errors are given in terms of 2σ.

4.1.1 Features of the Standard Fit

Recalling Section 2.3, the CMSSM is a model with R-parity conservation and the lightest of four neutralinos as LSP and DM candidate which is assumed to provide the relic density of CDM in the Universe. Under this assumption, the standard fit leads to very restricted preferred regions of parameter space with a low overall χ^2 due to one or many constraining observables, while other regions are entirely excluded due to a large total χ^2. The overall χ^2/ndf is $13.1/9$ as can be taken from Table 4.2. The errors correspond to the 2σ values of the parameters. The large errors

are due to a relatively flat scan of the parameter space. With over 138 million points of χ^2 value of 30 or lower, high statistics are provided. The wide-spread distribution in the parameter space is a hint for a non-convergence of the model. Values of several hundreds of GeV for the M_0 and $M_{1/2}$ parameter can be extracted from the Table. Evidently, such light sparticles inducing a light relic neutralino from the early Universe have not been found during jets+E_T^{miss} searches at the LHC. The $\tan\beta$ parameter was fit to moderate to large values of $\tan\beta \gtrsim 35$, which is compatible with the expected remaining regions where the right CDM relic abundance can be achieved. This is a reaction to the high $M_{1/2}$ value of the fit and a preferred higher $\tan\beta$ value from the observables $\Omega_{\text{CDM}}h^2$ and $(g-2)_\mu$, which are both more agreeable to moderate to higher values of $\tan\beta$. A low $\tan\beta$ in the discussed scenario would only be essential for the h-pole region which has been heavily disfavored when studying benchmark scenarios before, considering the non-detection of light sparticles, bounds for the Higgs mass and predictions for the neutralino mass. From the fit, the h-pole region can be ruled out entirely. The values for M_0 and $\tan\beta$ are too large, and the neutralino mass is fit nowhere near the range of $2m_\chi \gg m_h$ in order for neutralinos to have annihilated via h-resonance in the early Universe. A_0 is fit to large values of ≈ 900 GeV. Such a value is not only in agreement with bounds on m_h, but also allows m_h to be ≈ 126 GeV. The observable that puts boundaries to A_0 is the upper limit on σ_{SI} from direct DM searches. The stop-coannihilation region, a strip of very large $M_{1/2}$ and small M_0 and with particular A_0 values, is also excluded with the LHC constraints, as M_0 values are much higher in the fit and the lightest stop mass is significantly higher than the neutralino mass, which can be seen in Figure 4.3. The best fit regions for the parameters M_0, $M_{1/2}$, A_0 and $\tan\beta$ are shown in the profiled M_0–$M_{1/2}$ and A_0–$\tan\beta$ planes. Hidden dimensions are fully considered.

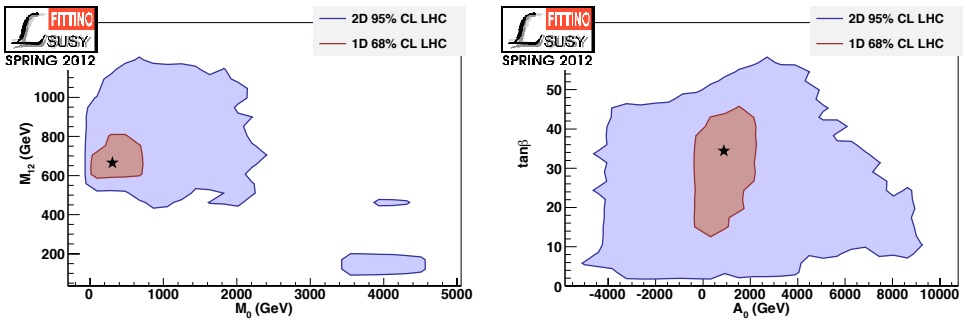

Figure 4.1: Best fit regions for the CMSSM parameters from the standard fit. The 1σ region is shown in red with a cross specifying the best fit point. The 2σ region is shown in blue color.

In a pull plot (4.2), the contributions from individual observables to the overall fit are shown. Slight tensions can be seen between the non-detection from SUSY searches at the LHC and the $(g-2)_\mu$ observable. The contributions from indirect searches for DM are not shown explicitly, as they are always zero or negligible within a 2σ range of the fit.

In the standard fit, the neutralino mass is best fit to $m_\chi = 270$ GeV, which is in

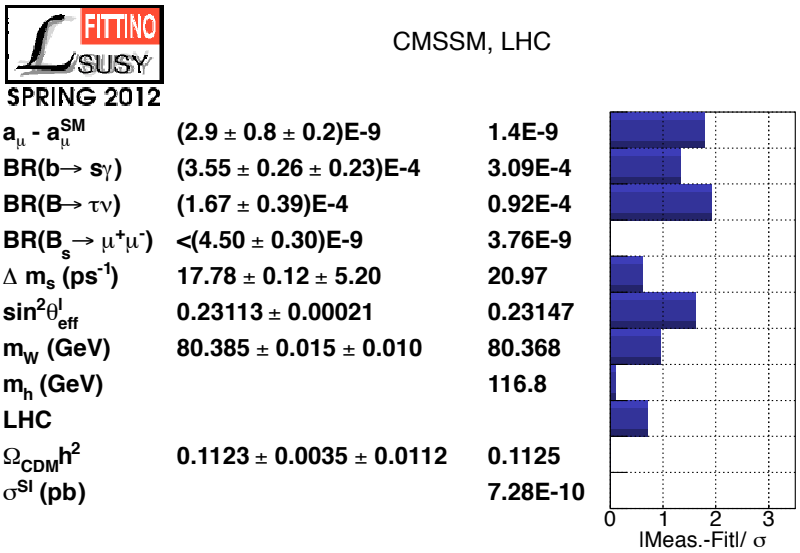

Figure 4.2: Pull plot demonstrating the $\Delta\chi^2$ contributions from individual observables to the standard fit. Contributions from indirect DM searches, which are zero within the relevant regions for all fit scenarios, are left out here and in all following pull plots.

a potential range for astrophysical detection and still allows the possibility for DM to be a SUSY neutralino. Strong constraints on the parameter space are especially given by the relic density of CDM and the $(g-2)_\mu$ observable. Remarkable impact can also be noticed from the jets+E_T^{miss} input as well as the variation of the Higgs mass. In the standard fit, tensions already occur between certain inputs. A conflict arises between the LHC input and the $(g-2)_\mu$ observable as there is no model that fits both observables well at the same time, leading to relatively high contributions from the $(g-2)_\mu$ observable eventually in the standard fit scenario. The best fit mass of the lightest neutral Higgs boson is $m_{h^0} \approx 117$ GeV in the standard fit. This is in good agreement with the 95% confidence level bound from `Higgsbounds` but shows potential conflicts when assuming that the measurement of a neutral boson at the LHC is indeed a discovery of the lightest neutral Higgs boson.

The resulting SUSY mass spectrum of the fit and the CMSSM parameters are shown in Figure 4.3. Referring again to the regions of CMSSM parameter space that allow the correct relic density of CDM, the bulk and h-pole regions and the stop co-annihilation strip are excluded as discussed above. This leaves the stau-coannihilation region, the funnel region and the focus point region to discuss. The latter, usually shown as a strip at very low $M_{1/2}$ and moderate to high M_0 values, is excluded below $M_0 = 3.5$ TeV in the standard fit. Above this edge, no LHC exclusion could take place in the fit due to lack of available published data. SUSY at such high mass scales is not of relevance, as it does not cover solutions to problems of the SM as the hierarchy problem or EWSB. At such high M_0 values, fine-tuning becomes a physical and technical problem, which makes the appearing focus point region unattractive as a possible solution. Furthermore, such a focus point region correlates to high

neutralino masses of TeV scale, which is, albeit possible, not covered by the uncertainty band of the SUSY mass spectrum, which strongly prefers a neutralino mass of roughly $200-500$ GeV. Thus, even though the focus point region is not excluded directly from the fit, the models from this region have shown to be not reasonable in accordance to measured data and theoretical motivations.

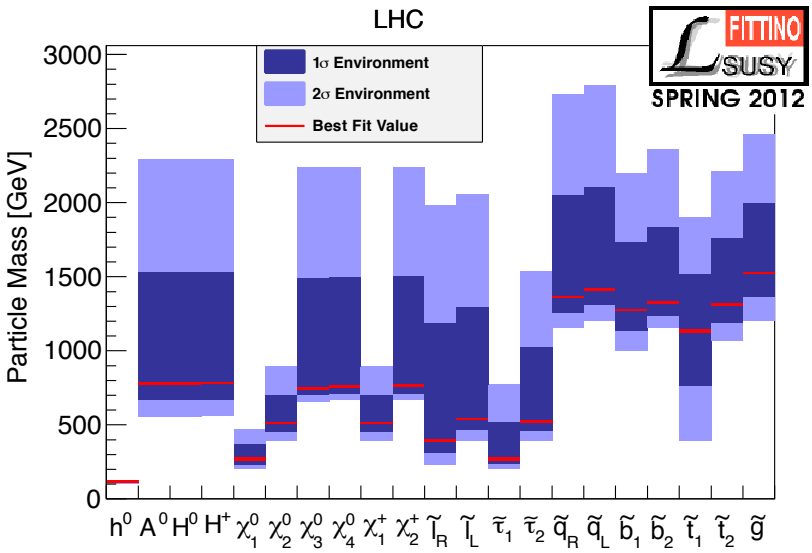

Figure 4.3: CMSSM mass spectrum of SUSY particles. The best fit value is shown in red, while the dark blue and light blue areas indicate the 1σ and 2σ bands, respectively. The full band for each sparticle mass represents the one-dimensional 2σ uncertainty with $\Delta\chi^2 < 4$ after profiling over all hidden dimensions. The mass of the lightest neutralino is best fit at $m_\chi = 270$ GeV. The mass of the lightest stau and the CP-odd Higgs particle allow models in the stau co-annihilation and funnel region, while the mass of the lightest stop particle and the comparison between the mass of the lightest neutral Higgs to the neutralino mass disfavor the stop co-annihilation and h-pole region of the CMSSM parameter space, which are indeed excluded in the standard fit.

4.1.2 Determining the Co-Annihilation and Funnel Region

For the analysis and searches for DM, it is of great interest which regions of parameter space remain still valid when confronting the CMSSM with actual data. The remaining regions of interest are the stau co-annihilation region and the funnel region. For the understanding of cosmological production of DM, it is especially relevant to distinguish the regions in the profiled M_0–$M_{1/2}$ plane where the right relic density of CDM is achieved via stau co-annihilation or H/A-resonance. Since the $\tan\beta$ value of each model point is not known in the two-dimensional representation and is independent from the M_0 and $M_{1/2}$ values at each point, the co-annihilation and funnel regions cannot be pointed out frugally. Therefore, to discern these regions in the resulting 1σ and 2σ regions of the standard fit, the following approximation was used. As co-annihilations with the stau in the early Universe would have occurred if the neutralino had similar or greater mass than the stau, the co-annihilation region was determined by taking all points within the 2σ region that matched the condition $m_{\chi_1^0}/m_{\tilde{\tau}} \geq 1$. For the A-funnel region, a relation between the lightest neutralino and

the pseudoscalar Higgs boson (which is similar to the heavy neutral Higgs) is drawn. All points within the 2σ of the M_0–$M_{1/2}$ plane are taken into consideration that fulfill the requirement $2m_{\chi_1^0}/m_{A^0} \geq 1$. The effect can be seen in Figure 4.4.

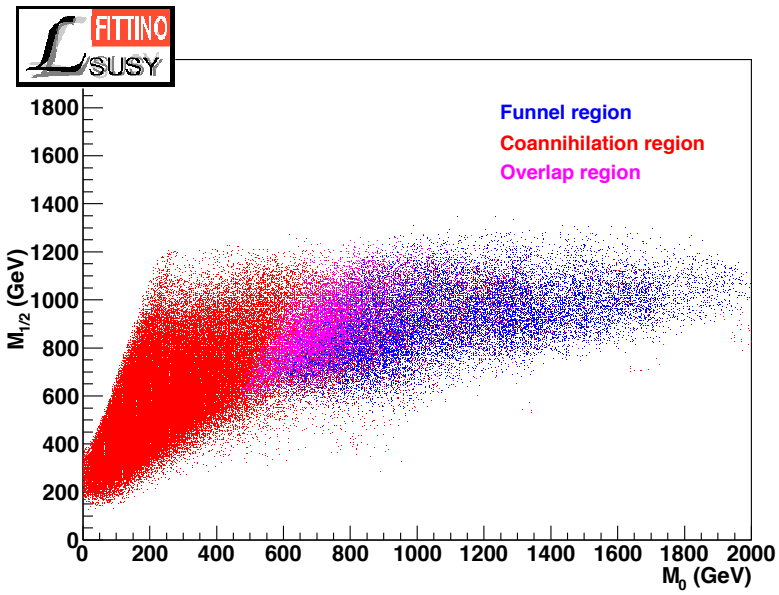

Figure 4.4: Approximation for the stau co-annihilation and funnel region within the M_0–$M_{1/2}$ plane of an example fit. Red points mark the co-annihilation region while blue points show the models referring to the funnel region. An overlap region occurs between the two regions, marked with points in dark magenta.

4.2 The Impact of Particular Observables

After recapitulating the general outcome of the standard fit and the preferred regions of parameter space both for the parameters as well as for the regions matching the relic abundance of CDM, I will now proceed to discuss the effects of the relic density input, the LHC input, the direct and indirect detection upper limits and the presumable mass of the lightest neutral Higgs boson of ~ 126 GeV, starting with the relic density of CDM, as it is the most important observable for DM research.

4.2.1 The Relic Density of Cold Dark Matter

For a study of the results from the standard fit, the relic density of CDM still plays the most vital role, as it excludes large regions of parameter space that do not produce the right relic density. It remains one of the most stringent constraints for SUSY studies in general and studies of the CMSSM in particular. Most parameter regions are disfavored by the relic density, because they produce a too high abundance of DM particles that does not meet the measured value. Thus, the remaining regions of parameter space from a global fit must match the relic density observable. Former studies have singled out the CMSSM parameter regions consistent with the measured

relic density for thermally produced neutralino DM, as shown in Section 2.3.2. From the bulk region, the focus point region, the stop co-annihilation region, the stau co-annihilation region and the funnel region, only the stau co-annihilation and the funnel region remain valid towards thermally produced neutralinos when taking into consideration all available observables now used in the standard fit. Aside from these, there is still the focus point region under reservations, which will become more pronounced when considering the input from direct DM detection and latest LHC data. Here, I will show the impact of the relic density observable by showing the results of the standard fit with and without the relic density input.

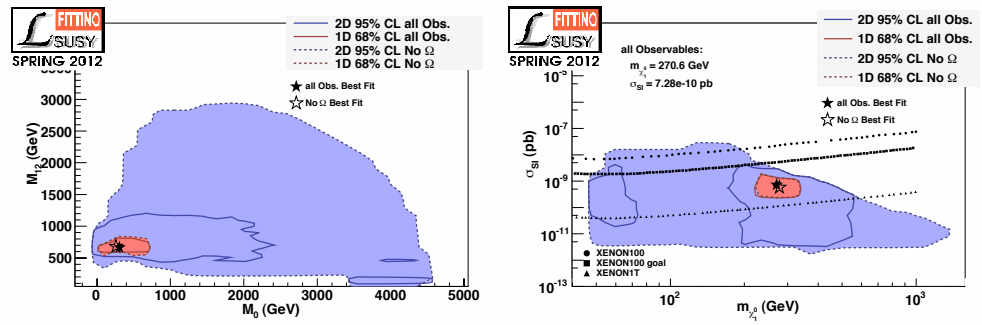

Figure 4.5: Results of fits with and without relic density input for the M_0–$M_{1/2}$ plane and the direct detection plane. The solid lines display the resulting 1σ and 2σ region in red and blue, respectively, with the best fit point at the total χ^2_{min} of the fit with a black star. The dashed lines mark the 1σ and the 2σ region for the allowed parameter space without Ωh^2 constraint with a blank star denoting the best fit point. In both projections, the 2σ region is apparently much wider.

In Figure 4.5, the impact of the Ωh^2 observable is demonstrated both in the M_0–$M_{1/2}$ plane and the σ_{SI}–m_χ plane (direct detection plane). As one can see, leaving out the relic density constraint enables the 2σ containment region to spread across a wide space of the CMSSM. While a fit leaving out the relic density observable still leads to similar preferences for the resulting 1σ region and best fit point, the 2σ becomes arbitrary.

For the M_0–$M_{1/2}$ plane, this demonstrates the importance of the cosmological DM model. If the neutralino is indeed the sole DM particle, the measured relic abundance of these particles stress the fact that only small parts of the otherwise huge allowed parameter space are fit to agree with thermally produced DM. Subsequently, in the direct detection plane one can see that, considering all input information from astroparticle and collider physics, the neutralino needs to have a mass of $200 - 500$ GeV. Otherwise, without Ωh^2 input, the neutralino mass could span from tens of GeV up to the order of 1 TeV. Adding the relic density, a small region for the allowed neutralino mass remains also in the range of $50 - 70$ GeV which refers to the focus point region. The latter is, however, disfavored, as I have explained above and will stress again when discussing the impact of the latest LHC data, the σ_{SI} observable and the input of a Higgs boson of mass ~ 126 GeV. One can also note that the relic density does not constrain the spin-independent WIMP-nucleon cross-section and is in agreement with the σ_{SI} results from the fit.

Using the measured relic density as observable to the fit has demonstrated the expected great impact, as quantities such as the WIMP annihilation cross-section and the branching fractions to various standard models depend on it (Caceres [2009]). Furthermore, the mass for a neutralino WIMP is fit to $\sim 200-500$ GeV, rather than broadly allowed from $O(10\,\text{GeV}-1\,\text{TeV})$.

4.2.2 SUSY Searches at the LHC

Direct SUSY searches and indirect searches for DM at the LHC have had a great effect on the CMSSM parameter space. This is evaluated by leaving out the jets+E_T^{miss} observable from the fit in the LEO fit. The total minimum χ^2 of the fit without direct SUSY searches at LHC is 10.3 per 8 degrees of freedom. This is a better fit compared to the standard scenario, showing that the LHC input in combination with other observables brings tension into the model. This is mainly due to the incoherence between the upper limits on sparticle masses and the $(g-2)_\mu$ observable. The effect is demonstrated in Figure 4.6, where the rising contribution of $(g-2)_\mu$ to the total fit in the standard fit can be seen in comparison to the LEO fit.

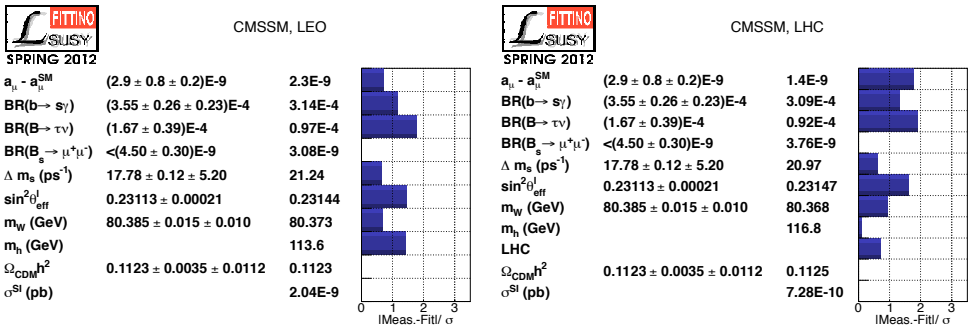

Figure 4.6: Contributions of individual observables to the overall fit. The observables are given on the left, in most cases with measured values and uncertainties. On the right, the best fit values from the theoretical prediction are given for the LEO and LHC (standard) fit, respectively. The blue bars indicate their relative contribution to the total χ^2 of the fit.

The addition of LHC data also had the effect to lift the best fit Higgs mass slightly from 113.6 to 116.8 GeV, which does not affect the parameters significantly. In both scenarios, the relic density of CDM is reached in good agreement, also. What does change significantly are the best fit regions of the CMSSM parameters. $M_{1/2}$ is shifted upwards, with the best fit point moving from 304.4 GeV in the LEO fit to $M_{1/2} = 664.6$ GeV in the LHC fit. M_0 is shifted from 84.4 to 304.4 GeV. The difference in the M_0–$M_{1/2}$ plane is shown in Figure 4.7. The interrelation between $M_{1/2}$ and $\tan\beta$ through the Ω_{CDM} and $(g-2)_\mu$ observables causes a rise in $\tan\beta$ from a best fit value of 14.9 to 34.4 GeV. An enormous change on A_0 can be seen. Demonstrated in the A_0–$\tan\beta$ plane, the 2σ region of A_0 is seen narrowly distributed around 0 for the LEO fit, while in the LHC fit, the magnitude of A_0 is extended widely, preferring positive values. In summary, all parameter values are higher when using the LHC

input.

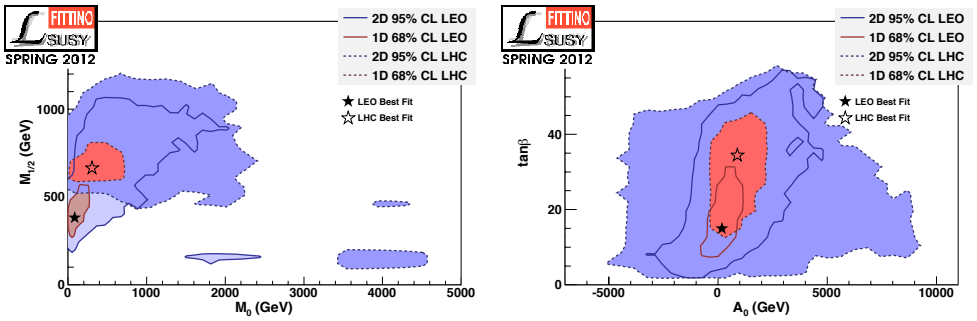

Figure 4.7: The best fit regions for the LEO and LHC fit are shown in comparison. The 1σ and 2σ regions without input from sparticle searches at the LHC are shown in solid red and blue lines with a filled black star as best fit point. The standard fit with LHC input is shown with dashed lines and is the same as in 4.1 with an empty star denoting the best fit point. The best fit points are shifted to higher M_0, $M_{1/2}$, $\tan\beta$ and A_0 values.

In summary, adding jets+E_T^{miss} data from two years of LHC observations with 5fb^{-1} integrated luminosity and a $\sqrt{s} = 7$ TeV center-of-mass energy alters the fit by increasing the values of the CMSSM parameters and thus lifting the entire CMSSM mass spectrum significantly. Moreover, the significance of the fit is slightly deteriorated due to tensions between the non-observation of sparticles at LHC and the $(g-2)_\mu$ observable. The effect of leaving out specific electroweak precision data in global fits, both in general and specified to the $(g-2)_\mu$ observable, has been studied in Buchmueller et al. [2009] and Fowlie et al. [2012]. In the standard fit presented here, although the $(g-2)_\mu$ contribution to the χ^2_{min} is high, the most preferred regions of parameter space, the stau co-annihilation and the funnel region, remain the same, even if the observable is left out. In terms of DM, the CMSSM still offers solutions for a neutralino-only DM scenario, which becomes increasingly difficult to explore at the LHC with $\sqrt{s} = 7$, as no observations of sparticles and no missing E_T from possible neutralino events have been reported.

4.2.3 Direct Detection Signals and Upper Limits

Measurements from direct detection instruments have been a center of discussion and used in a complementary approach in various CMSSM fits (e.g. see Buchmueller et al. [2012], Martinez et al. [2009b]). Including direct detection measurements into the global fits yields different results depending on the experiment. First, I will shortly refer to the conflict between claimed detection regions, e.g. by the DAMA/LIBRA and CoGeNT collaborations (see Bernabei et al. [2010], Aalseth et al. [2012]), opposed to upper limits on the elastic spin-independent scattering cross-section σ_{SI} (see Aprile et al. [2011], Ahmed et al. [2010]) and the effect of both towards the global fit. Using upper limits from a non-detection together with the other input observables resulted in the standard fit described above. I will briefly summarize the result achieved with a signal region input, before continuing with the upper limits on σ_{SI}.

Signal regions When using signal regions from DAMA/LIBRA and CoGeNT, no χ^2_{min} value of 50 or lower could be reached as a consequence of the excessively high $\Delta\chi^2_{\text{direct}}$ contribution from the σ_{SI} observable. All three claimed signals have been tested individually, as they do not resemble each other in the σ_{SI}–m_χ direct detection plane. For all three regions, the renunciative result for a CMSSM fit is similar. It can therefore be concluded that such signal regions cannot be accommodated as a WIMP signal in the CMSSM. It should however be emphasized that, from an experimental point of view, all possible DM signals should be investigated independently of theoretical models to understand the cause of the measurement, unbiased from a belief whether or not a signal has been found.

Upper limits Leaving the discussion on signal regions and focusing on the input of upper limit on σ_{SI}, a good agreement with the overall fit can be found. In the standard fit, the Xenon100 upper limits (Aprile et al. [2011]) were used. They were the lowest available limits on σ_{SI} during the setup of the fits and have since then only been updated by the Xenon100 collaboration itself. In this way, the limit represents all other limits, for example upper limits from the EDELWEISS and CDMS collaborations in all respects. Bearing in mind that not only one collaboration but many provide such upper limits stresses the prominence of the observable.

In the following, I will comment on how the σ_{SI} upper limit input from Xenon100 influenced the standard fit and how future results from direct detection as predicted with the Xenongoal upper limits for a higher runtime of the Xenon100 experiment and Xenon1T upper limits from an experiment with a higher fiducial mass of one ton would affect the fit.

Adding the Xenon100 upper limits does not have a further constraining effect as already obtained with LHC data. This shows the good concurrence of both inputs related to the CMSSM fit. Adding predicted information for Xenongoal upper limits does not change the outcome of the fit more than statistical effects would allow. Eventually, pursuing a supplemental lowering of the limit as planned with Xenon1T has a noticeable effect on the fit. The result of a fit with predicted Xenon1T information as an exchange for the Xenon100 data of the standard fit can be seen in Table 4.2 in the category labeled as LHC+XENON1T. The significance of the fit is substantially declined, as the χ^2_{min} rises to 15.0 compared to 13.1 at 9 degrees of freedom. This circumstance connotes that if a non-detection of a WIMP signal with the Xenon1T instrument were the case, it would strain the compatibility with other experimental input in a CMSSM framework. This is an important conclusion, since it would mean that upcoming observations with direct detection instruments could well account for final statements on the CMSSM as a DM explaining model. Either a WIMP detection will occur with such instruments in the near future or the CMSSM will severely suffer from a non-detection. If that is the case, global fits will mainly concentrate on other models to overcome shortcomings of the SM and solving the DM problem simultaneously, as the CMSSM would deficiently be able to do so.

In terms of the SUSY mass spectrum, a slightly higher mass spectrum, especially in the Higgs sector, is reached and the 2σ band is broadened by the moderately higher χ^2_{min} of the fit, as can be seen in Figure 4.8. The contributions to the χ^2_{min} are shown in a pull plot in Figure 4.9. The addition of the Xenon1T upper limit to the fit causes conflicts mainly with the $(g-2)_\mu$ observable, but also with the FCNCs and the other low energy precision data.

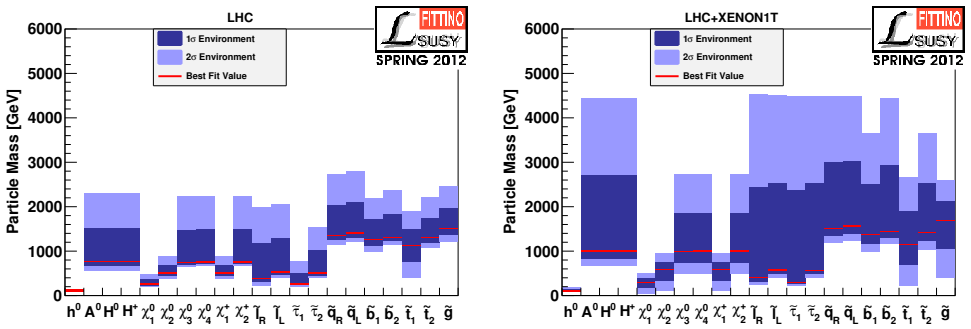

Figure 4.8: Mass distributions of SUSY particles in the standard fit compared to the LHC+Xenon1T fit. Tendencies towards higher masses can be observed as well as an increase in the width of the 2σ environment.

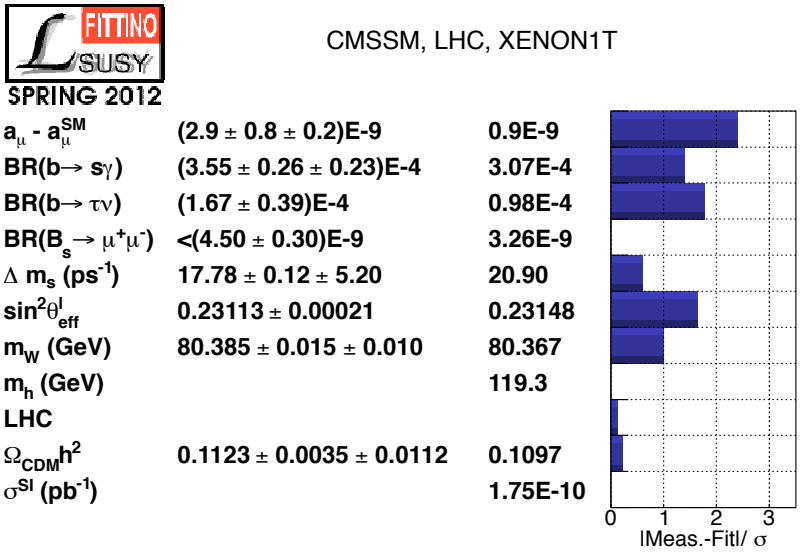

Figure 4.9: Pull plot demonstrating the $\Delta\chi^2$-contributions to the LHC+Xenon1T fit. Tensions occur especially for the $(g-2)_\mu$ observable, but also for other low energy observables. The Xenon1T upper limit is well in agreement with the LHC data.

Adding the Xenon1T input to the fit also restricts the allowed parameter region even further. This is demonstrated in Figure 4.10. In the M_0–$M_{1/2}$ plane of the fit, the stau co-annihilation and the funnel region are constrained, which has been tested as described in Section 3.4.4. The remaining parameter space for thermally produced DM is thus reduced supplementary. The focus point region is constrained in a way that one of the "islands" is now entirely missing, while the other island is

slightly larger. This is caused by the higher overall χ^2_{min}, allowing higher χ^2 values to contribute to the 1σ and 2σ regions. This is also the reason for the enlarged 1σ region that expands towards higher $M_{1/2}$ values. In the A_0–$\tan\beta$ plane, there is no influence on the $\tan\beta$ parameter. Instead, the allowed range for A_0 is limited with regard to high positive values, counteracting the influence of the LHC input in this domain and thus providing complementary limitations. The constraint from direct detection upper limits on σ_{SI} seeks a symmetrical A_0 distribution, constraining the stau co-annihilation region that needs $A_0 \gg 0$.

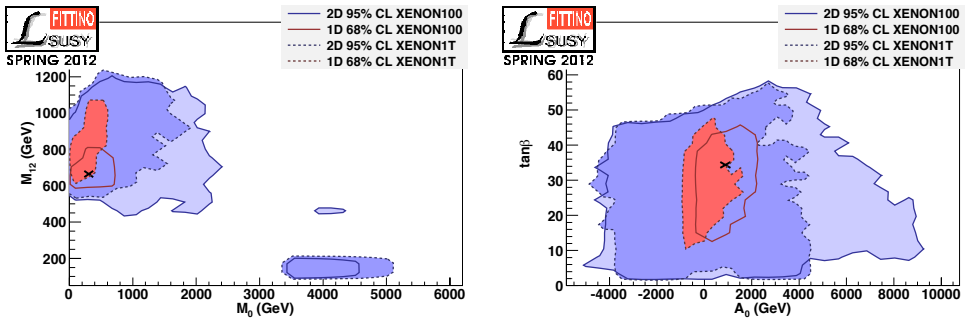

Figure 4.10: Overlay plots of the $M0$–$M_{1/2}$ and the A_0–$\tan\beta$ plane of the LHC+Xenon1T fit compared to the standard fit. The region surrounded by the solid lines resemble the results of the standard fit, while the regions within the dashed lines demonstrate the result of the LHC+Xenon1T fit. In both planes, additional constraints are put on the parameter space.

In the projection into the direct detection plane of Figure 4.11, it is shown that a lowering of the upper limit on σ_{SI} results in further restricted 1σ and 2σ regions, showing cuts on the region of a $50-70$ GeV neutralino mass corresponding to the focus point region and the larger region around 350 GeV, including the point with the χ^2_{min} and corresponding to both the stau-coannihilation and funnel region. The 1σ region is lowered by approximately an order of magnitude in the σ_{SI} scale. Both the 1σ and 2σ regions stretch out above the Xenon1T upper limit. There are several reasons for this occurrence. First, with a χ^2_{min} of 15.0 of the fit, model points are accepted up to a total χ^2 of up to 20.99 to contribute to the 2σ region. And second, an additional scope is allowed arising from the inclusion of a theoretical uncertainty as discussed in Section 3.4.2. While the lowering of the upper limit naturally prefers fit regions below the limit, the other observables of the fit contribute by provoking the regions to remain close to the limit. In doing so, again, the complementary nature of the fit is explicitly demonstrated. Either a neutralino is found in this region, or the CMSSM is put to the test.

Summarizing the result from the CMSSM fit for global fits with direct detection signals and upper limits, it can be concluded that apposite theoretical predictions, signal regions of a WIMP of ~ 10 GeV cannot be accommodated in the CMSSM, leading to unacceptably high χ^2-contributions that do not give significant results, while all current upper limits on the WIMP scattering cross-section are in agreement with the fit, especially with the non-detection of sparticles at the LHC. This does not necessarily mean that the signal measured by DAMA/LIBRA and CoGeNT is not

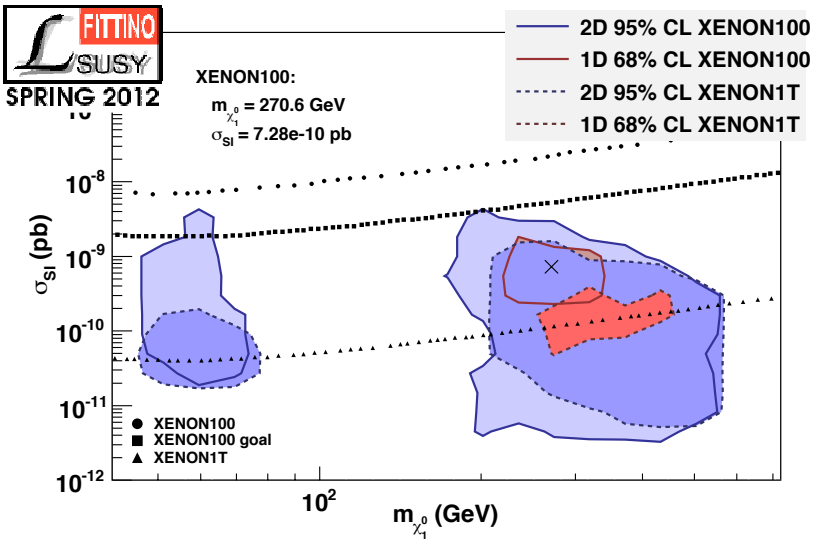

Figure 4.11: Overlay plot illustrating the impact of a Xenon1T input compared to that standard fit with the current input from Xenon100. The 1σ and 2σ regions from a fit with Xenon1T, shown in dashed lines, are further restricted compared to the standard fit as explained in the text.

a WIMP signal. The conclusion that can be drawn from the fit is simply that if it were a WIMP signal it would not be suitable within a CMSSM and must therefore be probed to be suited in a different SUSY model. On the other hand, it could also be concluded that if the CMSSM or closely related models roughly resembled Nature, the existing upper limits from Xenon100, CDMS and EDELWEISS enjoy more confidence within the theory. Another solution would be the hypothesis of having different DM particles and not only neutralino WIMPs. Many studies have addressed the topic of material sensitivity (see Savage et al. [2011], Gelmini and Gondolo [2004], Cline [2011]), saying that some detector materials are more likely than others to detect a faint signal. So whether a signal is found or not would be highly dependent on the target material chosen and the expectation to find a signal or to exclude a signal and propose constantly improving upper bounds. Other remarks apply to the uncertainty in background estimations. A global fit does neither clarify nor deny one or the other deliberation, as only the derived value is naively used in the fit, enabling to treat all possible signals or upper limits with greatest impartiality in order to extract the result. In any case, the more results there are from direct WIMP searches, the better the investigation of both the underlying principles and the understanding for sources of possible errors.

An even more unbiased method to use information from direct searches in global fits would be to use the pure data from the experiment instead of or additionally to the lines of signal regions or upper limits from publications. If using the sole event rates in a global fit, probing different sensible background estimations, a more differentiated picture could be gained from such a fit about the highest or lowest consensus between SUSY model, global fit, experimental result and a priori assumptions made

of the density distribution and so on. Also, a fit using the model-independent residuals could be of interest. Nonetheless, one single fit can so far give precedence to agreements of certain experimental results to the specific BSM model in question. The more models tested with an increasing number of experimental results, the more a foundation can be laid for further investigations.

4.2.4 Observations with Indirect Detection Methods

Adding results from indirect detection methods to global fits is a relatively new topic as methods in indirect detection differ from the other methods. For example, results are mainly drawn from observations, and measurements and observations cannot be addressed as promptly, as they are irreproducible. Nevertheless, with sufficient time, strong information can be gained through indirect DM searches simply from observation, and new instruments in this field increase the sensitivities and lower the thresholds for observations. Furthermore, indirect detection channels for DM are aplenty. Adding information from indirect DM searches is therefore not only highly complementary and sustainable, but will likely yield new results within time.

One of the most discussed search channel for DM activity during the past three years has been the DM search in dwarf spheroidal galaxies and ultra-faint satellites (see Section 2.4). In this study, photon flux upper limits from the H.E.S.S. observation of the Carina dSPh galaxies and from the Fermi-LAT observation of the Ursa Minor DSph have been used, as they were the lowest available limit during the setup of the fits. Also, upper limits on the $b\bar{b}$ channel for the WIMP annihilation cross-section $\langle\sigma v\rangle_{b\bar{b}}$ from the prospective Segue1 source have been used. During the analysis, upper limits from the stacking of non-observational results for ten dwarf spheroidals from the Fermi collaboration Ackermann et al. [2011] became available and were taken into consideration in the evaluation.

In combination with all observables used in the standard fit, the input of the photon flux upper limits and the Segue1 upper limit on $\langle\sigma v\rangle_{b\bar{b}}$ do not constrain the CMSSM parameter space significantly. Observations from dSPhs are so far in good agreement with all observables from direct DM detection and particle physics, emphasizing the result of the allowed parameter region of the fit. Nonetheless, the influence of the observable and the complementary information it provides to the fit can be demonstrated autonomously and in interrelation with the results from direct detection.

I will first consider the potential influence of the input from indirect detection. In Figure 4.12, the best fit regions are drawn into the indirect detection plane of m_χ against $\langle\sigma v\rangle_{b\bar{b}}$. Both the upper limits from Segue1 and the stacked likelihood of ten dSphs are depicted as a dashed and solid line, respectively. It can be seen that although there is no $\Delta\chi^2_{\text{indirect}}$ contribution so far, the limits are in close approximation to the resulting regions, encouraging the actual result. The line from the stacked likelihood analysis is actually so close to the 2σ region of the fit that it can be ex-

pected from photon flux studies of the near future to add constrains to global fits. Furthermore, the standard fit has been conducted with great care of using most conservative and unbiased data. Hence, the information from the $b\bar{b}$ channel, assuming an annihilation of WIMPs into purely $b\bar{b}$ has been used, as it is the most model-independent. Lower limits are available from the same studies if other channels are considered. Also, analogically to the upper limits used from direct detection, published lines have so far been used in the fit. The raw spectral data rather than photon counts that have been assumed for the derivation of the upper limits could provide more in-depth information. Beyond that, the application of many indirect detection channels by adding information from neutrino and antimatter searches could be able to further corroborate the fit results or add new constraints.

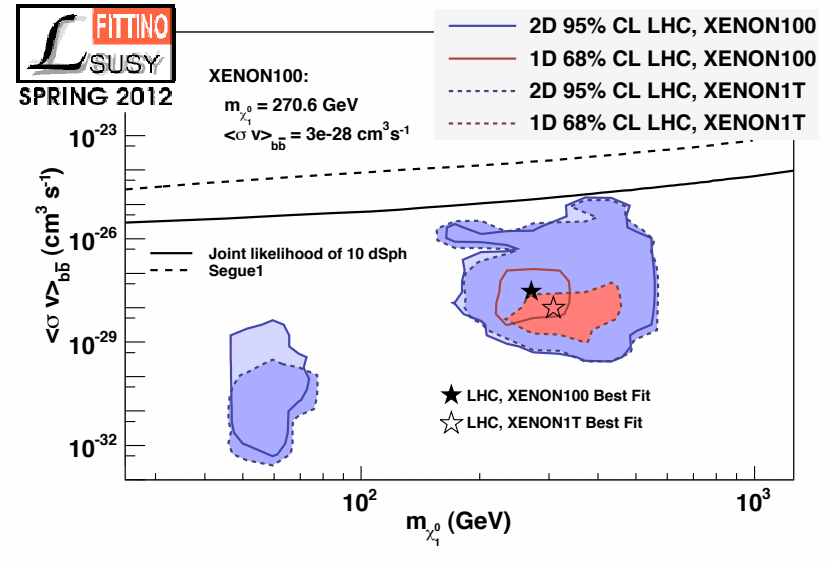

Figure 4.12: The 1σ and 2σ best fit regions from the perspective of the indirect detection plane. The inelastic WIMP-nucleon cross-section is shown on the x-axis, while the WIMP cross-section into photons is shown on the y-axis. The results for the standard LHC fit to the LHC+Xenon1T fit are again shown with solid and dashed lines with hardly any difference. The proximity of the limits to the best fit regions demonstrate the future prospect of additional constrains from indirect DM searches towards global fits, particularly in parameter regions not addressable by direct DM detection.

The highly complementary nature of the indirect detection observables towards direct detection methods is also exhibited in Figure 4.13. Both inputs, the information from indirect and direct DM searches, are displayed orthogonally to each other, narrowing down the CMSSM parameter space from different angles. Prospective Xenon1T information exert constraints on the parameter regions from the σ_{SI} direction, that is from the right side of the Figure, whereas future information from indirect searches will provide constraints from the $\langle\sigma v\rangle_{b\bar{b}}$ direction, in this case from above, putting further constraints on the fit from a new direction. Thus, it is particularly worthwhile to pursue the extension of global fits in the area of indirect detection.

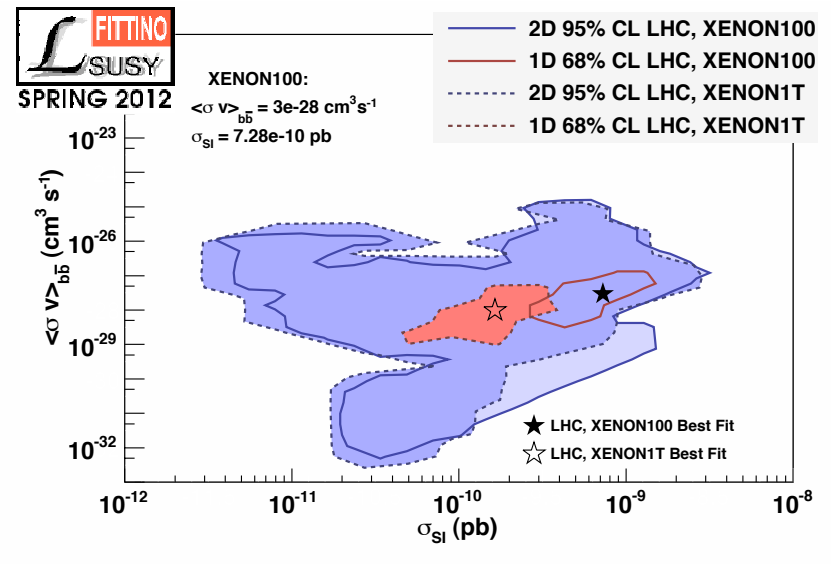

Figure 4.13: Projection of the 1σ and 2σ regions of the standard fit and the LHC+Xenon1T into the orthogonal direct vs. indirect detection plane. On the abscissa, the σ_{SI} observable is displayed, while on the ordinate, the $\langle\sigma v\rangle_{b\bar{b}}$ observable from indirect DM searches is shown. The supplementation of information to the fit from both directions is illustrated.

4.2.5 The Mass of the Lightest Neutral Higgs Boson

During the runs of the global fits for this study, the accordingly most intriguing discovery has taken place with the finding of the presumable Higgs boson of mass ~ 125 GeV (CMS) or ~ 126 GeV (ATLAS). Whether it is indeed the SM Higgs particle that has been predicted for decades or the lightest neutral Higgs boson in a SUSY framework or something totally different has yet to be determined (ATLAS Collaboration [2012], CMS Collaboration [2012]). Since this is an analysis of the CMSSM, the measurement is treated as the mass of the lightest neutral Higgs boson m_{h^0}. Compared to the standard fit, the LHC+$m_h = 126$ GeV fit deteriorates the fit significantly. A Higgs mass of $m_{h^0} = 126 \pm 3 \pm 2$ GeV, as available from the ATLAS collaboration with experimental and theoretical uncertainties, served as input in this fit scenario. As a result of the fit, the χ^2_{min} is raised to 18.4, making such a Higgs mass barely compatible with the CMSSM. The summary of the fit can be taken from Table 4.2.

First, it is of interest to single out the reason for such an increase in χ^2_{min}. In the pull plot (Figure 4.14), the $\Delta\chi^2$-contributions from individual observables can again be seen. While indirect searches for DM still remain without effect in a LHC+$m_h = 126$ GeV fit and the direct detection observable as well as jets+E_T^{miss} limits from the LHC are in excellent agreement with $m_h = 126$ GeV, serious tensions occur with regard to especially the $(g-2)_\mu$ observable and information from B-physics. The influence on B-physics is particular to the CMSSM. In more generic MSSM models the relation would be decoupled.

The standard fit prefers a Higgs mass of ~ 117 GeV. This is a significantly lower

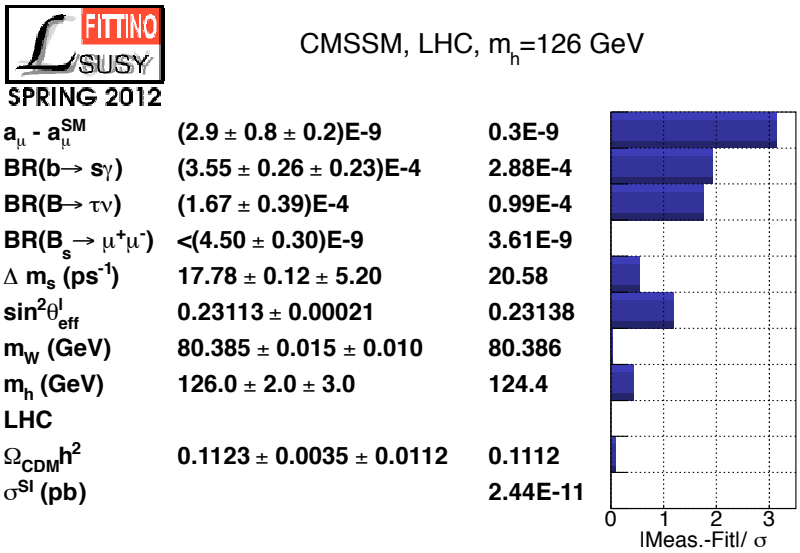

Figure 4.14: Pull plot for the LHC+$m_h = 126$ GeV fit scenario. High tensions occur in relation to the $(g-2)_\mu$ observable, decreasing the fit to $\chi^2_{min} = 18.4$ with 9 degrees of freedom.

value than ~ 126 GeV. The effect on the CMSSM parameters is demonstrated in the M_0–$M_{1/2}$ and A_0–$\tan\beta$ plane in Figure. Since the χ^2_{min} is rather high with 18.4, the best fit regions expand further into other parameter space, excepting points with worse χ^2-values compared to the standard fit. The best fit point moves to higher M_0 and $M_{1/2}$ values, which stresses the tension with the $(g-2)_\mu$ observable. A larger focus point region spanning from $M_0 \approx 3-5$ TeV also occurs as a result. Additionally, the fit prefers negative A_0 values of high magnitude, while the change in $\tan\beta$ is of less notice.

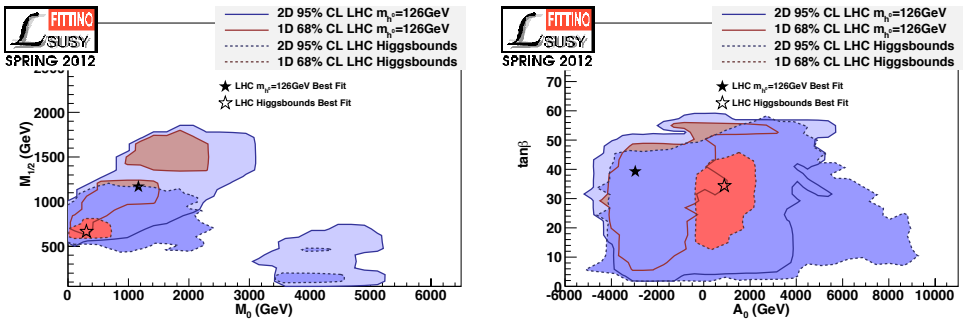

Figure 4.15: Results for the M_0–$M_{1/2}$ and A_0–$\tan\beta$ plane of the LHC+$m_h = 126$ GeV fit in comparison to the standard fit. Here, the solid lines denote the LHC+$m_h = 126$ GeV fit, while the dashed lines refer to the standard fit. The overall fit quality was found to be degenerate, leading to much broader 1σ regions. The best fit points are marked with a black and an empty star according to the lettering.

In terms of DM, the neutralino mass is pushed from 270 GeV to 497 GeV which has a major influence towards DM detection. This can be seen in the SUSY mass spectrum for the fit, where due to the worsened fit the 2σ band is once more very large compared to the standard fit. The effect of a higher neutralino mass can also be

seen in Figure 4.17. The larger 1σ region and the spread 2σ region are, as before, a sign of the worse quality of the fit. In the direct detection plane, the best fit point not only moves to higher neutralino masses, it also shifts towards lower σ_{SI} values. In this fit scenario, recent data from direct and indirect searches for DM as well as latest results from LHC searches for SUSY and DM have been used. Searches for DM and SUSY are ongoing, so that new data will continuously be available. Some of these I will mention in Chapter 5.

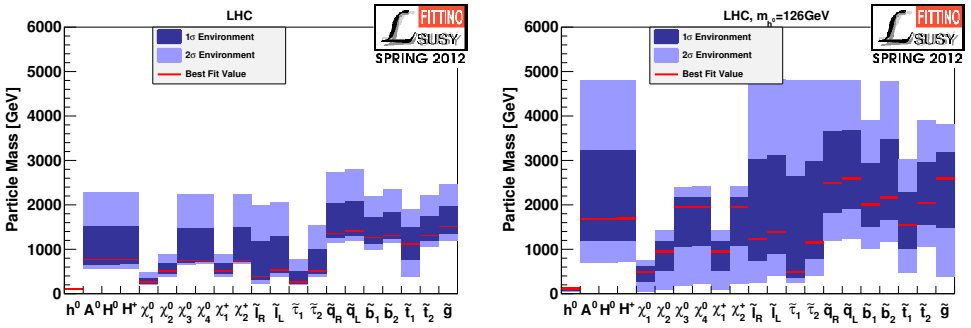

Figure 4.16: Mass spectrum of SUSY particles for the $m_h = 126$ GeV fit in comparison to the standard fit. The neutralino masses increase significantly as a result of the fit, while the overall worse fit quality causes a large 2σ band.

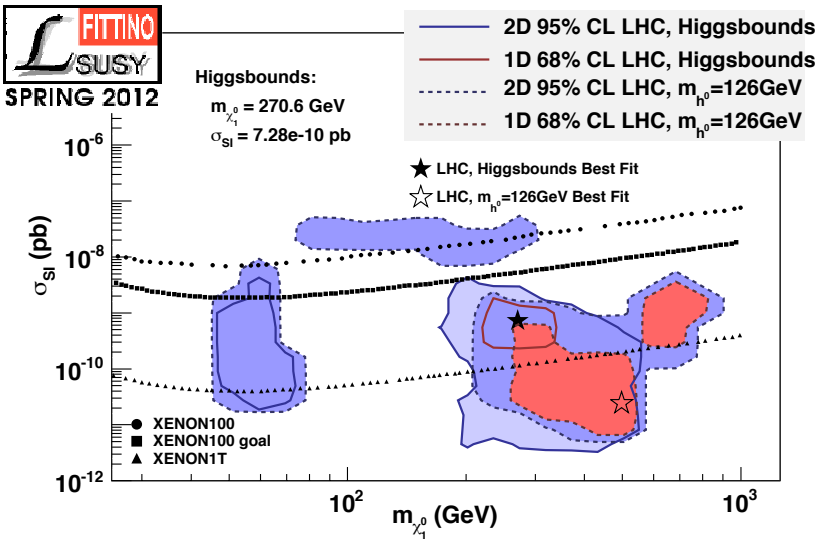

Figure 4.17: The effect of $m_h = 126$ GeV in the direct detection plane. The worse quality of the fit is noticeable in the wider 1σ and 2σ regions. The best fit point moves to higher neutralino masses and lower σ_{SI} values.

In conclusion, the finding of the Higgs boson at the LHC is an important milestone not only to prove a theory predicted for over 40 years, but also for searches for particles beyond the SM. The Higgs mechanism has been introduced to solve problems concerning particle masses. It has been a well-motivated theory that has helped

particle physicists design experiments to gain insight and proof that profound theoretical predictions are accurate. This still holds true for the wide belief that there must be physics beyond the SM that is not yet understood and that the Higgs boson is only the first step of understanding BSM processes. If the theory stopped with the Higgs boson, there would still be no quantum theory of particles, and the Universe would have to be incredibly fine-tuned. If the theory does not stop with the Higgs boson, then SUSY searches gain even higher justification. As there are already many BSM theories, it would be necessary to catch up with experimental proof or falsification to lower the number of theoretical options and to make progress in the discovery of new particles and their characteristics. Moreover, it would be the goal to find the one theory that is capable to describe all particle behavior and offer solutions to the present problems, be it DM, neutrino masses or the hierarchy problem rather than making up even more theories.

In this way, the discovery of a Higgs-like boson with ATLAS and CMS has been a most positive event in the process of proving or falsifying the first exemplary models as the CMSSM and NUHM1, putting powerful constraints on the supersymmetrical mass spectrum and consequently the annihilation mechanism of neutralino WIMPs in the early Universe (see also Baer et al. [2012]). Global fits including a Higgs mass of $\simeq 126$ GeV put great tension to the CMSSM and neutralino DM, putting this particular SUSY model to dispute and opening the door for models that shelter a 126 GeV Higgs superiorly and give better space for a corresponding DM particle. The inclusion of the Higgs mass, just recently made possible by confirmation of a signal from ATLAS and CMS, has thus changed the quality of the fits to being able to make very different conclusions compared to former fits with observables from LEP and Tevatron only. Even though the CMSSM can still hold with this measurements, tensions have highly increased and will eventually lead to pinpointing the right particle masses and couplings rather sooner than later or excluding the model eventually which at this point seems more likely.

Chapter 5

Summary and Conclusions

In particle physics, astrophysics and cosmology, fundamental problems remain unsolved. The DM problem is common to all of these disciplines. In BSM theories of particle physics, explanations for DM are mostly included as one fragment within a larger theory. In cosmology, DM is a sensitive component in structure formation and the evolution of the Universe. In astrophysics, observations and their interpretation are influenced by the DM content. With the observation of particle fluxes in the Universe and the production of new particles at the LHC, astrophysics and particle physics increasingly approach the same central problems. DM is the strongest argument to pursue theories in which these central problems are related (see also Feng [2010]). From a phenomenological point of view, it is beneficial to analyze results in a wider, interdisciplinary angle and compare the results from complementary detection methods.

A plethora of theories offer solutions to both the DM enigma and other open issues of the SM at the same time. It needs advanced experimental techniques to probe these theories, detect new particles and observe DM signatures. Most of them require high energies, long run times and a good background rejection. Particle colliders such as the LHC and the two inherent experiments ATLAS and CMS are designed to search for direct evidence of BSM particles and indirect DM signatures from missing transverse energy in the reconstruction of events. Direct detection instruments in underground laboratories allow the detection of weak interactions between DM particles coming towards the Earth with target nuclei. Observations with satellites, balloon-borne experiments or IACTs enable a detailed study of astroparticle processes, providing information of DM annihilation in particle spectra. Particle data have the potential to not only confine or exclude particular theoretical models, but also to observe yet unexpected events that may help understand particle and astroparticle physics.

Global fits In order to confront the overwhelming choice of theories with actual data, global fits are a useful tool, as many parameters can be fit simultaneously (see Chapter 3). Among the many BSM models, the CMSSM is a good choice for first

series of fits, since its number of parameters is limited to five and the neutralino as DM particle candidate in the CMSSM would be observable by a large number of complementary search instruments. Additionally, it offers solutions to other current shortcomings of the SM and is motivated by GUT theories, unifying the gauge couplings at $O(10^{16}\text{GeV})$. The first global fits were performed with information from collider experiments only (see Bardin et al. [1992]). Progressively, measurements from the relic density of CDM have been added. Of late, information from direct detection experiments have also been included into recent studies using global fits.

AstroFit In the last three years, I have worked on the development of `AstroFit` (described in Section 3.4), which takes the approach to combine all available DM related observations for the usage in global fits. Since global fits alone are already consequently updated in the particle physics sector, `AstroFit` provides an interface for adding complementary information from astrophysics and cosmology to global fits. The resulting study using the `Fittino` fit program in combination with `AstroFit`, published in Bechtle et al. [2012], is currently the only study of this manner including experimental data from the LHC, direct detection and indirect searches for DM. A different approach could be pursued if astroparticle information were implemented directly into fit programs. If the complementary approach is established in BSM research, it might as well be a standard expansion of global fits. Yet, I support the idea of stand-alone programs for each field of activity contributing to a global fit, because it encourages fruitful discussions on methods and results, as each field brings its unique expertise into the match. With many programs at hand for theoretical predictions of low-energy measurements, LHC observables and astrophysical input, each global fit consists of a main body and additional construction sets. These sets could incorporate contributions from different fields of research.

The development of AstroFit has not ceased yet. On the contrary, the implementation of increasingly more important knowledge from indirect detection is still in progress. For example, observations of antiparticle spectra already provide additional information that should be included in global fits. Also, bounds from neutrino experiments like IceCube, Super-Kamiokande and ANTARES can play an important role in putting constraints on the results from direct detection of WIMPs, even if they do not yet provide strong evidence for DM by themselves. I have shown in Chapter 4 that indirect detection of DM constrains the CMSSM parameter region from a new angle that cannot be approached by data from direct detection experiments or the LHC. Therefore, extending the range of global fits with astroparticle data from indirect DM searches is an important step to improve the information content of results.

Bayesian and frequentist interpretation The number of programs that perform global fits is increasing with the need to study BSM phenomena. Both Bayesian and frequentist interpretations are studied. The frequentist approach described in this work scans the entire parameter space without prior assumptions and therefore no

a priori knowledge or preference of parameter values. A frequentist interpretation can be interpreted as more unbiased than a Bayesian scan of parameter space, where priors are defined. However, both methods have their advantages and disadvantages. The frequentist approach needs very high statistics and thereby long computational time, and it remains a demanding task to check if the χ^2_{min} of the fit indeed corresponds to the global minimum of parameter space. This given, such an analysis is of high informative value. The Bayesian approach with defined priors to the fit offers only a hypothetical statement towards the result of the fit dependent on the prior. Yet, it is a sophisticated method to perform very precise scans of multidimensional parameter space, especially if other SUSY models with more parameters than the CMSSM are fit. With `Fittino`, both interpretations are possible. Therefore, consistency checks between both methods have been done, affirming the results. For DM phenomenology with so many BSM models to test, the frequentist interpretation offers a good method to compare the results of different models based upon same information of input.

Results from a CMSSM fit The analysis of the CMSSM (Chapter 4) showed that new knowledge from state-of-the-art experiments from particle and astroparticle experiments and observation severely constrained the CMSSM parameter space, decreasing the size of regions still allowed. The contributions from direct SUSY searches at LHC together with the low energy observables and precision data show great tension, leading to an overall higher χ^2_{min} of the entire fit compared to former fits without the LHC information. Even higher tensions occur with the inclusion of the measurement of the Higgs-like boson of mass $m = 125 - 126$ GeV at LHC if it was interpreted as the lightest neutral Higgs boson in the CMSSM. Together with the upper limits on the spin-independent WIMP-nucleon scattering cross-section σ_{SI} from Xenon100, the χ^2_{min} highly deteriorates. It would also suffer critically if the non-observation of a WIMP signal via the σ_{SI} channel continued and the predicted upper limits for the Xenon1T were affirmed. Information from indirect searches for DM of astroparticle physics become increasingly important, as the analysis has shown that already most conservative data lead to a close-in on the remaining CMSSM parameter regions. It has been shown that new physics from the LHC, upper limits from direct detection instruments and photon flux upper limits from indirect searches for DM constrain the CMSSM parameter space from different directions. If all three approaches continue in the predicted way, the CMSSM parameter space would narrow down entirely. I will briefly summarize the main results from the fit in Table 5.1.

The remaining regions of CMSSM parameter space from a fit with recent information from LHC, Xenon100 and Fermi-LAT upper limits on photon fluxes from dSPhs are the stau co-annihilation region, the funnel region and the focus-point region. Each of these regions has been constrained in those parts that were more agreeable with data and theory, e.g. the focus point region has been cut off in parts that were in better agreement with fine-tuning, while the remaining part can be probed both with direct and indirect detection methods. All accepted points within a 2σ region suffer from an increased χ^2_{min} arising from tensions among the input observables.

This is the most important information for discouraging the CMSSM as DM model. If e.g. the $(g-2)_\mu$ observable and the measurements at LHC are correct, they cannot be well accommodated in the CMSSM at the same time. With the correspondence principle that requires new physics to describe known phenomena accurately, a BSM model has to be able to incorporate all existing measurements in a new theory. The somewhat high tensions of the observables, namely the sparticle searches at LHC, the low energy observables, the hypothesis of the Higgs boson, and the upper limits on σ_{SI} strongly disfavor the CMSSM as the model to explain new physics phenomena such as DM.

Testing hypotheses When I say hypothesis, it implies that of course all hypotheses need to be clarified, as a wrong hypothesis cannot lead to a right interpretation. However, a hypothesis can be tested within a theoretical model. The hypothesis of the measured boson at LHC to be a Higgs boson remains a hypothesis as long as the exact spin of the measured particle is not identified. Yet, even if the Higgs mass did not enter the fit directly, but constraints on the Higgs mass, computed with `HiggsBounds` only from LEP and Tevatron bounds were used, the result of the fit still shows tensions between observables and small regions of parameter space left. The indirect detection information is held as conservative as possible without any boost factors and using only $b\bar{b}$ upper limits. In this way, it is mostly independent from assumptions, except for the J-factor for the dark matter density. Using these deliberate steps from very cautious to more probable interpretations, it is safe to say that photon flux upper limits will have higher impact and help restrict the CMSSM parameter space even further with any additional information. The σ_{SI} information is debatable, since both upper limits and signal regions have been found by different experiments. Therefore, both containment regions and upper limits have been tested in individual CMSSM fits. The signal regions with a preferred neutralino mass of $m_\chi \approx 10$ GeV led to incompatible results with the CMSSM. Upper limits from Xenon100, representing also higher limits from other experiments, are in agreement with latest LHC data. They were used in the standard fit. Predictions for a non-detection outcome of the Xenon1T have only been tested in an additional scenario. The constraining character of the fit was able to show that if combined forces of the LHC and direct detection experiments did not find any signal for neutralino DM and SUSY in general, new BSM theories must be considered.

Outlook As a general outcome of the analysis, latest experimental results from complementary DM searches have shown that a different DM model is more likely to explain both DM and other BSM phenomena than the CMSSM. The CMSSM has been a well-motivated BSM model that was preferable for global fits, because of its few parameters. The focus, however, moves towards other models. For instance, non-unifying SUSY models and UED are discussed for the next set of global fits. Before the CMSSM can be entirely excluded, the parameter space left should nonetheless be further probed with upcoming experimental data. New experimental constraints have been available after the setup of this study, e.g. on B-physics from Aaij et al. [2012a]

and on σ_{SI} from Xenon100 (Aprile et al. [2012]). From the LHC, more detailed information on the Higgs boson search will be available. Reconstruction of the decay channels of the boson of mass around $125 - 126$ GeV, detected with the ATLAS and CMS experiment, can give more information on particle physics in general. The conflict between signal regions and non-detection of a WIMP signal with direct detection instruments remains intriguing. Careful studies will follow the current status, leading to a better understanding. The many possible indirect detection signals will be able to contribute to global fits. Here, only photon flux upper limits have been used, but other signals and upper limits, e.g. from neutrino fluxes and antimatter fluxes, are already available, as further photon flux data from other sky regions, such as the Galactic center or Galactic halo. These information have the power to constrain BSM models even further, while offering a good opportunity for specific DM studies. Especially promising is the planned observation of the Galactic center with CTA (Doro et al. [2012]) in the near future. Another hypothesis that can be tested is the indication for a gamma-ray line as possibly observed with the Fermi-LAT instrument (Weniger [2012], Hektor et al. [2012], Su and Finkbeiner [2012] and others).

Concluding remarks In this work, I presented a unique study, using combined and complementary information from direct and indirect searches for DM with astrophysical instruments and results from collider experiments in one global fit of the CMSSM parameter space. I also showed the concept, development and usage of the `AstroFit` program and the results from a combined fit of the CMSSM with `Fittino` and `AstroFit` as one example of usage. I have described possible extensions and future prospects for the `AstroFit` project. In the context of DM, I have been able to conclude that latest experimental results and observation from astroparticle physics in addition to particle physics data constrain the CMSSM parameter space severely. Especially data from direct detection and latest LHC result are only marginally compatible with low energy precision data, while indirect searches for DM still bear great potential for model constraints. With recent prospects in each of these research fields, the probability of explaining the DM enigma within the CMSSM will be slim, and large constraints have already been put to formerly preferred parameter regions. Other DM models will therefore stand in the focus of global fits and DM phenomenology.

Subject	Conclusion
CMSSM regions	The parameter space of the CMSSM that suits all current input is reduced to the stau co-annihilation region and the funnel region. The focus point region remains to some part, but is disfavored for physical reasons.
SUSY searches at LHC	Upper limits from the non-detection of sparticles severely constrain the CMSSM in the lower energy region, ruling out the bulk region. Tensions to the $(g-2)_\mu$ observable occur. A CMSSM parameter scan becomes flat, so that the confidence regions are large.
Ω_{CDM}	The relic density of CDM remains the most stringent constraint on the CMSSM parameter space as only very limited parts match the measured relic abundance, whereas most other regions correspond to a calculated Ω_{CDM} value that is too high for a good fit.
σ_{SI} signal regions	Signal regions on σ_{SI} from DAMA/LIBRA and CoGeNT are not compatible with the CMSSM. The overall χ^2-values for the standard fit with such signal regions do not reach a value of lower than 50 for any model point.
Xenon100	Upper limits on σ_{SI} from Xenon100 are in good agreement with the LHC input.
Xenon1T	Estimated upper limits from the Xenon1T experiment would constrain the CMSSM to a point where neutralino DM becomes unreasonable. Furthermore, such limits would lead to a deterioration of the fit.
Indirect searches	Results from indirect searches do not yet constrain the CMSSM significantly. However, future prospects, i.e. with CTA (Doro et al. [2012]), are very promising, and many other channels offer supplemental information. The complementary behavior of direct and indirect searches as well as collider results have been shown.
Higgs boson	If the discovery of a Higgs boson of $m_h \approx 126$ GeV can be assumed, such an observable would lead to severe tensions within the observables in a CMSSM fit. The quality of fit is impaired to a point where the CMSSM becomes disputable.

Table 5.1: Summary of results.

Appendices

Appendix A

Example of AstroFit Input File

This is an example of an `AstroFit` input file. The file is divided into three parts: 1. relic density, 2. indirect detection, 3. direct detection. Different data files can be chosen as input for the fit. A choice of other available data files are commented out with a # symbol but are kept visible, so that they can be addressed easily, if the user wishes to change the data they want to use.

```
################################################################################
#  AstroFit input file                                                         #
#                                                                              #
#  Used to specify input data as well as various settings of AstroFit          #
#  Don't exceed line length of 80 chars (indicated by this '#' box length)!   #
################################################################################

########## 1. RELIC DENSITY ##########

# relic density
#FLAG   relic
HOW    relic    1
DATA   Oh2      0.1123 +/- 0.0035


########## 2. INDIRECT DETECTION ##########

# photon fluxes
FLAG photons
HOW  photons     0
FLAG photon_dSph
HOW  photon_dSph  1
FLAG photon_sv

#choose data files according to your choices in photon fluxes

#DATAFILE    dSph_int   dSph_int_Fornax.dat
#DATAFILE    dSph_int   dSph_int_Coma.dat
#DATAFILE    dSph_int   dSph_int_Draco.dat

DATAFILE    dSph_int   dSph_int_UMi_bbar.dat
DATAFILE    dSph_int   dSph_int_Carina_bbar.dat
#DATAFILE    dSph_int   dSph_int_Sculptor_bbar.dat
#DATAFILE    dSph_int   dSph_int_Fornax_bbar.dat

# thermal average sigma v from indirect detection
# to activate this option, you need to activate HOW photon_sv
# however only if no other HOW photon_xx option is active

#choose data files according to your sources for sigma v

DATAFILE    svind     svind_Segue1.dat
#DATAFILE   svind     svind_Carina.dat
#DATAFILE   svind     svind_Sculptor.dat
#DATAFILE   svind     svind_UMi.dat


########## 3. DIRECT DETECTION #########

# direct detection
FLAG direct

#choose data files according to your choices in direct detection

DATAFILE    direct   dd_xenon100_2012.dat
#DATAFILE    direct   dd_xenon100_100d.dat
#DATAFILE    direct   dd_cresst_1s_2011.dat
#DATAFILE    direct   dd_cresst_2s_2011.dat
#DATAFILE    direct   dd_dama_90.dat
#DATAFILE    direct   dd_dama_3s.dat
#DATAFILE    direct   dd_cogent_90.dat
#DATAFILE    direct   dd_cogent_3s.dat

###############################
# End of AstroFit input file #
###############################
```

Appendix B

Example of AstroFit Data File

Here, an example of an `AstroFit` data file. This particular file delivers the data on σ_{SI} upper limits from Xenon100 (Aprile et al. [2012]). The user can fill in information on the name of the experiment, the target material, the type of information (signal regions or upper limit), the given confidence interval (in terms of $X\sigma$ or percentage), the source of the information, and the data.

```
# Data file for elastic scattering cross section from direct detection.
# Please use exactly the same syntax if you add more of these files

# Name of experiment
Xenon100 2012

# Element
Xe

# Type
limit

# Confidence limit [%]
90

# data taken from [1207.5988]

# WIMP mass[GeV] | si elastic scattering cross-section [pb]
#............       ..............
  0.5971E+01            7.327E-04
  0.6001E+01            5.948E-04
  0.6061E+01            4.930E-04
  0.6122E+01            4.002E-04
  0.6153E+01            3.181E-04
  0.6184E+01            2.749E-04
  0.6246E+01            2.278E-04
  0.6278E+01            1.888E-04
  0.6341E+01            1.565E-04
  0.6373E+01            1.297E-04
  0.6405E+01            1.075E-04
  0.6469E+01            8.912E-05
  0.6501E+01            7.542E-05
  0.6534E+01            6.122E-05
  0.6600E+01            5.074E-05
  0.6633E+01            4.294E-05
  0.6700E+01            3.559E-05
  0.6733E+01            2.950E-05
  0.6801E+01            2.394E-05
  0.6835E+01            2.026E-05
  0.6869E+01            1.679E-05
  0.6904E+01            1.335E-05
  0.7008E+01            1.106E-05
  0.7150E+01            8.801E-06
  0.7222E+01            7.448E-06
  0.7331E+01            6.046E-06
  0.7405E+01            5.012E-06
  0.7555E+01            4.069E-06
  0.7669E+01            3.372E-06
  0.7785E+01            2.681E-06
  0.7903E+01            2.222E-06
  0.7983E+01            1.920E-06
  0.8103E+01            1.625E-06
  0.8267E+01            1.376E-06
  0.8351E+01            1.189E-06
  0.8435E+01            1.027E-06
  0.8605E+01            9.070E-07
  0.8692E+01            7.838E-07
  0.8868E+01            5.977E-07
  0.9092E+01            4.955E-07
  0.9369E+01            4.023E-07
```

0.9559E+01	3.266E-07
0.9752E+01	2.765E-07
1.0000E+01	2.245E-07
1.0250E+01	1.940E-07
1.0510E+01	1.642E-07
1.0830E+01	1.361E-07
1.1100E+01	1.129E-07
1.1330E+01	9.556E-08
1.1730E+01	7.759E-08
1.2030E+01	6.568E-08
1.2330E+01	5.677E-08
1.2580E+01	4.907E-08
1.3160E+01	3.822E-08
1.3570E+01	3.304E-08
1.3910E+01	2.916E-08
1.4260E+01	2.573E-08
1.4620E+01	2.271E-08
1.4990E+01	2.090E-08
1.5380E+01	1.923E-08
1.5690E+01	1.733E-08
1.6080E+01	1.529E-08
1.6570E+01	1.407E-08
1.6990E+01	1.268E-08
1.7510E+01	1.167E-08
1.7960E+01	1.074E-08
1.8410E+01	9.682E-09
1.8880E+01	8.725E-09
1.9550E+01	7.702E-09
2.0050E+01	6.941E-09
2.0760E+01	6.256E-09
2.1400E+01	5.757E-09
2.2050E+01	5.298E-09
2.2720E+01	4.978E-09
2.3300E+01	4.776E-09
2.4130E+01	4.583E-09
2.4860E+01	4.130E-09
2.5620E+01	3.881E-09
2.6800E+01	3.498E-09
2.7760E+01	3.153E-09
2.8890E+01	3.026E-09
3.0530E+01	2.728E-09
3.2100E+01	2.618E-09
3.3740E+01	2.461E-09
3.5480E+01	2.361E-09
3.7480E+01	2.266E-09
3.8820E+01	2.221E-09
4.0410E+01	2.176E-09
4.2270E+01	2.132E-09
4.3780E+01	2.133E-09
4.5570E+01	2.090E-09
4.7670E+01	2.091E-09
4.9860E+01	2.092E-09
5.2160E+01	2.094E-09
5.5390E+01	2.095E-09
5.8530E+01	2.097E-09
6.1220E+01	2.098E-09
6.3730E+01	2.099E-09
6.8350E+01	2.101E-09
7.0790E+01	2.191E-09
7.3680E+01	2.239E-09

7.7080E+01	2.335E-09
8.1850E+01	2.437E-09
8.6920E+01	2.543E-09
9.1380E+01	2.598E-09
9.6550E+01	2.654E-09
1.0150E+02	2.769E-09
1.0610E+02	2.889E-09
1.1160E+02	3.014E-09
1.1910E+02	3.145E-09
1.2520E+02	3.351E-09
1.3300E+02	3.496E-09
1.4190E+02	3.648E-09
1.4990E+02	3.886E-09
1.5760E+02	3.971E-09
1.6410E+02	4.057E-09
1.7170E+02	4.321E-09
1.8050E+02	4.508E-09
1.8880E+02	4.703E-09
1.9650E+02	4.805E-09
2.0450E+02	5.012E-09
2.1500E+02	5.229E-09
2.2490E+02	5.455E-09
2.3530E+02	5.573E-09
2.4740E+02	5.937E-09
2.5750E+02	6.065E-09
2.6670E+02	6.327E-09
2.7620E+02	6.463E-09
2.8320E+02	6.601E-09
2.9480E+02	6.744E-09
3.0380E+02	7.034E-09
3.1300E+02	7.185E-09
3.2420E+02	7.340E-09
3.4430E+02	7.820E-09
3.5650E+02	7.989E-09
3.6930E+02	8.333E-09
3.8050E+02	8.512E-09
3.9210E+02	8.878E-09
4.0810E+02	9.070E-09
4.2060E+02	9.460E-09
4.3780E+02	9.868E-09
4.5570E+02	1.029E-08
4.6960E+02	1.051E-08
4.9370E+02	1.097E-08
5.1380E+02	1.144E-08
5.4570E+02	1.219E-08
5.8230E+02	1.272E-08
6.0610E+02	1.327E-08
6.3410E+02	1.384E-08
6.5670E+02	1.444E-08
6.7670E+02	1.506E-08
7.0080E+02	1.571E-08
7.2950E+02	1.638E-08
7.5550E+02	1.709E-08
7.9030E+02	1.783E-08
8.3510E+02	1.860E-08
8.6920E+02	1.941E-08
9.0920E+02	2.067E-08
9.5110E+02	2.156E-08
9.8010E+02	2.249E-08

```
# END of file
#
```

Appendix C

Example of AstroFit Output File

An example of an output file handed from `AstroFit` to `Fittino` is shown below. It is kept as simple as possible. The keywords as well as the value following the keywords are read out by according functions in `Fittino` and can be used in the fit. The syntax of the output file can be changed by request.

```
BLOCK AF_OBS
relic  0.138603
chi2_relic  5.00260164
photon  0.
chi2_photon  3.84182612E-09
svind  3.67864485E-27
chi2_svind  1.4776143E-54
direct  2.42189317E-08
chi2_direct  3.88688837
```

Bibliography

[Aad et al., 2012] Aad, G., et al., 2012. Search for squarks and gluinos with the ATLAS detector in final states with jets and missing transverse momentum using 4.7 fb^{-1} of $\sqrt{s} = 7$ TeV proton-proton collision data.

[Aaij et al., 2012a] Aaij, R., et al., 2012a. First evidence for the decay $B_s \to \mu^+\mu^-$.

[Aaij et al., 2012b] Aaij, R., et al., 2012b. Strong constraints on the rare decays $B_s \to \mu^+\mu^-$ and $B^0 \to \mu^+\mu^-$. Phys.Rev.Lett. 108, 231801.

[Aalseth et al., 2011] Aalseth, C., et al., 2011. Results from a Search for Light-Mass Dark Matter with a P-type Point Contact Germanium Detector. Phys.Rev.Lett. 106, 131301.

[Aalseth et al., 2012] Aalseth, C., et al., 2012. CoGeNT: A Search for Low-Mass Dark Matter using p-type Point Contact Germanium Detectors.

[Abdallah et al., 2003] Abdallah, J., et al., 2003. Searches for supersymmetric particles in e+ e- collisions up to 208-GeV and interpretation of the results within the MSSM. Eur.Phys.J. C31, 421–479.

[Abdo et al., 2010] Abdo, A., et al., 2010. Observations of Milky Way Dwarf Spheroidal galaxies with the Fermi-LAT detector and constraints on Dark Matter models. Astrophys.J. 712, 147–158.

[Abdo et al., 2009] Abdo, A. A., et al., 2009. Measurement of the Cosmic Ray e+ plus e- spectrum from 20 GeV to 1 TeV with the Fermi Large Area Telescope. Phys.Rev.Lett. 102, 181101.

[Abe et al., 2008] Abe, K., Fuke, H., Haino, S., Hams, T., Itazaki, A., et al., 2008. Measurement of cosmic-ray low-energy antiproton spectrum with the first BESS-Polar Antarctic flight. Phys.Lett. B670, 103–108.

[Abramowski et al., 2011a] Abramowski, A., et al., 2011a. H.E.S.S. constraints on Dark Matter annihilations towards the Sculptor and Carina Dwarf Galaxies. Astropart.Phys. 34, 608–616.

[Abramowski et al., 2011b] Abramowski, A., et al., 2011b. Search for a Dark Matter annihilation signal from the Galactic Center halo with H.E.S.S. Phys.Rev.Lett. 106, 161301.

[Abramowski et al., 2012] Abramowski, A., et al., 2012. Search for Dark Matter Annihilation Signals from the Fornax Galaxy Cluster with H.E.S.S. Astrophys.J. 750, 123.

[Ackermann et al., 2011] Ackermann, M., et al., 2011. Constraining Dark Matter Models from a Combined Analysis of Milky Way Satellites with the Fermi Large Area Telescope. Phys.Rev.Lett. 107, 241302.

[Adriani et al., 2009] Adriani, O., et al., 2009. An anomalous positron abundance in cosmic rays with energies 1.5-100 GeV. Nature 458, 607–609.

[Adriani et al., 2010] Adriani, O., et al., 2010. PAMELA results on the cosmic-ray antiproton flux from 60 MeV to 180 GeV in kinetic energy. Phys.Rev.Lett. 105, 121101.

[Aharonian et al., 2006a] Aharonian, F., et al., 2006a. H.E.S.S. observations of the Galactic Center region and their possible dark matter interpretation. Phys.Rev.Lett. 97, 221102.

[Aharonian et al., 2006b] Aharonian, F., et al., 2006b. Observations of the Crab Nebula with H.E.S.S. Astron.Astrophys. 457, 899–915.

[Ahmed et al., 2010] Ahmed, Z., et al., 2010. Dark Matter Search Results from the CDMS II Experiment. Science 327, 1619–1621.

[Ahmed et al., 2012] Ahmed, Z., et al., 2012. Search for annual modulation in low-energy CDMS-II data.

[Albert et al., 2008] Albert, J., et al., 2008. VHE Gamma-Ray Observation of the Crab Nebula and Pulsar with MAGIC. Astrophys.J. 674, 1037–1055.

[Angloher et al., 2012] Angloher, G., Bauer, M., Bavykina, I., Bento, A., Bucci, C., et al., 2012. Results from 730 kg days of the CRESST-II Dark Matter Search. Eur.Phys.J. C72, 1971.

[Aprile et al., 2010] Aprile, E., et al., 2010. First Dark Matter Results from the XENON100 Experiment. Phys.Rev.Lett. 105, 131302.

[Aprile et al., 2011] Aprile, E., et al., 2011. Dark Matter Results from 100 Live Days of XENON100 Data. Phys.Rev.Lett.

[Aprile et al., 2012] Aprile, E., et al., 2012. Dark Matter Results from 225 Live Days of XENON100 Data.

[Arens et al., 2008] Arens, T., Hettlich, F., Karpfinger, C., Kockelkorn, U., Lichtenegger, K., Stachel, H., 2008. Mathematik. Spektrum Akademischer Verlag Heidelberg.

[Arguelles and Kopp, 2012] Arguelles, C. A., Kopp, J., 2012. Sterile neutrinos and indirect dark matter searches in IceCube. JCAP 1207, 016.

[Armengaud et al., 2010] Armengaud, E., Augier, C., Benoit, A., Berge, L., Besida, O., et al., 2010. First results of the EDELWEISS-II WIMP search using Ge cryogenic detectors with interleaved electrodes. Phys.Lett. B687, 294–298.

[Asner et al., 2010] Asner, D., et al., 2010. Averages of b-hadron, c-hadron, and τ-lepton Properties.

[ATLAS Collaboration, 2012] ATLAS Collaboration, 2012. Observation of a new particle in the search for the Standard Model Higgs boson with the ATLAS detector at the LHC. Physics Letters B 716 (1), 1 – 29.

[Atwood et al., 2009] Atwood, W., et al., 2009. The Large Area Telescope on the Fermi Gamma-ray Space Telescope Mission. Astrophys.J. 697, 1071–1102.

[Baer, 2011] Baer, H., 2011. Theoretical expectations for dark matter detection at the LHC. PoS IDM2010, 129.

[Baer et al., 2012] Baer, H., Barger, V., Mustafayev, A., 2012. Neutralino dark matter in mSUGRA/CMSSM with a 125 GeV light Higgs scalar. JHEP 1205, 091.

[Baer et al., 1999] Baer, H., Chen, C.-h., Drees, M., Paige, F., Tata, X., 1999. Probing minimal supergravity at the CERN LHC for large tan Beta. Phys.Rev. D59, 055014.

[Baer and List, 2012] Baer, H., List, J., 2012. Post LHC7 SUSY benchmark points for ILC physics.

[Bardin et al., 1992] Bardin, D. Y., Bilenky, M. S., Chizhov, A., Fedorenko, O., Ganguli, S. N., et al., 1992. ZFITTER: An Analytical program for fermion pair production in e+ e- annihilation.

[Battaglia et al., 2004] Battaglia, M., De Roeck, A., Ellis, J. R., Gianotti, F., Olive, K., et al., 2004. Updated post - WMAP benchmarks for supersymmetry. Eur.Phys.J. C33, 273–296.

[Battiston, 2009] Battiston, R., 2009. The Anti Matter Spectrometer (AMS-02): A particle physics detector in space.

[Bechtle et al., 2011] Bechtle, P., Brein, O., Heinemeyer, S., Weiglein, G., Williams, K. E., 2011. HiggsBounds 2.0.0: Confronting Neutral and Charged Higgs Sector Predictions with Exclusion Bounds from LEP and the Tevatron. Comput.Phys.Commun. 182, 2605–2631.

[Bechtle et al., 2012] Bechtle, P., Bringmann, T., Desch, K., Dreiner, H., Hamer, M., et al., 2012. Constrained Supersymmetry after two years of LHC data: a global view with Fittino. JHEP 1206, 098.

[Bechtle et al., 2010] Bechtle, P., Desch, K., Uhlenbrock, M., Wienemann, P., 2010. Constraining SUSY models with Fittino using measurements before, with and beyond the LHC. Eur.Phys.J. C66, 215–259.

[Bekenstein, 2004] Bekenstein, J. D., 2004. Relativistic gravitation theory for the MOND paradigm. Phys.Rev. D70, 083509.

[Belanger et al., 2010] Belanger, G., Boudjema, F., Pukhov, A., Semenov, A., 2010. micrOMEGAs: A Tool for dark matter studies.

[Beltran et al., 2010] Beltran, M., Hooper, D., Kolb, E. W., Krusberg, Z. A., Tait, T. M., 2010. Maverick dark matter at colliders. JHEP 1009, 037.

[Bennett et al., 2006] Bennett, G., et al., 2006. Final Report of the Muon E821 Anomalous Magnetic Moment Measurement at BNL. Phys.Rev. D73, 072003.

[Bergstrom, 2000] Bergstrom, L., 2000. Nonbaryonic dark matter: Observational evidence and detection methods. Rept.Prog.Phys. 63, 793.

[Bergstrom, 2012] Bergstrom, L., 2012. Dark Matter Evidence, Particle Physics Candidates and Detection Methods.

[Beringer et al., 2012] Beringer, J., et al., 2012. Review of Particle Physics (RPP). Phys.Rev. D86, 010001.

[Bernabei et al., 2008] Bernabei, R., et al., 2008. First results from DAMA/LIBRA and the combined results with DAMA/NaI. Eur.Phys.J. C56, 333–355.

[Bernabei et al., 2010] Bernabei, R., et al., 2010. New results from DAMA/LIBRA. Eur.Phys.J. C67, 39–49.

[Bertone, 2010] Bertone, G., 2010. Particle Dark Matter. Cambridge University Press.

[Bertone et al., 2005] Bertone, G., Hooper, D., Silk, J., 2005. Particle dark matter: Evidence, candidates and constraints. Phys.Rept. 405, 279–390.

[Bradac et al., 2008] Bradac, M., Allen, S. W., Treu, T., Ebeling, H., Massey, R., et al., 2008. Revealing the properties of dark matter in the merging cluster MACSJ0025.4-1222.

[Bringmann et al., 2008] Bringmann, T., Bergstrom, L., Edsjo, J., 2008. New Gamma-Ray Contributions to Supersymmetric Dark Matter Annihilation. JHEP 0801, 049.

[Bringmann et al., 2012] Bringmann, T., Huang, X., Ibarra, A., Vogl, S., Weniger, C., 2012. Fermi LAT Search for Internal Bremsstrahlung Signatures from Dark Matter Annihilation.

[Buchmueller, 2012] Buchmueller, O., 2012. Global (SUSY) Fits in 2012 (Frequentist Approach). darkattack2012 Workshop.

[Buchmueller et al., 2012] Buchmueller, O., Cavanaugh, R., Citron, M., De Roeck, A., Dolan, M., et al., 2012. The CMSSM and NUHM1 in Light of 7 TeV LHC, B_s to $\mu^+\mu^-$ and XENON100 Data.

[Buchmueller et al., 2009] Buchmueller, O., Cavanaugh, R., De Roeck, A., Ellis, J., Flacher, H., et al., 2009. Likelihood Functions for Supersymmetric Observables in Frequentist Analyses of the CMSSM and NUHM1. Eur.Phys.J. C64, 391–415.

[Caceres, 2009] Caceres, G., 2009. Explaining the WMAP Haze with Neutralino Dark Matter.

[Cerdeno and Green, 2010] Cerdeno, D. G., Green, A. M., 2010. Direct detection of WIMPs.

[Challinor, 2012] Challinor, A., 2012. CMB anisotropy science: a review.

[Chandra X-Ray Observatory, 2009] Chandra X-Ray Observatory, Apr. 2009. http://chandra.harvard.edu/photo/2006/1e0657/.

[Cheng et al., 2002] Cheng, H.-C., Feng, J. L., Matchev, K. T., 2002. Kaluza-Klein dark matter. Phys.Rev.Lett. 89, 211301.

[Chou et al., 2008] Chou, A. S., et al., 2008. Search for axion-like particles using a variable baseline photon regeneration technique. Phys.Rev.Lett. 100, 080402.

[Ciuchini et al., 1998] Ciuchini, M., Degrassi, G., Gambino, P., Giudice, G., 1998. Next-to-leading QCD corrections to B $\rightarrow$ X(s) gamma in supersymmetry. Nucl.Phys. B534, 3–20.

[Cline, 2011] Cline, D. B., 2011. Recent results on the low mass dark matter WIMP controversy: 2011.

[Clowe et al., 2006] Clowe, D., Bradac, M., Gonzalez, A. H., Markevitch, M., Randall, S. W., et al., 2006. A direct empirical proof of the existence of dark matter. Astrophys.J. 648, L109–L113.

[CMS Collaboration, 2012] CMS Collaboration, 2012. Observation of a new boson at a mass of 125 GeV with the CMS experiment at the LHC. Physics Letters B 716 (1), 30 – 61.

[Cottingham and Greenwood, 2007] Cottingham, W., Greenwood, D., 2007. An Introduction to the Standard Model of Particle Physics, 2nd Edition. Cambridge University Press.

[Davier et al., 2010] Davier, M., Hoecker, A., Lopez Castro, G., Malaescu, B., Mo, X., et al., 2010. The Discrepancy Between tau and e+e- Spectral Functions Revisited and the Consequences for the Muon Magnetic Anomaly. Eur.Phys.J. C66, 127–136.

[de Austri et al., 2006] de Austri, R. R., Trotta, R., Roszkowski, L., 2006. A Markov chain Monte Carlo analysis of the CMSSM. JHEP 0605, 002.

[De Jesus, 2004] De Jesus, M., 2004. WIMP / neutralino direct detection. Int.J.Mod.Phys. A19, 1142.

[Dedes et al., 2001] Dedes, A., Dreiner, H. K., Nierste, U., 2001. Correlation of $B_s \rightarrow \mu^+\mu^-$ and $(g-2)_\mu$ in minimal supergravity. Phys.Rev.Lett. 87, 251804.

[Djouadi et al., 2005] Djouadi, A., Drees, M., Kneur, J.-L., 2005. Neutralino dark matter in mSUGRA: Reopening the light Higgs pole window. Phys.Lett. B624, 60–69.

[Doro and consortium, 2011] Doro, M., consortium, f. t. C., 2011. CTA - A Project for a New Generation of Cherenkov Telescopes. Nucl.Instrum.Meth. A630, 285–290.

[Doro et al., 2012] Doro, M., et al., 2012. Dark Matter and Fundamental Physics with the Cherenkov Telescope Array.

[Ehret et al., 2010] Ehret, K., Frede, M., Ghazaryan, S., Hildebrandt, M., Knabbe, E.-A., et al., 2010. New ALPS Results on Hidden-Sector Lightweights. Phys.Lett. B689, 149–155.

[Einasto, 2009] Einasto, J., 2009. Dark Matter.

[Ellis, 2011] Ellis, J., 2011. Casting Light on Dark Matter.

[Ellis, 2012] Ellis, J., 2012. Outstanding questions: Physics beyond the Standard Model. Phil.Trans.Roy.Soc.Lond. A370, 818–830.

[Ellis and Olive, 2010] Ellis, J., Olive, K. A., 2010. Supersymmetric Dark Matter Candidates.

[Ellis and Olive, 2012] Ellis, J., Olive, K. A., 2012. Revisiting the Higgs Mass and Dark Matter in the CMSSM. Eur.Phys.J. C72, 2005.

[Ellis et al., 2001] Ellis, J. R., Falk, T., Ganis, G., Olive, K. A., Srednicki, M., 2001. The CMSSM parameter space at large tan beta. Phys.Lett. B510, 236–246.

[Ellis et al., 1998] Ellis, J. R., Falk, T., Olive, K. A., 1998. Neutralino - Stau coannihilation and the cosmological upper limit on the mass of the lightest supersymmetric particle. Phys.Lett. B444, 367–372.

[Ellis et al., 2000] Ellis, J. R., Falk, T., Olive, K. A., Srednicki, M., 2000. Calculations of neutralino-stau coannihilation channels and the cosmologically relevant region of MSSM parameter space. Astropart.Phys. 13, 181–213.

[Feldman and Cousins, 1998] Feldman, G. J., Cousins, R. D., 1998. A Unified approach to the classical statistical analysis of small signals. Phys.Rev. D57, 3873–3889.

[Feng, 2010] Feng, J. L., 2010. Dark Matter Candidates from Particle Physics and Methods of Detection. Ann.Rev.Astron.Astrophys. 48, 495–545.

[Fitzpatrick et al., 2010] Fitzpatrick, A. L., Hooper, D., Zurek, K. M., 2010. Implications of CoGeNT and DAMA for Light WIMP Dark Matter. Phys.Rev. D81, 115005.

[Fowlie et al., 2012] Fowlie, A., Kazana, M., Kowalska, K., Munir, S., Roszkowski, L., et al., 2012. The CMSSM Favoring New Territories: The Impact of New LHC Limits and a 125 GeV Higgs.

[Fox et al., 2012] Fox, P. J., Kopp, J., Lisanti, M., Weiner, N., 2012. A CoGeNT Modulation Analysis. Phys.Rev. D85, 036008.

[Gelmini and Gondolo, 2004] Gelmini, G., Gondolo, P., 2004. DAMA dark matter detection compatible with other searches.

[Gondolo et al., 2010] Gondolo, P., Edsjo, J., Ullio, P., Bergstrom, L., Schelke, M., Baltz, E., Bringmann, T., Duda, G., Sep. 2010. Darksusy home page. http://www.darksusy.org.

[Gondolo et al., 2002] Gondolo, P., Edsjo, J., Ullio, P., Bergstrom, L., Schelke, M., et al., 2002. Darksusy - a numerical package for supersymmetric dark matter calculations, 256–261.

[Gondolo et al., 2004] Gondolo, P., Edsjo, J., Ullio, P., Bergstrom, L., Schelke, M., et al., 2004. DarkSUSY: Computing supersymmetric dark matter properties numerically. JCAP 0407, 008.

[Grasso et al., 2009] Grasso, D., et al., 2009. On possible interpretations of the high energy electron-positron spectrum measured by the Fermi Large Area Telescope. Astropart.Phys. 32, 140–151.

[Griffith, 2010] Griffith, D., 2010. Introduction to Elementary Particles, 4th Edition. Wiley-VCH.

[Hektor et al., 2012] Hektor, A., Raidal, M., Tempel, E., 2012. An evidence for indirect detection of dark matter from galaxy clusters in Fermi-LAT data.

[Hooper and Baltz, 2008] Hooper, D., Baltz, E. A., 2008. Strategies for Determining the Nature of Dark Matter. Ann.Rev.Nucl.Part.Sci. 58, 293–314.

[Hooper and Kelso, 2011] Hooper, D., Kelso, C., 2011. Implications of CoGeNT's New Results For Dark Matter. Phys.Rev. D84, 083001.

[iSGTW, 2012] iSGTW, Aug. 2012. Go on a particle quest at the first cern hackfest. http://www.isgtw.org/spotlight/go-particle-quest-first-cern-hackfest.

[Jungman et al., 1996] Jungman, G., Kamionkowski, M., Griest, K., 1996. Supersymmetric dark matter. Phys.Rept. 267, 195–373.

[Kamionkowski, 1997] Kamionkowski, M., 1997. WIMP and axion dark matter.

[Kane et al., 1994] Kane, G. L., Kolda, C. F., Roszkowski, L., Wells, J. D., 1994. Study of constrained minimal supersymmetry. Phys.Rev. D49, 6173–6210.

[Kappl and Winkler, 2012] Kappl, R., Winkler, M. W., 2012. Dark Matter after BESS-Polar II. Phys.Rev. D85, 123522.

[Komatsu et al., 2011] Komatsu, E., et al., 2011. Seven-Year Wilkinson Microwave Anisotropy Probe (WMAP) Observations: Cosmological Interpretation. Astrophys.J.Suppl. 192, 18.

[Kuhlen, 2010] Kuhlen, M., 2010. The Dark Matter Annihilation Signal from Dwarf Galaxies and Subhalos. Adv.Astron. 2010, 162083.

[Ludwig, 2010] Ludwig, D., 2010. The global electroweak fit and constraints on new physics with Gfitter. PoS ICHEP2010, 404.

[Mangano, 2012] Mangano, S., 2012. Selected results from the ANTARES neutrino telescope.

[Martin, 1997] Martin, S. P., 1997. A Supersymmetry primer.

[Martinez et al., 2009a] Martinez, G. D., Bullock, J. S., Kaplinghat, M., Strigari, L. E., Trotta, R., 2009a. Indirect Dark Matter Detection from Dwarf Satellites: Joint Expectations from Astrophysics and Supersymmetry. JCAP 0906, 014.

[Martinez et al., 2009b] Martinez, G. D., Bullock, J. S., Kaplinghat, M., Strigari, L. E., Trotta, R., 2009b. Indirect Dark Matter Detection from Dwarf Satellites: Joint Expectations from Astrophysics and Supersymmetry. JCAP 0906, 014.

[McMahon, 2008] McMahon, D., 2008. Quantum Field Theory Demystified, 1st Edition. McGraw-Hill.

[Melbeus et al., 2012] Melbeus, H., Merle, A., Ohlsson, T., 2012. Higgs Dark Matter in UEDs: A Good WIMP with Bad Detection Prospects. Phys.Lett. B715, 164–169.

[Merten et al., 2011] Merten, J., Coe, D., Dupke, R., Massey, R., Zitrin, A., et al., 2011. Creation of cosmic structure in the complex galaxy cluster merger Abell 2744. Mon.Not.Roy.Astron.Soc. 417, 333–347.

[Milgrom, 1983] Milgrom, M., 1983. A Modification of the Newtonian dynamics as a possible alternative to the hidden mass hypothesis. Astrophys.J. 270, 365–370.

[Mohanty et al., 2012] Mohanty, S., Rao, S., Roy, D., 2012. Predictions of a Natural SUSY Dark Matter Model for Direct and Indirect Detection Experiments.

[Moskalenko and Strong, 1998] Moskalenko, I., Strong, A., 1998. Production and propagation of cosmic ray positrons and electrons. Astrophys.J. 493, 694–707.

[Munoz, 2012] Munoz, C., 2012. Indirect Dark Matter Searches and Models.

[NASA, 2011] NASA, Jun. 2011. WMAP-recommended Parameter Constraints. `http://lambda.gsfc.nasa.gov/product/map/current/best_params.cfm`.

[Nath et al., 2010] Nath, P., Nelson, B. D., Davoudiasl, H., Dutta, B., Feldman, D., et al., 2010. The Hunt for New Physics at the Large Hadron Collider. Nucl.Phys.Proc.Suppl. 200-202, 185–417.

[Nguyen et al., 2012] Nguyen, N., Horns, D., Bringmann, T., Feb. 2012. AstroFit: An Interface Program for Exploring Complementarity in Dark Matter Research. ArXiv e-prints.

[Paczynski, 1986] Paczynski, B., May 1986. Gravitational microlensing by the galactic halo. Astrophys. J.304, 1–5.

[Papini et al., 2004] Papini, P., Piccardi, S., Spillantini, P., Vannuccini, E., Ambriola, M., et al., 2004. High-energy deuteron measurement with the CAPRICE98 experiment. Astrophys.J. 615, 259–274.

[Pavan et al., 2002] Pavan, M., Strakovsky, I., Workman, R., Arndt, R., 2002. The Pion nucleon Sigma term is definitely large: Results from a G.W.U. analysis of pi nucleon scattering data. PiN Newslett. 16, 110–115.

[Peccei and Quinn, 1977] Peccei, R., Quinn, H. R., 1977. CP Conservation in the Presence of Instantons. Phys.Rev.Lett. 38, 1440–1443.

[Perkins, 2003] Perkins, D., 2003. Particle Astrophysics. Oxford University Press.

[Peskin and Schroeder, 1995] Peskin, M., Schroeder, D., 1995. Introduction to Quantum Field Theory. Westview Press.

[Picozza et al., 2007] Picozza, P., Galper, A., Castellini, G., Adriani, O., Altamura, F., et al., 2007. PAMELA: A Payload for Antimatter Matter Exploration and Light-nuclei Astrophysics. Astropart.Phys. 27, 296–315.

[Plambeck, 2011] Plambeck, N., 2011. Komplementäre Analyse von Suchen nach dunkler Materie und Ergebnissen von Beschleunigerphysik mit AstroFit.
URL `http://wwwiexp.desy.de/groups/astroparticle/de/forschung/nils_plambeck.pdf`

[Porter et al., 2011] Porter, T. A., Johnson, R. P., Graham, P. W., 2011. Dark Matter Searches with Astroparticle Data. Ann.Rev.Astron.Astrophys. 49, 155–194.

[Press et al., 2007] Press, W., Teukolsky, S., Vetterling, W., B.P., F., 2007. Numerical Recipes - The Art of Scientific Computing, 3rd Edition. Cambridge Press.

[Press et al., 1992] Press, W., Teukolsky, S., Vetterling, W., Flannery, B., 1992. Numerical Recipes in Fortran 77. Cambridge University Press.

[Roszkowski et al., 2001] Roszkowski, L., Ruiz de Austri, R., Nihei, T., 2001. New cosmological and experimental constraints on the CMSSM. JHEP 0108, 024.

[Sanchez-Conde et al., 2010] Sanchez-Conde, M. A., Paneque, D., Bloom, E. D., Prada, F., Dominguez, A., 2010. The Search of Axion-Like-Particles with Fermi and Cherenkov Telescopes.

[Santoso, 2003] Santoso, Y., 2003. The MSSM with nonuniversal Higgs masses, 184–188.

[Savage et al., 2011] Savage, C., Gelmini, G., Gondolo, P., Freese, K., 2011. XENON10/100 dark matter constraints in comparison with CoGeNT and DAMA: examining the Leff dependence. Phys.Rev. D83, 055002.

[Schnee, 2011] Schnee, R., 2011. Introduction to dark matter experiments.

[Scott, 2011] Scott, P., 2011. Searches for Particle Dark Matter: An Introduction.

[Scott et al., 2010] Scott, P., Conrad, J., Edsjo, J., Bergstrom, L., Farnier, C., et al., 2010. Direct Constraints on Minimal Supersymmetry from Fermi-LAT Observations of the Dwarf Galaxy Segue 1. JCAP 1001, 031.

[Servant and Tait, 2003] Servant, G., Tait, T. M., 2003. Is the lightest Kaluza-Klein particle a viable dark matter candidate? Nucl.Phys. B650, 391–419.

[Shears, 2012] Shears, T., 2012. The Standard Model. Phil.Trans.Roy.Soc.Lond. A370, 805–817.

[Simon, 2012] Simon, M., 2012. The space experiment PAMELA. Phys.Unserer Zeit 43N1, 18–24.

[Skands et al., 2004] Skands, P. Z., Allanach, B., Baer, H., Balazs, C., Belanger, G., et al., 2004. SUSY Les Houches accord: Interfacing SUSY spectrum calculators, decay packages, and event generators. JHEP 0407, 036.

[Skielboe et al., 2012] Skielboe, A., Wojtak, R., Pedersen, K., Rozo, E., Rykoff, E. S., 2012. Spatial anisotropy of galaxy kinematics in SDSS galaxy clusters.

[Su and Finkbeiner, 2012] Su, M., Finkbeiner, D. P., 2012. Strong Evidence for Gamma-ray Line Emission from the Inner Galaxy.

[Tanaka et al., 2011] Tanaka, T., et al., 2011. An Indirect Search for WIMPs in the Sun using 3109.6 days of upward-going muons in Super-Kamiokande. Astrophys.J. 742, 78.

[Tempel et al., 2012] Tempel, E., Hektor, A., Raidal, M., 2012. Fermi 130 GeV gamma-ray excess and dark matter annihilation in sub-haloes and in the Galactic centre. JCAP 1209, 032.

[Trotta and Cranmer, 2011] Trotta, R., Cranmer, K., 2011. Statistical Challenges of Global SUSY Fits.

[Trotta et al., 2008] Trotta, R., Feroz, F., Hobson, M. P., Roszkowski, L., Ruiz de Austri, R., 2008. The Impact of priors and observables on parameter inferences in the Constrained MSSM. JHEP 0812, 024.

[Trotta et al., 2011] Trotta, R., Johannesson, G., Moskalenko, I., Porter, T., de Austri, R. R., et al., 2011. Constraints on cosmic-ray propagation models from a global Bayesian analysis. Astrophys.J. 729, 106.

[van den Aarssen et al., 2012] van den Aarssen, L. G., Bringmann, T., Goedecke, Y. C., 2012. Thermal decoupling and the smallest subhalo mass in dark matter models with Sommerfeld-enhanced annihilation rates. Phys.Rev. D85, 123512.

[Weekes et al., 2002] Weekes, T., Badran, H., Biller, S., Bond, I., Bradbury, S., et al., 2002. VERITAS: The Very energetic radiation imaging telescope array system. Astropart.Phys. 17, 221–243.

[Weniger, 2012] Weniger, C., 2012. Tentative observation of a gamma-ray line at the Fermi LAT.

[Zechlin et al., 2012] Zechlin, H., Fernandes, M., Elsaesser, D., Horns, D., 2012. Dark matter subhaloes as gamma-ray sources and candidates in the first Fermi-LAT catalogue. Astron.Astrophys. 538, A93.

[Zechlin and Horns, 2012] Zechlin, H.-S., Horns, D., 2012. Unidentified sources in the Fermi-LAT second source catalog: the case for DM subhalos.

[Zee, 2010] Zee, A., 2010. Quantum Field Theory in a Nutshell, 2nd Edition. Princeton University Press.

[Zornoza, 2012] Zornoza, J., 2012. Dark matter search with the ANTARES neutrino telescope.